MANGANESE CENTERS IN OXALATE DECARBOXYLASE

By

ELLEN WINGER MOOMAW

A DISSERTATION PRESENTED TO THE GRADUATE SCHOOL
OF THE UNIVERSITY OF FLORIDA IN PARTIAL FULFILLMENT
OF THE REQUIREMENTS FOR THE DEGREE OF
DOCTOR OF PHILOSOPHY

UNIVERSITY OF FLORIDA

2007

To my parents and to my sisters

ACKNOWLEDGMENTS

There are many people that I would like to thank for their help and support throughout my doctoral research at the University of Florida. I am particularly indebted to my advisor Dr. Nigel G. J. Richards and EPR collaborator Dr. Alexander Angerhofer for making this work a reality as well as for their guidance. I thank Dr. George Christou, Dr. Thomas J. Lyons, and Dr. Daniel L. Purich for their input and support as members of my doctoral dissertation committee. This study was supported by grants from the National Institutes of Health (DK61193 and DK61666) and by the University of Florida Chemistry Department.

I am grateful to my coworkers and friends in the Richards research group, especially Dr. Patricia Moussatche, for the molecular biological training and collaboration that she provided. I also thank Kai Li, Ewa Wroclawska, Dr. Drazenka Svedruzic, Dr. Christopher Chang, Cory Toyota, and Dr. Jemy Gutierrez for technical assistance, training, and helpful discussions.

I owe a debt of gratitude to my EPR collaborators in addition to Dr. Alexander Angerhofer, Dr. Andrew Ozarowski and Dr. Jurek Kryztek of the National High Magnetic Field Laboratory, Dr. Ines Garcia-Rubio of the ETH Zurich, and Dr. Ralph T. Weber of the Bruker Biospin Corp.

I appreciate the technical support of Vijay Antharam and Omjoy Ganesh for the CD studies and of Witcha Imaram for the EPR spin-tapping experiments.

I thank Dr. Ben Smith, Graduate Coordinator, and Lori Clark in the Graduate Student Office for their help and advice.

TABLE OF CONTENTS

page

LIST OF TABLES

LIST OF FIGURES

Abstract of Dissertation Presented to the Graduate School
of the University of Florida in Partial Fulfillment of the
Requirements for the Degree of Doctor of Philosophy

STUDIES OF THE MANGANESE CENTERS IN OXALATE DECARBOXYLASE

By

Ellen Winger Moomaw

August 2007

Chair: Nigel G. J. Richards
Major: Chemistry

Oxalate decarboxylase (OxDC) catalyzes the conversion of oxalate into CO_2 and formate by a mechanism that remains poorly understood. The bacterial form of the enzyme, present in *Bacillus subtilis*, is composed of two cupin domains, each of which contains a Mn(II) ion coordinated by four conserved residues. My work reports an *in vivo* strategy for obtaining recombinant, wild type OxDC in which manganese is substituted by cobalt, together with the first conditions for *in vitro* reconstitution of the apoenzyme with Mn(II). My work also examines the question of whether both Mn-binding sites in *Bacillus subtilis* OxDC can independently catalyze the decarboxylation reaction by expressing and characterizing a series of OxDC mutants in which metal binding is perturbed. A linear relationship between Mn occupancy and catalytic activity is demonstrated. Electron Paramagnetic Resonance (EPR) measurements reveal that the apparent line broadening observed for the Mn signals of wild type OxDC arises from dipolar coupling between neighboring Mn ions. These results are consistent with the proposal that there is only a single catalytic site in the enzyme.

The similarity between the two Mn(II) sites has precluded previous attempts to distinguish them spectroscopically and complicated efforts to understand the catalytic mechanism. My research utilizes a multifrequency EPR approach to distinguish the two Mn ions on the basis of

their differing fine structure parameters, and observed that acetate and formate bind to Mn(II) in only one of the two sites. The EPR evidence is consistent with the hypothesis that this Mn-binding site is located in the N-terminal domain, in agreement with predictions based on a recent X-ray structure of the enzyme.

CHAPTER 1
INTRODUCTION

Oxalic Acid in Biological Systems

Oxalate producing plants, which include numerous crop plants, accumulate oxalate in the range of 3% to 80% (w/w) of their dry weight either as the free acid, as sodium or potassium oxalate, or as an insoluble salt, most commonly calcium oxalate (*1-4*). A number of possible pathways for the biosynthesis of oxalic acid in plants have been described (*5*). These pathways include the oxidation of glycolate and glyoxylate (byproducts of photorespiration) by glycolate oxidase (*6, 7*) and the activity of isocitrate lyase on isocitrate (*8, 9*). Possible functions of soluble oxalate and calcium oxalate crystals in plants include protection against insects and foraging animals, ion regulation, and detoxification of heavy metals (*2, 4, 10*).

Oxalic acid and its calcium salt accumulate in many fungi but knowledge of its biosynthetic pathway remains fragmentary. Oxaloacetase, which cleaves oxaloactetate to yield acetate and oxalate, is present in many fungal species and has been proposed as one biosynthetic route (*5, 11, 12*). Phytopathogenic fungi use oxalic acid at the site of infection to lower the pH which enhances the activity of lytic enzymes such as polygalacturonase and cellulase (*13, 14*). Utilization of oxalate by wood rotting fungi to degrade lignin and cellulose has been the subject of much research (*15-18*).

Bacteria capable of using oxalate as a sole carbon and energy source (oxalotrophic) play essential roles in soil fertility and retention and/or recycling of elements necessary for plant growth and are important modulators in the biological carbon cycle (*19, 20*). Oxalotrophic bacteria inhabiting the gastrointestinal tracts of mammals provide the only known route for the catabolism of dietary oxalate in these organisms.

At high concentrations, oxalate causes death in humans and animals as a result of its corrosive properties. At lower concentrations, oxalate leads to a variety of pathological disorders, including hyperoxaluria, pyridoxine deficiency, cardiomyopathy, cardiac conductance disorders, calcium oxalate stones and renal failure (*20-24*). The administration of oxalate degrading bacteria (*Oxalobacter formigenes)* has been proposed as a treatment for hyperoxaluria (*25*).

Several oxalate degrading enzymes have either actual or potential commercial significance with applications in medicine, agriculture, and industry. Oxalate oxidase and oxalate decarboxylase are used in clinical assays of oxalate in blood and urine (*26, 27*). Transgenic plants have been engineered to express oxalate degrading enzymes as a means of protection against pathogens and to reduce the amount of oxalate present (*28, 29*). Structural, mechanistic, and biochemical information is needed in order to further the application of oxalate degrading enzymes in medicine, agriculture, and industry (*28, 30, 31*).

Oxalate Degrading Enzymes

Three major classes of enzymes have evolved to degrade oxalate. Plants employ oxalate oxidase (*32*), fungi (*33*) and soil bacteria (*34*) utilize oxalate decarboxylase, and bacteria exploit oxalyl-CoA decarboxylase (*35*) (Figure 1.1A). Oxalate oxidases (OxOx), also known as germins, catalyze the oxygen-dependent oxidation of oxalate to carbon dioxide in a reaction that is coupled with the formation of hydrogen peroxide (*32, 36, 37*). Hydrogen peroxide formation is believed to serve as a defense mechanism against infection by pathogens (*38, 39*) and to contribute to cell wall crosslinking (*40*). X-ray crystallographic structure determination revealed that OxOx crystallizes as a hexamer (*41*) and electron paramagnetic resonance (EPR) studies demonstrated the presence of Mn(II) in the resting enzyme (*36*). The Mn ion is coordinated by four conserved residues (three His and a Glu) (*42*) and each monomer possesses the β–barrel

topology characteristic of the cupin superfamily of enzymes (*28, 43-46*). EPR spectroscopic changes of the Mn signal upon the addition of oxalate supports the hypothesis that the Mn ion is the site of catalysis (*47*). UV-visible spectroscopy, spin trapping studies, and structural studies have lead to proposed mechanisms that involve the binding of oxalate directly to Mn(II), the formation of Mn(III), and a radical intermediate species (*36, 37, 48*).

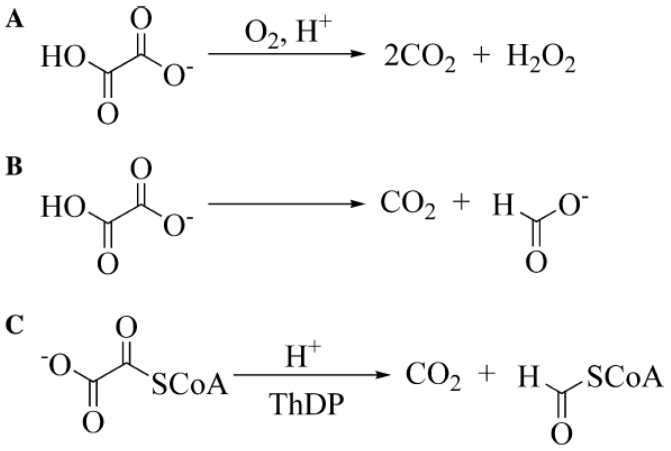

Figure 1-1 Enzymes that catalyze oxalate degradation. (A) Oxalate oxidases, found in plants. (B) Oxalate decarboxylases, present in fungi and in some bacteria (C) Oxalyl-CoA decarboxylases, thiamin-dependent enzymes present in bacteria.

Oxalyl-CoA decarboxylase (OXC) catalyzes the cleavage of oxalyl-CoA to formyl CoA and carbon dioxide (*37, 49, 50*) (Figure 1-1C). In *Oxalobacter formigenes* OXC is coupled to formyl-CoA transferase, which catalyzes an acyl transfer from formyl-CoA to oxalate to yield formate and oxalyl-CoA (*51*). The overall coupled reactions convert oxalate to formate and carbon dioxide with the consumption of a proton. Insight into this system was provided by the isolation and characterization of a membrane bound formate-oxalate antiporter (*52-54*), which imports oxalate into the cell and exports formate, creating a proton gradient across the membrane which is then used to drive ATP synthesis (*55, 56*).

Oxalate Decarboxylase

Biological Distribution

Oxalate decarboxylase (OxDC) catalyzes the difficult carbon-carbon bond cleavage of oxalate to yield carbon dioxide and formate (*57*) (Figure 1-1B). This enzyme was first reported in the basidiomycete fungi *Collybia (Flammulina) velutipes* and *Coriolus hersutus* more than 50 years ago (*33, 58*). OxDC has since been reported in a number of fungal species including the following: *Sclerotinia sclerotiorum* (*59*) , *Coriolus (Trametes) versicolor* (*18*), *Mythrothecium verrucaria* (*60*), *Aspergillus niger* (*61, 62*), *Agaricus bisporus* (*63*) and *Postia placenta* (*64*). Fungal OxDCs can be both an intracellular enzyme (*18*) or excreted from the hyphal cells (*18, 64, 65*). Expression of OxDC in fungal cultures is induced by decreasing the pH and/or adding carboxylic acids such as oxalate, glycolate, and citrate (*18, 59-61, 66, 67*). It has been proposed that differences in the regulation of OxDC expression may imply differences in the function of the enzyme in a specific organism (*34, 68*). Acid-induced OxDCs might be involved in proton consumption whereas those induced by oxalate may protect the organism from the harmful metabolic effects of oxalate.

The first prokaryotic OxDC was reported in 2000 when *Bacillus subtilis,* a soil bacterium, was shown to express a cytosolic OxDC. Bacterial OxDC is induced by acid but not by oxalate which may suggest that its metabolic function is not related to its oxalate degrading activity (*34, 69*). This enzyme, encoded by the *yvrK* gene (renamed *oxdC*) has been overexpressed in *E. coli* and further characterized (*57, 70-74*). Comparison of the OxDC fungal sequences with the *B. subtilis* genome (*75*), suggested that two other genes, *yoaN* (renamed *oxdD*) and *yxaG* may also code for enzymes with OxDC activity (*70*). The *yoaN* gene product OxdD was shown to have low levels of OxDC activity (*70*) and the *yxaG* gene product has been reported to be a novel Fe-containing quercetin 2,3-dioxygenase (*76-78*).

Oxalate Decarboxylase Belongs to the Cupin Superfamily (DSBH) of Proteins

The cupin superfamily of proteins have been well recognized as possessing remarkable functional diversity with representatives found in Archaea, Eubacteria, and Eukaryota (*28, 43-46*). The identification of the cupin superfamily was originally based on the recognition that the wheat protein germin shared a nine amino acid sequence with another protein, spherulin, produced by the slime mold *Physarum polycephalun* during starvation (*44*). This sequence similarity was also observed in a number of seed storage proteins called germin-like proteins (GLPs). Knowledge of the three dimensional structures of these proteins led to the collective name cupin on the basis of their β–barrel shape ('cupa' means "small barrel" in Latin) (*46*). Characteristic features of proteins with this fold include high thermal stability and resistance to proteases. These features are consistent with a high degree of subunit contacts, hydrophobic interactions, and short loops. The cupin domain was originally described as two conserved motifs, each composed of two β–strands separated by a less conserved region composed of another two β–strands separated by a loop of varying length (*28, 45*). Motif 1 was originally designated as $G(X)_5HXH(X)_{3,4}E(X)_6G$ (shown in blue in Figure 1-2) and Motif 2 as $G(X)_5PXG(X)_2H(X)_3H(X)_3N$ (shown in red in Figure 1-2). With more sequences analyzed, it has become clear that the primary sequence of the two motifs is not as highly conserved as previously thought (*42, 43*).

The cupin superfamily of proteins exemplifies a general trend emerging from comparative genomics: classes of proteins are being expanded beyond the presence of a set of conserved residues which had previously been the cornerstone of their identification. In 2003, Anantharaman et al. described the use of information from recently reported X-ray

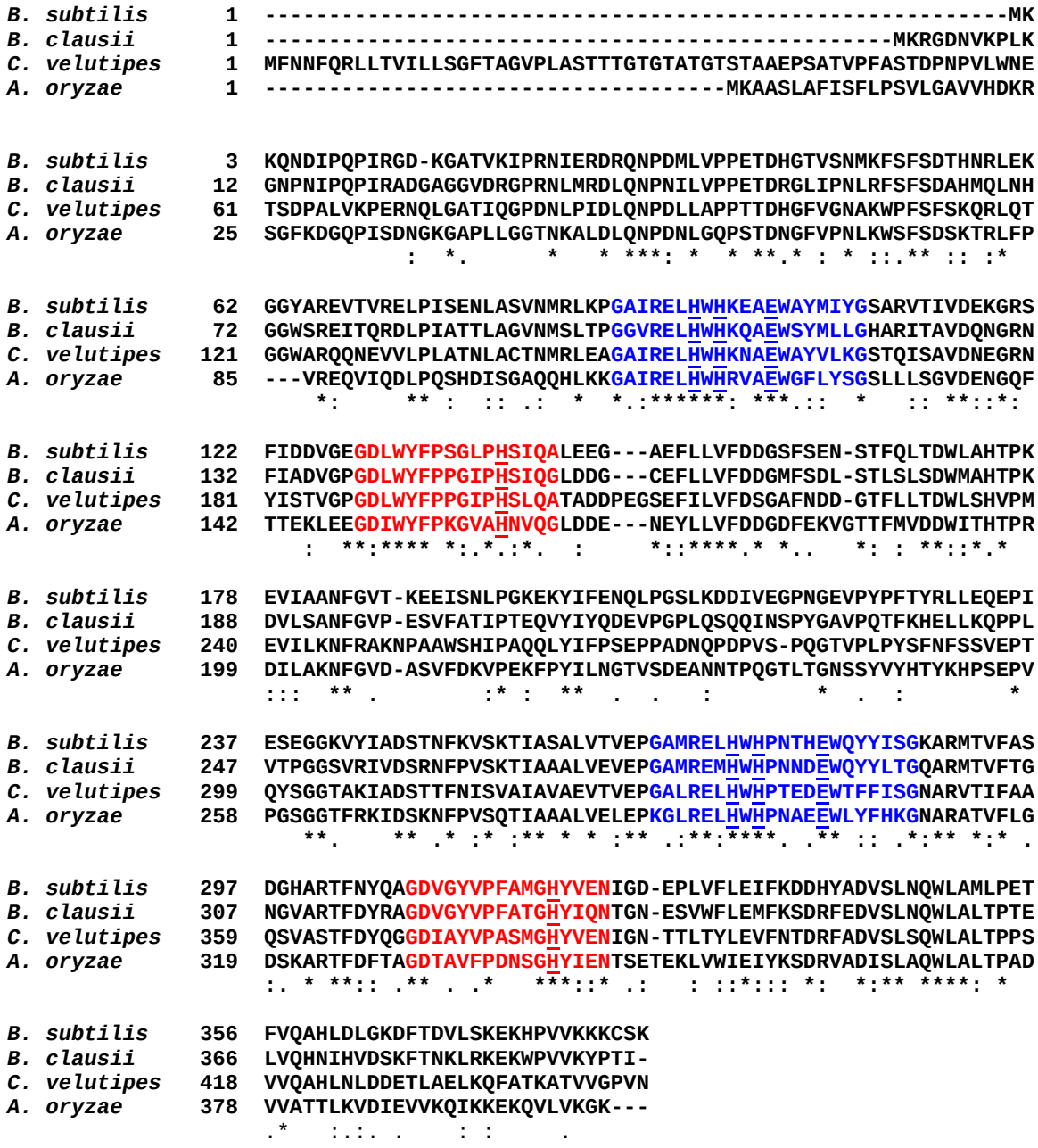

Figure 1-2 Sequence alignments of OxDCs from *Bacillus subtilis*, *Bacillus clausii*, *Collybia velutipes*, and *Aspergillus oryzae* showing the positions of the two conserved motifs (motif 1 in blue and motif 2 in red) in the two domains. Alignment was made using the Clustal W method (*79*, *80*). Asterisks indicate identical residues, colons(:) indicate conservative substitutions, and periods (.) indicate semi-conservative substitutions. The Mn-binding residues of the *Bacillus subtilis* OxDC are underlined.

crystallographic structures and sequences to gain a perspective on the major principles that appear to have shaped the emergence of diverse enzymatic activities within structurally similar

and evolutionarily related scaffolds (*81*). The absence or presence of various metals such as Ni, Fe, Zn, Mn, or Cu contribute to the functional diversity of the cupin superfamily (*43, 78*). The term cupin has been expanded into the Structural Classification of Proteins (SCOP) (http://scop.berkeley.edu/data/scop.b.html) database as the double-stranded β-helix (DSBH) multicatalytic fold. The terms cupin and DSBH are now used synonymously (*82-84*). Since OxDC has two of these characteristic DSBH domains it is further classified as a bicupin. It has been suggested that OxDC evolved from OxOx by gene duplication and selection (*28, 37, 45*). This suggestion is consistent with current models of enzyme evolution (*85, 86*).

Anantharaman et al. (*81*) propose that ancestral forms of the DSBH can be evolutionarily reconstructed as simple, small-molecule-binding domains that perhaps bound sugars and cyclic nucleotides (*45, 81, 87*) and that it is from these sugar-binding domains that sugar-modifying domains such as isomerases and epimerases arose. They further propose (*81*) that a set of conserved histidine residues employed in sugar-binding in the ancestral non-enzymatic domain evolved into the metal coordinating histidine residues observed in germin (*88*) and oxalate decarboxylase (*72*) and that another lineage of DSBH domains acquired a new set of conserved residues with the ability to bind 2-oxoglutarate which gave rise to the iron-2-OG-dependent dioxygenases.

Structural Features

High resolution X-ray crystal structures of *Bacillus subtilis* OxDC (*72, 73*) have confirmed that the OxDC monomer is composed of two β-barrel domains, each of which contains a metal-binding site (Figure 1-3A). These metal ions are 26 angstroms apart from each other in the monomer. Evidence from inductively-coupled plasma mass spectrometry (ICP-MS) (*89*) and

EPR spectroscopy initially suggested that OxDC activity was Mn-dependent (*70*). This hypothesis is consistent with crystallographic observations (*72, 73*).

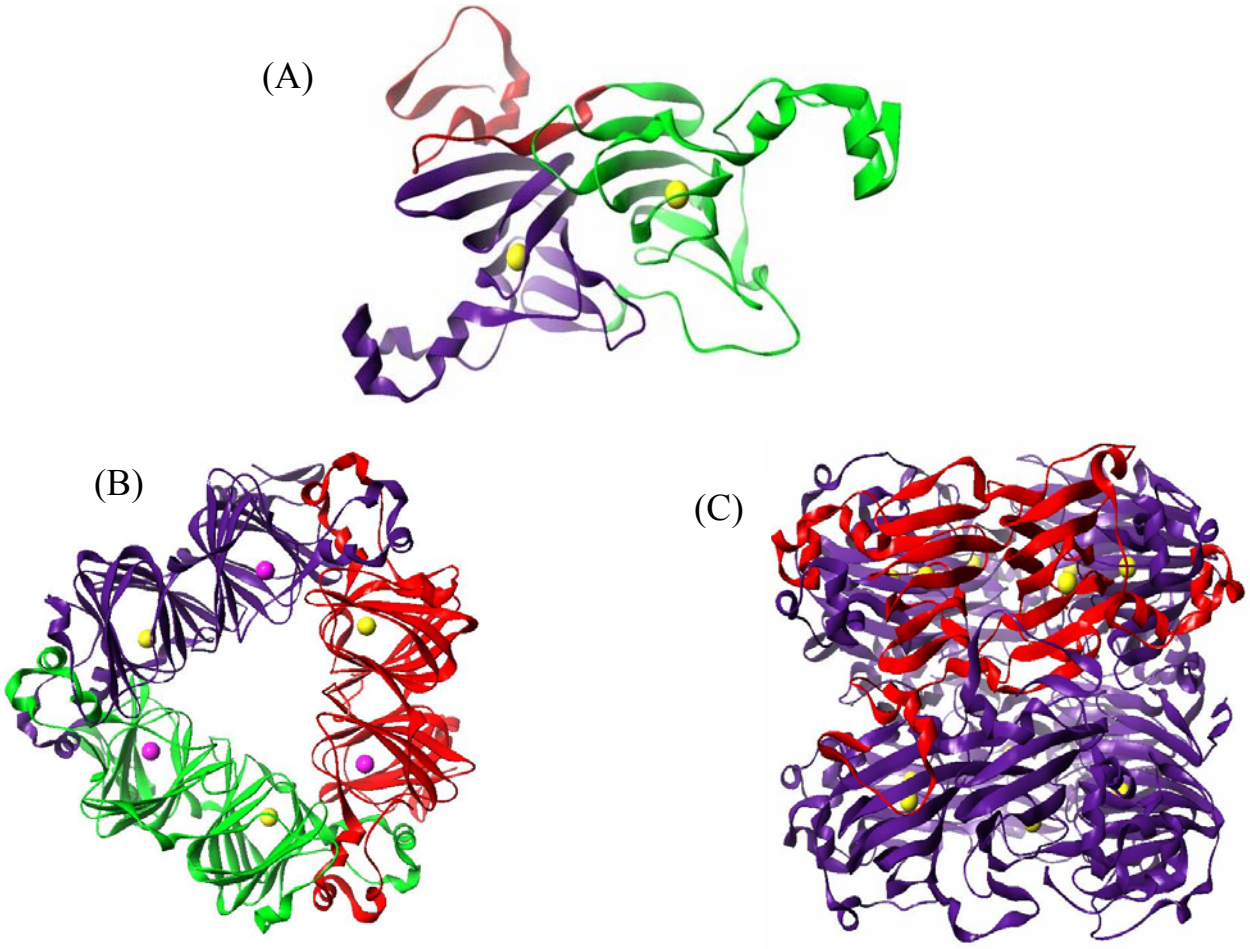

Figure 1-3 Ribbon structures of the *Bacillus subtilis* OxDC monomer, trimer, and hexamer. (A) The N- and C-terminal cupin domains of the OxDC monomer are colored green and purple, respectively, and the N-terminal segment that contributes to the secondary structure of the C-terminal domain is colored red. The yellow spheres show the locations of the two Mn centers. (B) Structure of an OxDC trimer in which the monomers are colored red, green and purple. The locations of Mn ions are shown by the purple (N-terminal domain) and yellow spheres (C-terminal domain). (C) Structure of the OxDC hexamer in which one monomer is colored red to emphasize the role of α-helical regions in mediating monomer/monomer interactions. These structures were visualized using the CAChe Worksystem Pro V6.5 software package (Fujitsu America Inc., Beaverton, OR).

The quaternary structure of OxDC is hexameric (Figure 1-3C) composed of two trimeric layers (Figure 1-3B) packed face to face that have 32 (D_3) point symmetry. The OxDC trimer resembles the OxOx hexamer (37). The OxDC hexamer has a diameter of approximately 90 angstroms and a thickness of 85 angstroms. A large solvent channel (15 angstroms wide) runs through the hexamer along the 3-fold axis (72). The trimeric layers of the hexamer are stabilized by α-helical protrusions of adjacent monomers (Figure 1-3C).

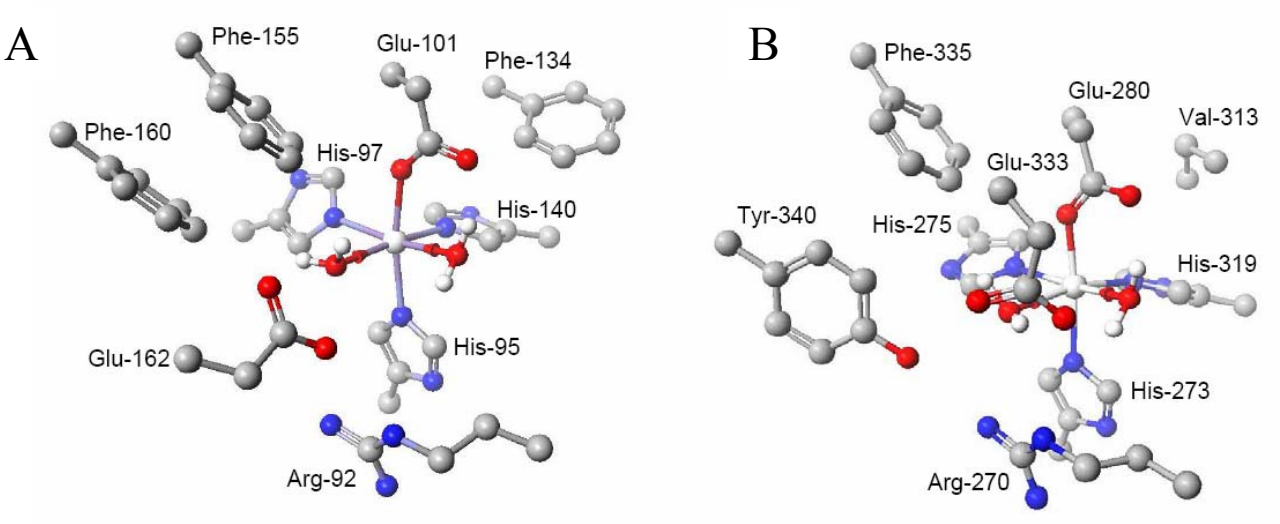

Figure 1-4 Residues defining the Mn-binding sites in A) the N-terminal (1UW8) domain of OxDC and B) the C-terminal (1J58) domain of OxDC. Residue numbering is for the enzyme encoded by the OxdC gene in Bacillus subtilis. For clarity, hydrogen atoms bound to carbon atoms are omitted. Atom coloring: C, black; H, white; N, blue; O, red; Mn, silver. These structures were visualized using the CAChe Worksystem Pro V6.5 software package (Fujitsu America Inc., Beaverton, OR).

Both of the Mn-binding sites in the OxDC monomer resemble the Mn-binding site of OxOx in that each Mn ion is coordinated by the side chains of four conserved residues (Figure 1-4) in a distorted octahedral environment. The manganese-binding residues in the N-terminal domain are His95, His 97, His 140, and Glu101 and in the C-terminal domain are His273, His275, His319, and Glu280. In one of the available X-ray crystallographic structures ("open" conformation), the N-terminal Mn-binding site contains one water molecule and one formate

molecule while the C-terminal Mn-binding site contains two water molecules (*72*). In another available X-ray crystallographic structure ("closed" conformation), however, the N-terminal Mn-binding site contains two water molecules and the C-terminal Mn-binding site contains a single water molecule in a penta-coordinated form (*73*).

Not only do oxalate oxidase and oxalate decarboxylase possess remarkably similar Mn-binding sites, the metal-binding cavity is also intriguingly similar in that it is lined primarily by hydrophobic residues. Given these similarities and common substrate, it appears that only subtle changes are necessary to promote different biochemical activities. It has been proposed that the absence of a proton donor in the active site of OxOx prevents it from catalyzing the decarboxylation of oxalate (*72*). The putative proton donor(s) in OxDC have been proposed to be Glu162 in the N-terminal domain (*73*) and/or Glu333 in the C-terminal domain (*72*).

Mechanistic Information

Oxalate decarboxylase requires molecular oxygen for catalytic turnover (*57, 58, 61, 70*) even though the production of formate and CO_2 from oxalate involves no net oxidation or reduction. Furthermore, all of the OxDCs that have been characterized possess optimum activity at acidic pH and exhibit a high substrate specificity for oxalate (*37, 57, 58, 70*). Efforts to elucidate the catalytic mechanism through the use of heavy atom isotope effects (*57*), electron paramagnetic resonance spectroscopy (*71*), density functional theory calculations (*90*), homology modeling with oxalate oxidase sequences (*91*), structural information and site-directed mutagenesis studies (*72, 73*) have led to a number of mechanistic proposals.

Heavy-atom (^{13}C and ^{18}O) kinetic isotope effect (KIE) measurements (*92*) were used to probe the structure of the transition state for the decarboxylation step for the recombinant, wild type OxDC from *B. subtilis* (*57*). Since V/K KIEs were measured in these competition experiments, no information can be obtained for the steps that occur after carbon-carbon bond

cleavage (*93*). The pH dependence of the enzyme catalyzed reaction suggests that monoprotonated oxalate is the actual substrate for OxDC (*57*) and that the substrate likely binds directly to the Mn in the enzyme-substrate complex (*37*).

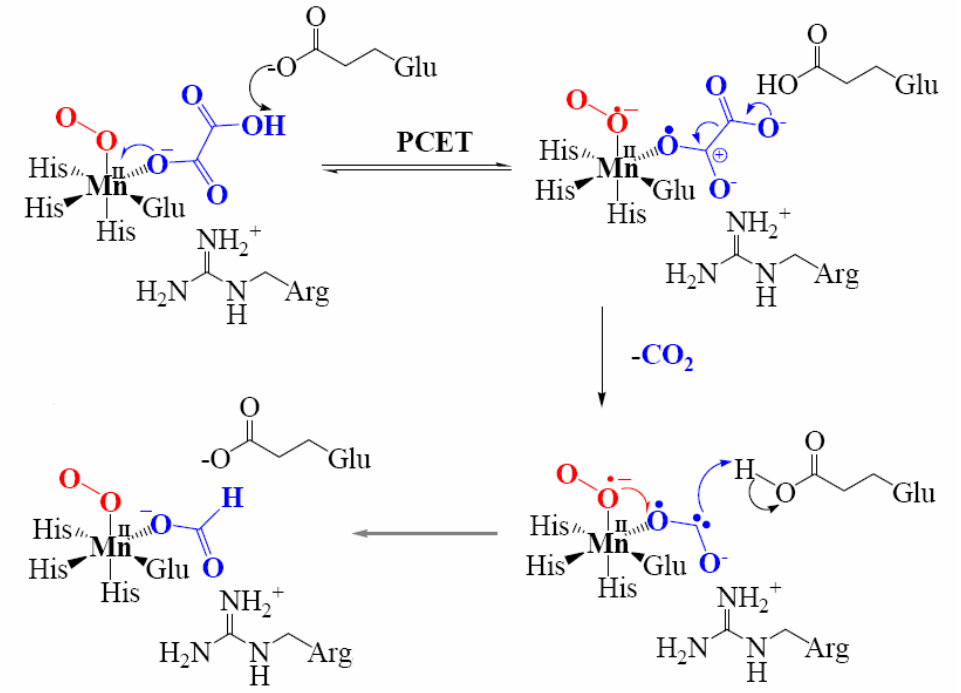

Figure 1-5 Proposed catalytic mechanism for oxalate decarboxylase based on heavy-atom isotope effect measurements.

Heavy-atom KIEs measured at pH 4.2 and 5.7 are consistent with a two step model in which a reversible step precedes carbon-carbon bond cleavage and decarboxylation (Figure 1-5) (*37*, *57*). In this proposal, a reversible proton-coupled electron transfer (*94*, *95*) yields a Mn-bound oxalate radical anion, which then decarboxylates to form CO_2 and a formate radical anion. Protonation of the Mn-bound formate radical anion produces formate which is then liberated from the enzyme. In this proposal, active site glutamate residue(s) serve as a general acid/base catalyst and active site arginine residue(s) act to polarize the oxalate carbonyl bond (*57*). The oxidation state in the above mechanism is purely hypothetical and remains to be demonstrated by

experimental methods. Other proposals have invoked that the oxidation state of manganese alternates during catalysis, between Mn(II) and Mn(III) (*70, 74*) or Mn(III) and Mn(IV) (*72*). Only Mn(II) has been detected experimentally by either standard perpendicular-mode or parallel-mode EPR spectroscopy of the resting enzyme (*70, 71, 74*) or during turnover (*71*).

Oxygen Dependence and the Formation of Hydrogen Peroxide

The first report of an oxalate decarboxylase observed that decarboxylation did not proceed under strictly anaerobic conditions and that the introduction of air into the manometric apparatus restored the activity to the original level (*33*). Subsequently reported OxDCs have shown a similar oxygen dependence (*37, 57, 58, 60-62, 70*) but vary with respect to the level of activity restored upon the reintroduction of oxygen. The role of dioxygen in the catalytic cycle is unknown and cannot be replaced by other oxidizing agents such as H_2O_2, paraquinone, 2-methyl-1,4-naphthoquinone, flavin adenine dinucleotide, flavin mononucleotide, and cytochrome c (*58*).

The most extensive characterization of the oxygen dependence of OxDC was carried out on the enzyme from *Aspergillus niger* using manometric techniques (*62*). In this study, the influence of the partial pressure of O_2 on the enzyme was observed by replacing the air in the Warburg apparatus by mixtures of O_2 and N_2. In the absence of *o*-phenylenediamine (oPDA), maximal activity was obtained at 0.04 atm of O_2, whereas, in the presence of oPDA maximal activity was obtained at 0.2 atm. Pressures greater than optimal accelerated the irreversible inactivation of the enzyme even in the presence of oPDA. Inactivation occurs, however, only during catalytic turnover since bubbling O_2 through the enzyme solution prior to the addition of substrate did not affect product formation. This suggests that if O_2 binds directly to the metal, it does so after oxalate binding. Oxalate oxidase activity has been reported for both fungal and bacterial oxalate decarboxylases. The rate of oxalate oxidation relative to decarboxylation is 1.5-

3.0% for the *A. niger* enzyme (*62*) and 0.2% for the recombinant, wild type *B. subtilis* enzyme (*70*).

Research Objectives

The overarching goals of this research are motivated by the fact that the metal centers in oxalate decarboxylase and oxalate oxidase are evolutionarily related (*28*) even though the chemical transformations catalyzed by the enzymes are different (*32, 33*). This research seeks to employ the techniques of bioinorganic chemistry, molecular spectroscopy, enzyme kinetics, and protein engineering to characterize oxalate decarboxylase. Increased knowledge of this enzyme may impact our general understanding of metalloenzyme evolution and the role of the protein environment in modulating reactivity (*86, 96*).

The specific objectives of the presented work were: 1) to optimize the expression and purification procedures to obtain OxDC with high manganese occupancy; 2) to characterize the manganese dependence of the enzyme; 3) to distinguish the manganese-binding sites spectroscopically; and, 4) to determine which manganese center is the site(s) of catalysis.

CHAPTER 2
CHARACTERIZATION OF THE MN-DEPENDENCE OF OXALATE DECARBOXYLASE ACTIVITY

Introduction

Three pieces of indirect evidence support the idea that OxDC activity is Mn-dependent. First, Mn(II) is present in the resting form of recombinant, wild type *Bacillus subtilis* OxDC when the enzyme is expressed in *Escherichia coli* (*70, 71*). Second, the successful expression of correctly folded OxDC with reasonable catalytic activity specifically requires the presence of Mn(II) in the growth medium (*70*). Third, the X-ray scattering factors for Mn which were used in the refinement of the high-resolution structures of recombinant *Bacillus subtilis* OxDC were fully consistent with this metal being bound within both DSBH domains (*72, 73*). On the other hand, the native form of OxDC from *Bacillus subtilis* could not be purified in sufficient quantities for accurate metal analysis (*34*), and other enzymes in the bicupin family appear to be able to employ a variety of metals in catalysis (*76, 78, 97*). In order to characterize the Mn-dependence of recombinant *B. subtilis* OxDC, an *in vivo* strategy was employed for obtaining recombinant, wild type OxDC in which Mn is substituted by Co, and *in vitro* conditions for re-constituting the recombinant enzyme with Mn were developed.

Results and Discussion

Optimization of Expression of Recombinant Wild Type OxDC

Expression conditions for obtaining OxDC were optimized so that pure samples of the enzyme could be routinely obtained with a metal content of 1.6-1.9 Mn/monomer rather than the 0.86-1.14 Mn/monomer reported in prior studies of the enzyme (*57, 70*). At this level of Mn incorporation, recombinant OxDC exhibits a specific activity of 40-65 U/mg as measured in an endpoint assay employing formate dehydrogenase (FDH) (*98*). To obtain reproducibly high levels of Mn incorporation, protein expression was induced at a lower optical (0.6 at 600 nm)

density than previously reported (*57*), and cells were grown at a post-induction temperature of 30^{o}C so as to promote the transport of manganese ions into the bacterial cells (*99, 100*). Consistent with previous reports, we observed the oxalate dependence of the decarboxylase activity followed Michaelis-Menton kinetics, with our K_m value being lower than previously reported (8.4 vs. 15 mM) (*70*).

Effect of Addition of Other Metals in the Growth Medium

Having established conditions for obtaining recombinant OxDC with high specific activity, we next investigated whether including other salts in the growth medium might yield enzyme in which manganese had been replaced by other transition metals. Introducing $FeCl_2$, $FeCl_3$, or $CoCl_2$ into to the growth medium in place of $MnCl_2$ yielded samples of the recombinant, wild type enzyme with varying levels of Mn incorporation. All of these variants behaved similarly to the wild type, Mn containing OxDC on purification but exhibited activities that correlated best with their Mn content leading to the conclusion that metals such as Co or Fe do not support catalysis.

When $CoCl_2$ (2 mM) was used as a supplement, ICP-MS analysis showed that samples of recombinant OxDC contained 0.80 Co/monomer and 0.05 Mn/monomer (Table 2-1). Given the very low specific activity of the Co-substituted OxDC was similar to that expected solely on the amount of Mn present in the enzyme sample, we assumed that enzyme-bound Co(II) did not catalyze the decarboxylation reaction and therefore investigated the effects of expressing the enzyme with mixtures of the chloride salts of both Co(II) and Mn(II) in the growth medium (Table 2-1). We anticipated that different concentration ratios of the exogenous salts would yield OxDC samples substituted with different levels of Mn, and this proved to be the case although no obvious correlation was observed between the Mn:Co ratio and the extent to which Mn or Co was incorporated into the recombinant enzyme.

Table 2-1 Effect of $MnCl_2$ and $CoCl_2$ in the growth medium on metal incorporation and specific activity of recombinant, wild type OxDC. Metal content is expressed as the number of metal ions/OxDC monomer. n. d. indicates that the value was not determined. These samples contained <0.01 atoms/monomer Mg.

OxDC Preparation	$MnCl_2$ (mM)	$CoCl_2$ (mM)	Mn	Co	Zn	Fe	Cu	Specific Activity (U/mg)
1	5	0	1.87	n.d.	0.51	0.07	0.01	61.2
2	5	0	1.87	n.d.	0.13	0.19	< 0.01	50.1
3	5	0	1.63	n.d.	0.08	< 0.01	< 0.01	40.9
4	0	2	0.05	0.80	0.14	< 0.01	< 0.01	2.2
5	0.25	2	0.27	1.03	0.22	0.18	< 0.01	8.0
6	1	1	0.12	1.32	0.26	0.13	< 0.01	4.5
7	5	0.25	0.56	0.68	0.22	0.13	< 0.01	13.5
8	5	0.05	0.47	0.09	0.19	0.06	< 0.01	19.0

When a 20:1 Mn:Co ratio was employed the two metals were incorporated into the enzyme in approximately equal amounts. Increasing the amount of $MnCl_2$ relative to $CoCl_2$ in the growth medium, however, did not yield wild type OxDC containing more Mn than Co. This finding likely reflects the tight regulation of Mn metabolism that is observed in bacteria such as *Escherichia coli* (*100-103*). Although a positive correlation between Mn content and decarboxylation rate was evident on assaying the activity of the Mn/Co-substituted enzymes, we could not definitely conclude that decarboxylase activity was linearly correlated with Mn content on the basis of these *in vivo* experiments because no expression conditions could be identified that gave OxDC samples containing 0.7-1.5 Mn/monomer.

Preparation of the OxDC "Apoenzyme" and Reconstitution of the Wild Type, Mn-Containing Enzyme

In order to correlate specific activity with metal content in the 0.7 – 1.5 Mn/monomer range, we examined alternate strategies to obtain samples of the OxDC apoenzyme (*104-109*), then prepare enzyme samples reconstituted with manganese. Following procedures that had been reported for removing the metals from other metalloenzymes, we tried a variety of chelating agents with and without chaotropic agents. In contrast to the bicupin quercetin 2,3-

dioxygenase (*76, 78, 97*), it proved remarkably difficult to remove the metal ion from wild type OxDC. Many literature conditions either did not remove the metal or led to irreversible protein denaturation. The removal of Mn from recombinant OxDC and its subsequent reconstitution with Mn was eventually accomplished, however, following a protocol based on that used to obtain the apoenzyme of Mn-dependent superoxide dismutase (Mn-SOD) (*110-112*).

Table 2-2 Metal content of "apoenzyme" and enzyme reconstituted with Mn. Metal content is expressed as the number of metal ions/OxDC monomer. n. d. indicates that the value was not determined.

Enzyme Preparation	Mn	Co	Zn	Fe	Cu	Mg	Specific Activity
WT OxDC	1.87	n.d.	0.51	0.07	0.01	0.01	61.2 U/mg
"Apoenzyme"	0.01	n.d.	2.0	0.01	0.01	0.01	0 U/mg
Reconstituted OxDC **1**	0.90	n.d.	0.79	0.14	0.01	0.01	25.1 U/mg
Reconstituted OxDC **2**	0.64	0.01	1.20	0.01	0.02	n.d.	14.4 U/mg
Reconstituted OxDC **3**	0.84	0.01	0.60	0.01	0.01	n.d.	19.5 U/mg

This multi-step procedure (see Experimental Methods section) involved partially unfolding the protein in 3.5 M guanidinium hydrochloride (GuHCl) with ethylenediaminetetraacetic acid (EDTA) present. Refolding samples into a buffered solution without added metals resulted in a manganese-free "apoenzyme" (2 Zn/monomer) in which Zn(II) had replaced Mn(II) in wild type OxDC (Table 2-2). Alternate metal ions could also be introduced into the "apoenzyme" by refolding samples into a buffered solution containing salts such as $MnCl_2$. These conditions were used to prepare samples of recombinant OxDC containing 0.64, 0.84, and 0.90 Mn/monomer (the remaining metal sites being occupied by Zn) for kinetic characterization. The specific activities of these samples were determined (Table 2-2). Combining these data with the data obtained adding $CoCl_2$ to the growth medium resulted in a plot of manganese content vs. specific activity which suggests a linear correlation between decarboxylation rate and Mn incorporation (Figure 2-1)

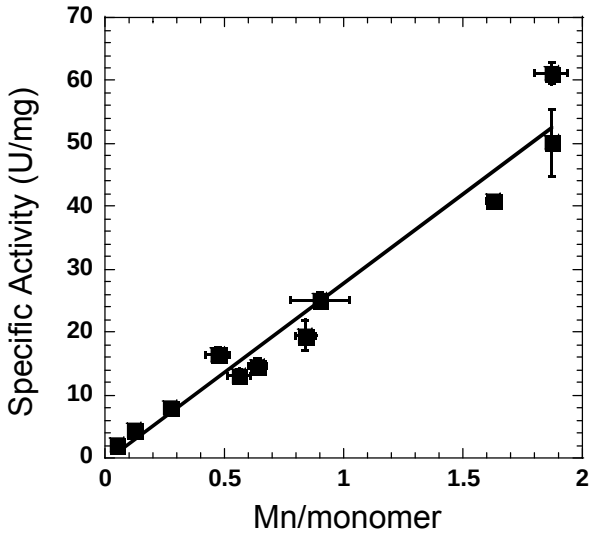

Figure 2-1 The dependence of OxDC specific activity on the extent of Mn incorporation. The line shows the specific activity that would be expected assuming a linear correlation with Mn content.

Gepasi Simulations

The observation of a linear dependence of OxDC specific activity on Mn incorporation places an important constraint on kinetic models for the number of active sites in OxDC that may mediate catalysis. The fact that OxDC is a bicupin capable of binding up to 2 Mn/monomer raises questions concerning the number and location of the catalytic sites that mediate C-C bond cleavage (*72, 73*). Previous efforts to address these questions by steady state kinetic characterization of OxDC mutants in which residues implicated in proton transfer (Glu-162 and Glu-333) were site-specifically modified have given ambiguous results (*72, 73*). The steady-state behavior of seven kinetic models was, therefore, simulated using the GEPASI simulation package (*113, 114*) to evaluate the effects of varying active site number and Mn-binding site affinity on the observed Mn-dependence of catalytic activity.

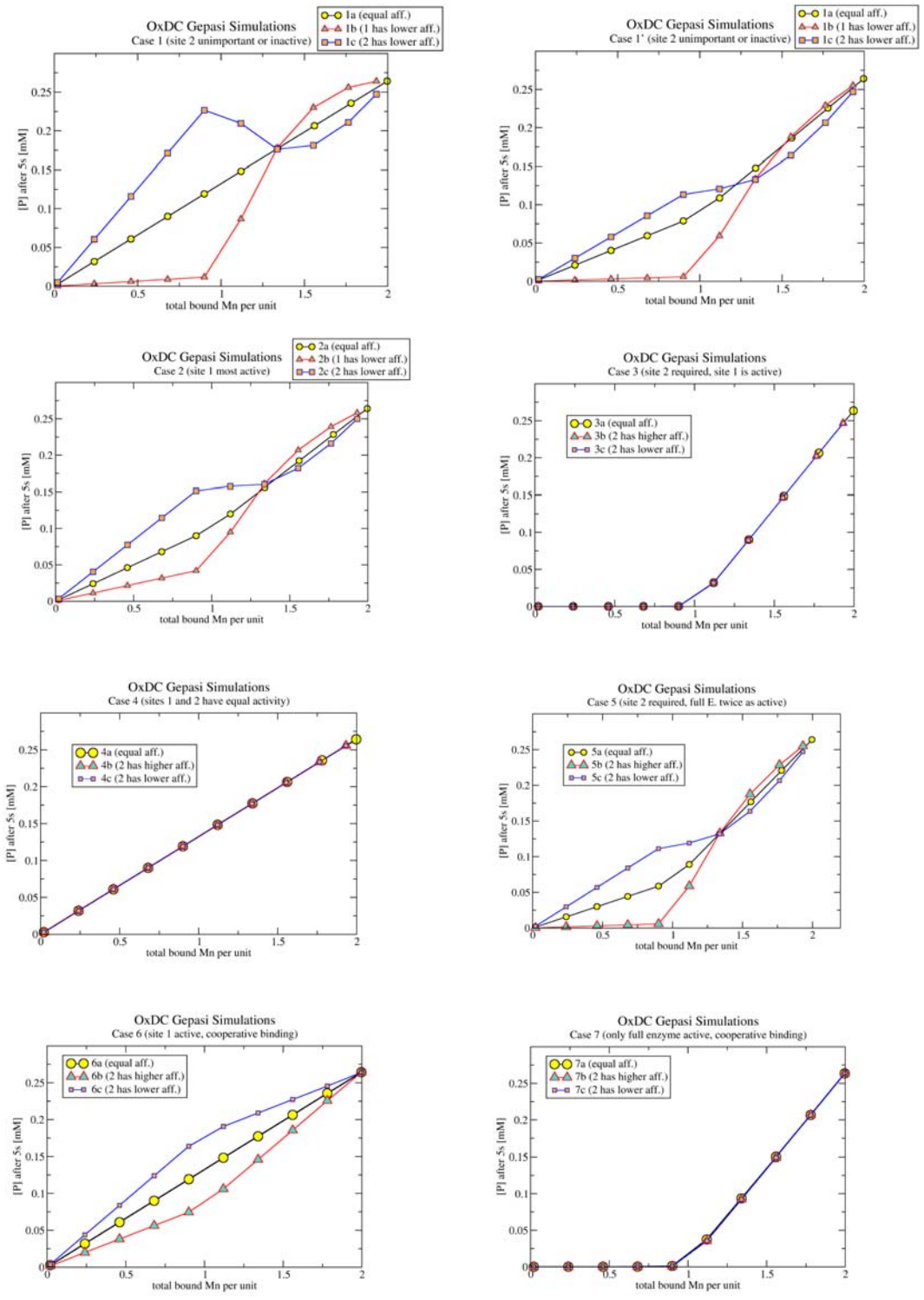

Figure 2-2 Numerical simulations of the dependence of catalytic activity on the extent of Mn incorporation. Full details of the kinetic parameters used in the simulations are provided in Appendix A. All panels show the amount of product formed after a reaction time of 5 s. Note that site 1 and site 2 cannot be associated with a specific N- or C- terminal Mn-binding site.

To date only three models have been identified that are consistent with experimental observations (Case 1a, Case 4a,b,and c, and Case 6a)(Figure 2-2). In Case 1a one site (site ***1***) has catalytic activity that is independent of metal occupancy of the second, inactive Mn-binding site (site ***2***) and these two sites possess the same affinity for Mn. In Case 4 a linear relationship is observed independent of affinity for Mn as both sites have equal levels of catalytic activity. Case 6 assumes that although catalytic activity is only associated with a single site (site ***1***), the affinity of Mn for site ***2*** is increased 100-fold when Mn occupies the active site (site ***1***). Kinetic models that seek to simulate an earlier proposal (*8*) in which the N-terminal site is responsible for the majority (if not all) of activity, with the C-terminal site being primarily important in maintaining enzyme structure, only gave a non-linear relationship between activity and Mn incorporation (Cases 3, 5 and 7).

A model in which both sites have equal activities (Case 4) reproduces the observed linear relationship between activity and Mn content. On the other hand, for models where it is assumed that only a single site (site 1) can mediate catalysis, it is difficult to obtain a linear plot. For example, a model (Case 3) in which the catalytic activity of site 1 is turned on when Mn(II) occupies the second binding site (site 2) yields a non-linear relationship between activity and Mn incorporation. Similarly, permitting differences in the affinity of the two sites for Mn while requiring that catalytic activity be localized within a single site (site 1), irrespective of the occupation of the second site (site 2), results in non-linear behavior (Cases 1b and 1c, Cases 1'b and 1'c). Linear behavior is anticipated for this model only if the two sites initially have an equal affinity for Mn. It is possible, however, to obtain a linear dependence using a kinetic model (Case 6a) in which the affinities of the two binding sites are initially identical but Mn occupancy of site 1 results in an enhanced affinity of site 2 for the metal. We note that such a model

corresponds to a recent suggestion that structural interactions between the cupin domains may be important for yielding enzyme with full catalytic activity (*73*).

Experimental Section

Materials

Unless otherwise stated, all chemicals and reagents were purchased from Sigma-Aldrich (St. Louis, MO), and were of the highest available purity. Protein concentrations were determined using a modified Bradford assay (Pierce, Rockford, IL) for which standard curves were constructed with bovine serum albumin (*14*). All DNA primers were obtained from Integrated DNA Technologies, Inc. (Coralville, IA), and DNA sequencing was performed by the core facility in the Interdisciplinary Center for Biotechnology Research (ICBR) at the University of Florida. The metal content of wild type OxDC, and all site-directed OxDC mutants, was quantified at the University of Wisconsin Soil and Plant Analysis Laboratory on the basis of ICP-MS measurements (*89*).

Expression and Purification of Recombinant, Wild Type OxDC.

Recombinant wild-type *Bacillus subtilis* OxDC was expressed and purified using a modified literature procedure (*57*). Thus, Luria-Bertani broth (50 mL) containing 50 μg/mL kanamycin (LBK) was inoculated with oxdC:pET-9a/BL21(DE3) and incubated overnight at 37 ^{o}C. An aliquot (4 mL) of this stationary phase culture was then used to inoculate Luria-Bertani broth (5 x 400 mL) and the resulting cultures were incubated at 30 ^{o}C until reaching an OD_{600} value of 0.6. At this time, the bacteria were heat-shocked at 42 ^{o}C for 10 minutes before the addition of isopropyl thiogalactoside and $MnCl_2$ to final concentrations of 1 and 5 mM, respectively. The induced cells were then grown at 30 ^{o}C with shaking to ensure maximal aeration for 4 h. The cells were harvested by centrifugation (6000 rpm, 20 min, 4 ^{o}C), and the pellets re-suspended in 50 mM imidazole-Cl, pH 7.0, (100 mL) before sonication. The lysate was

clarified by centrifugation (10,000 rpm, 20 min, 4 °C) and stored overnight at 4 °C. The lysis pellets were re-suspended in 50 mM imidazole-Cl, pH 7.0, containing 1M sodium chloride, 10 μM $MnCl_2$, 0.1% Triton X-100, and 10 mM 2-mercaptoethanol (total volume 100 mL), and the resulting mixture stirred overnight at 4 °C. After centrifugation (10,000 rpm, 20 min, 4 °C), the solubilized extract was combined with the lysate and diluted 7-fold before being applied to a DEAE-Sepharose Fast Flow column (2.5 x 25 cm) equilibrated with 50 mM imidazole-HCl, pH 7.0 (buffer A). Elution was performed using a 500 mL linear gradient from buffer A to buffer A containing 1 M NaCl. Fractions containing OxDC were pooled, and solid $(NH_4)_2SO_4$ added to a final concentration of 1.7 M. The resulting solution was applied to a phenyl-Sepharose Hi-Performance column (2.5 x 18 cm) (GE Healthcare, Piscataway, NJ) equilibrated with 50 mM imidazole-Cl, pH 7.0, containing 1.7 M $(NH_4)_2SO_4$ (buffer B). Bound proteins were eluted using a 500 mL linear gradient from buffer B to buffer A, and fractions containing purified OxDC were pooled, and concentrated by ultrafiltration in an Amicon stirred cell (Millipore, Billerica, MA) to a final volume of 10 mL before being exhaustively dialyzed against 20 mM hexamethylenetetramine hydrochloride, pH 6.0, containing 0.5 M NaCl. The dialyzed enzyme was then concentrated to approximately 9 mg/mL, and stored in aliquots at -80 °C.

Expression and Purification of Co-Substituted, Wild Type OxDC

The recombinant Co-containing, wild-type enzyme was obtained following the standard protocol for expressing the Mn-substituted enzyme, except that $CoCl_2$ (Fisher Scientific, Pittsburgh, PA) or various $CoCl_2/MnCl_2$ mixtures were added to the cell culture in place of $MnCl_2$, after the heat shock step but prior to induction of OxDC expression. After cell lysis, and extraction of the recombinant protein from the crude lysate as described above for recombinant wild-type OxDC, the Co-containing enzyme was purified by DEAE column chromatography. Fractions containing OxDC were pooled and dialyzed for 4 h against 50 mM imidazole-HCl

buffer, pH 7.0 (2 L). The resulting sample was then applied to a Q-Sepharose Hi-Performance column (2.5 x 18 cm) column equilibrated with buffer A, and eluted using a 500 mL linear gradient from buffer A to buffer A containing 1 M NaCl. Fractions containing OxDC were pooled and exhaustively dialyzed against 20 mM hexamethylenetetramine hydrochloride, pH 6.0, containing 0.5 M NaCl. The purified, Co-substituted enzyme was concentrated and stored as described for recombinant, wild type OxDC.

Preparation of the OxDC "Apoenzyme" and Reconstitution of the Wild Type, Mn-Containing Enzyme

Recombinant Mn-containing, wild type OxDC was dialyzed against 3.5 M guanidinium hydrochloride (GuHCl), 20 mM Tris-HCl, and 10 mM EDTA, pH 3.1, for 8 h at 4 ^{o}C. A second round of dialysis against 2.5 M GuHCl, 20 mM Tris-HCl, and 10 mM EDTA, pH 7.0, was performed, and excess EDTA removed in a third dialysis against 2.5 M GuHCl containing 20 mM Tris-HCl, pH 7.0. Both of the latter steps were carried out for 8 h at 4 ^{o}C. At this stage, the protein could be re-folded by dialysis against 20 mM hexamethylenetetramine-HCl, pH 6.0, containing 0.5 M NaCl, over 8 h at 4 ^{o}C, to yield a Mn-deficient form of OxDC ("apoenzyme") that exhibited no catalytic activity when incubated with oxalate. Alternatively, a round of dialysis over 8 h, at 4 ^{o}C, against 20 mM Tris-HCl, pH 7.0, containing 10 mM $MnCl_2$ could be used to re-introduce Mn(II) into the enzyme before exhaustive exchange into 20 mM hexamethylenetetramine-HCl, pH 6.0, containing 0.5 M NaCl 4 ^{o}C. The latter re-folding step gave samples of reconstituted OxDC containing Mn.

Metal Content Determination

Two methods were used to prepare samples and blanks for determination of metal content by ICPMS (University of Wisconsin Soil and Plant Analysis Lab). In the first method, approximately 0.2 mM enzyme samples (200 μL of ~10 mg/mL) were made 1 mM

ethylenediaminetetracetic acid (EDTA) and incubated on ice for 15 minutes. Samples were then desalted on a G-25 pasteur pipet column equilibrated with dH_2O. The desalting column had been previously treated with EDTA. 200 μL of storage buffer was put through an identical procedure for use as a blank. In the second method, divalent cations were removed from 20 mM hexamethylenetetramine hydrochloride, pH 6.0 containing 0.5 M sodium chloride by passing through a 1.5 x 16 cm column containing Chelex 100 (Bio-Rad) in the Na^+ form. Purified protein samples were exchanged into the resulting buffer by washing 2.5 mg samples three times with 10-fold volumes of the "scrubbed" buffer in Centricon or Centriprep 30 (Amicon) concentrators (*104*). The final filtrates were recovered and used as blanks, which routinely possessed insignificant metal content. Samples were sent to the University of Wisconsin Soil and Plant Analysis Laboratory for the determination of metal content by ICPMS. Both methods yielded similar results, results reported here are from the second method.

Steady-State Kinetic Assays

Assay mixtures consisted of 50 mM NaOAc, pH 4.2, 0.2% Triton X-100, 0.5 mM *o*-phenylenediamine, 1-50 mM potassium oxalate, and either the wild type OxDC (1-4 μM) or OxDC mutant (80-120 μM) (100 μL total volume). Reactions were initiated by the addition of substrate, incubated at ambient temperature (21-23^o C), and quenched by the addition of 1 N NaOH (10 μL). The amount of formate product was determined by an end-point assay (*98*) consisting of 50 mM potassium phosphate, pH 7.8, 0.09 mM NAD^+, and 0.4-1.0 U/mg of formate dehydrogenase (1 mL final volume). The absorbance at 340 nm was measured after overnight incubation at 37^{o}C, and formate was quantitated by comparison to a standard curve generated by spiking pre-quenched OxDC assay mixtures with known amounts of sodium formate. Measurements were made at specific substrate and enzyme concentrations in duplicate,

and data were analyzed to obtain the specific activity by standard computer-based methods (*115*). The initial rate of formate production is expressed in millimoles per liter per minute.

Gepasi Simulations

The rates used for the reactions for the various simulations (Figure 2-2) have been cut and pasted from the Gepasi output files into Appendix A. The equations used for the simulations are given in Figure 2-3. To ensure that the binding equilibria for the Mn ions are well established before catalysis takes place, the k_1 values for the forward reaction in equations [R1-4] were chosen to be fairly large, i.e., close to the diffusion limit: k_1(R1-R4) = 1 x 10^9 $(sM)^{-1}$, k_2(R1-R4) = 5 $(s)^{-1}$.

$$\begin{aligned}
\mathrm{Mn + apo} &\underset{k_2(R1)}{\overset{k_1(R1)}{\rightleftharpoons}} \mathrm{EMn_A} \\
\mathrm{Mn + apo} &\underset{k_2(R2)}{\overset{k_1(R2)}{\rightleftharpoons}} \mathrm{EMn_B} \\
\mathrm{Mn + EMn_A} &\underset{k_2(R3)}{\overset{k_1(R3)}{\rightleftharpoons}} \mathrm{E} \\
\mathrm{Mn + EMn_B} &\underset{k_2(R4)}{\overset{k_1(R4)}{\rightleftharpoons}} \mathrm{E} \\
\mathrm{E + S} &\underset{k_2(R5)}{\overset{k_1(R5)}{\rightleftharpoons}} \mathrm{ES} \\
\mathrm{ES} &\xrightarrow{k_1(R6)} \mathrm{E + P} \\
\mathrm{EMn_A + S} &\underset{k_2(R7)}{\overset{k_1(R7)}{\rightleftharpoons}} \mathrm{EMn_AS} \\
\mathrm{EMn_B + S} &\underset{k_2(R8)}{\overset{k_1(R8)}{\rightleftharpoons}} \mathrm{EMn_BS} \\
\mathrm{EMn_AS} &\xrightarrow{k_1(R9)} \mathrm{EMn_A + P} \\
\mathrm{EMn_BS} &\xrightarrow{k_1(R10)} \mathrm{EMn_B + P}
\end{aligned}$$

Figure 2-3 Equations used for Gepasi simulations to describe the amount of product formed after 5 s as a function of Mn incorporation.

The rate constants for dissociation were small to ensure good binding. 5 s^{-1} represents a K_D of 5 nM. For low affinity 5,000 s^{-1} was chosen, representing 5 μM affinity with unchanged

k_1. As a result this ended up giving full sites for a complement of Mn ions present. The binding of substrate to enzyme is given by:

$k_1(R5,R7,R8) = 1 \times 10^8 \text{ (s M)}^{-1}$

$k_2(R5,R7,R8) = 8.4 \times 10^5 \text{ (s)}^{-1}$

These values were chosen to give a $K_m = \frac{k_2(R5,R7,R8) + k_1(R6,R9,R10)}{k_1(R5,R7,R8)} = 8.4$ mM

and $k_{cat} = k_1(R6,R9,R10) = 53 \text{ (s)}^{-1}$.

In order to simulate inactive sites, the k_{cat} value was reduced to 5×10^{-6} s^{-1}. For "less active" sites the k_{cat} value was changed to values between 17 and 35 s^{-1}. For "half active" sites the k_{cat} value was chosen to be 26.5 s^{-1}. In case 3 where site 2 was mechanistically required all $k_1(R9,R10) = 5 \times 10^{-6}$ s^{-1} and only $k_1(R6) = 53$ s^{-1}. This resulted in non-linear behavior in all instances due to the fact that only the full enzyme is capable of catalysis.

The linear relationships in Case 4 are due to the fact that each bound Mn participates equally in catalysis. This case is thus insensitive to the affinity of the two sites. To simulate cooperative binding (Case 6) positive feedback was assumed for the binding of the second site. Only site 1 is equally active in both the single Mn as well as the full enzyme. To simulate cooperativity of binding the second site was assumed to have a factor of 100 higher affinity once the first site was filled. To see what happens when only the full enzyme was active, case 7 was created which is otherwise equal to case 6. It shows essentially the same result as case 3 where only the full enzyme was capable of catalysis. In all cases, the starting conditions involved 1 mM apoenzyme concentration, up to 2 mM Mn concentration, and a saturating substrate concentration of 10 M.

Case 1 (site 1 active, site 2 unimportant): In this case only site 1 is active and the presence or absence of site 2 is simply irrelevant. However, as the results show it is not quite so irrelevant if

it is allowed to bind substrate (and thus sequester the enzyme in that state). Thus the "dip" seen in case 1c is artifactual since in reality one would expect the enzyme to also allow substrate to bind in the other site.

Case 1': To avoid the problem with the "dip" in case 1, a lower catalytic rate was assumed for the singly bound Mn, *i.e.*, 26.5 s^{-1} for the single Mn case vs. 53 s^{-1} for the full enzyme. As it turns out the difference in activities between the singly and doubly occupied enzyme starts to "curve" the former straight line predicted for equal affinity of the Mn sites. This is expected since the model introduces some form of cooperativity into the catalytic mechanism.

Case 2 (site 1 most active, site 2 less active): is another modification of case 1, in which the rates were input as 53s^{-1} for the full enzyme, 35 s^{-1} for site 1, and 8 s^{-1} for site 2.

Case 3 (site 1 active, and site 2 required structurally or mechanistically): The quadratic behavior of the case with equal affinity is confirmed and makes sense because the number of fully loaded enzymes is quadratic with the concentration of bound Mn.

Case 4 (site 1 and site 2 have equal activity): Case 4 doesn't show any difference in its kinetics except a small difference in total bound Mn for the different data points, just as expected.

Case 5 (site 2 required for full activity of the enzyme): This case is similar to case 3 but relaxes the necessity of the mechanistic site 2 a bit by allowing for "half activity" of site 1 when site 2 in not occupied.

Case 6 (site 1 is active, binding is cooperative with the affinity for the first Mn being different for the two sites): Case 6 represents cooperative binding of the Mn sites. It is assumed that the subsequent Mn binds with a 100 fold higher affinity than the first one. However, the cases 6b and 6c differ, just like in all other cases treated before, by 3 orders of magnitude in their initial affinity for sites 1 and 2. In other words, when the first affinity is 5 nM the second affinity is

now 50 pM, and when the first affinity is 5 μM the second is now 50 nM. It should be noted that the activity of site 1 was assumed to be 53 s^{-1} for both the fully loaded enzyme as well as for the singly loaded one at site 1.

Case 7: Case 7 is similar to case 6, except that it assumes only the full enzyme containing both Mn to be active.

CHAPTER 3
SPECTROSCOPIC CHARACTERIZATION OF THE TWO MANGANESE CENTERS

Introduction

Electron Paramagnetic Resonance Spectroscopy

Electron paramagnetic resonance is a spectroscopic technique for detecting species containing unpaired electrons, generally organic radicals or transition metal ions with partially filled *d* orbitals. Since an unpaired electron possesses circular motion about its axis (spin angular momentum) and a charge, it has a magnetic moment. An external magnetic field interacts with the magnetic moment of the unpaired electron (Zeeman interaction) and can result in two possible orientations, parallel to the magnetic field or antiparallel to it. The two orientations (states) possess different energies and the difference in energy (Zeeman energy) increases with increases in the magnetic field.

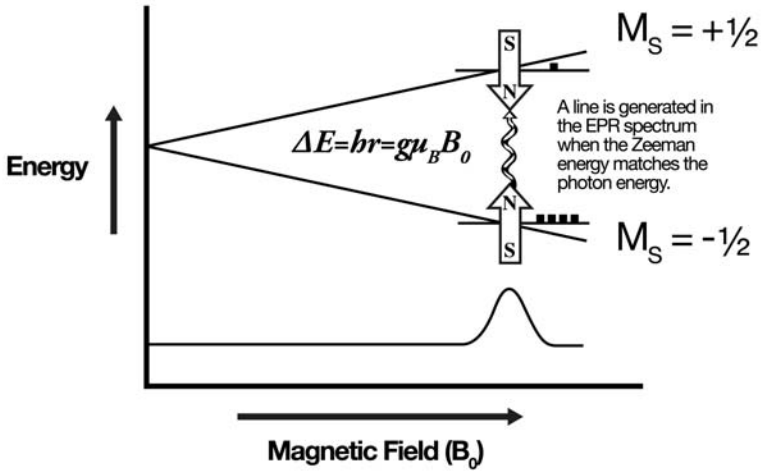

Figure 3-1 Absorption of microwave irradiation by an unpaired electron in a magnetic field. Figure adapted from http://www.bruker-biospin.com/cw.html.

Application of radiation at an appropriate frequency results in a transition between the two states (resonance condition, $\Delta E = h\upsilon = g\mu_B B_o$). In EPR spectroscopy, the sample is irradiated with a fixed frequency microwave energy and the magnetic field is gradually increased. A line is generated in the EPR spectrum when the Zeeman energy matches the photon energy (Figure 3-1) (*116*).

Electronic Configuration of Mn(II)

The shape of the magnetization of Mn(II) in any given coordination environment dictates its EPR properties. This shape is determined by the distribution of unpaired electrons around the Mn nucleus and is related to the types of ligands present and how they are geometrically arranged around the ion. As a free ion in the gaseous phase, Mn^{2+} possesses five 3*d* electrons in a spherical distribution around the nucleus (an S-state ion). Ligand interactions with the *d* electrons in the condensed phases break both the degeneracy of the 3*d* orbitals and their spherical symmetry which influences the EPR properties of Mn^{2+}. The splitting that results from a noncubic environment is known as zero-field splitting (zfs) or fine structure splitting (*117*).

Electron Paramagnetic Resonance Properties of Mn(II)

The characteristic six line EPR spectrum of Mn(II) arises from the interaction (hyperfine coupling) between the unpaired electrons ($S = 5/2$) and the ^{55}Mn nucleus ($I = 5/2$). While this interaction decreases the sensitivity of the EPR measurement by a factor of six, it provides a tool for distinguishing between octahedral and tetrahedral coordination states (*118*). Interactions between electron spin (M_s) and nuclear spin (M_I) result in 36 states and 30 allowed transitions where $\Delta M_s = \pm 1$ and $\Delta M_I = 0$ (five EPR transitions, each split by hyperfine fine coupling to a sextet) (Figure 3-2) (*117*).

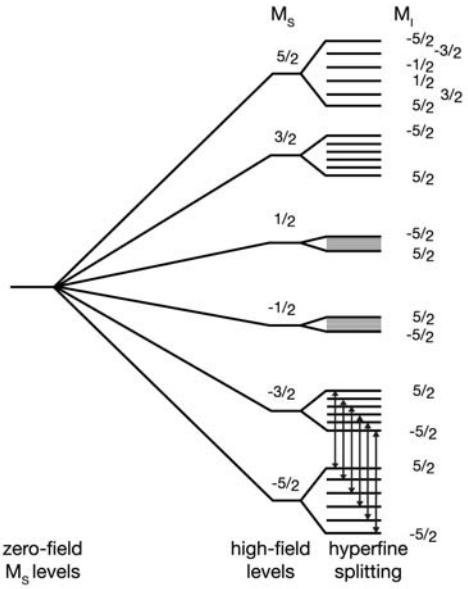

Figure 3-2 Electron spin energy levels and hyperfine splitting for Mn(II) in spherical symmetry. One sextet of the five-fold allowed transitions ($\Delta M_s = 1$, $\Delta M_I = 0$) is indicated by arrows. Figure adapted from (*117*).

The schematic representation in Figure 3-2 depicts the electronic Zeeman and nuclear hyperfine interactions of a hypothetical case in which there is a five-fold degeneracy of the $\Delta M_s = \pm 1$ fine structure transitions. This situation would yield a spectrum of six well resolved EPR signals and is close to what is observed for hexaaquo manganese in solution. For hexaaquo manganese there is, however, some inhomogenous broadening of the EPR lines that is the result of an inexact superpositioning of the five $\Delta M_s = \pm 1$ fine structure transitions (*117, 119*). When Mn(II) is bound in a symmetry lower than cubic, the asymmetry of the ligand field (or crystal field) removes the degeneracy of the electronic spin levels in the absence of an applied magnetic field. This means that the approximate degeneracy of the five $\Delta M_s = \pm 1$ fine structure transitions is lifted resulting in a zero field splitting. The three Kramers doublets (±5/2, ±3/2, ±1/2) possess different energies in the absence of an external magnetic field.

Four magnetic parameters are essential to define a paramagnetic species, these are *g, A, E,* and *D*. The gyromagnetic ratio of an electron, g_e, is the ratio of its magnetic dipole moment to its angular momentum. A free electron has a g value of 2.002319304386 (which is g_e, the electronic g-factor). When an unpaired electron is in an atom, it is affected by not only the external magnetic field, B_o, but also by any local magnetic fields. The effective field, B_{eff}, felt by an electron is described by

$$B_{eff} = \Delta E = h\upsilon = g\mu_B B_o\ (1-\sigma)$$

where σ allows for the effects of the local fields. The resonance condition is, therefore,

$$\Delta E = h\upsilon = g_e\mu_B B_o(1-\sigma)$$

The quantity $g_e(1-\sigma)$ is called the *g*-factor, given by the symbol *g*, so

$$\Delta E = h\upsilon = g\mu_B B_o$$

The *g*-factor (or *g*-value) is determined in an EPR experiment by measuring the field, B_o, and the frequency, υ, at which resonance occurs. If *g* is different than g_e, the ratio of the electron's magnetic moment to its angular momentum has changed from the free electron value. Since the electron's magnetic moment (the Bohr magneton, μ_B) is constant, it must have gained or lost angular momentum (*116*).

As illustrated in Figure 3-2, the hyperfine interaction is the interaction between the magnetic moment of an electron with the magnetic moment of the nucleus. The electron-nuclear interaction, depends on the projections of both electron and nuclear spins:

$$E_{electron\text{-}nuclear} = A\ M_I\ M_s$$

where *A* is the hyperfine coupling constant. *A* depends not only on the g-values for the electron and the nucleus but also on the distance between them and their orientation with respect to the external field.

The fine structure parameters *D* and *E*, reflect the deviation of the ligand field from spherical and axial symmetry, respectively. *D*- and *E*- strain reflect the inhomogeniety of these values and depend on the metal-ligand distances and bond angles (*117*).

Oxalate Decarboxylase EPR

Since the two Mn(II) ions in the resting monomer are in very similar coordination (Figures 1-4 and 3-3) environments, spectroscopic efforts to establish whether catalysis takes place in only one or both of the two metal sites have been significantly complicated. In previous X-band studies, it has been shown that addition of small molecules like formate and oxalate have small but reproducible effects on the Mn(II) EPR spectra indicating the possibility of using EPR as a sensitive probe of the ligand environment (74). Distinguishing which metal signal(s) was perturbed, however, is difficult in X-band because the signals are very broad.3.

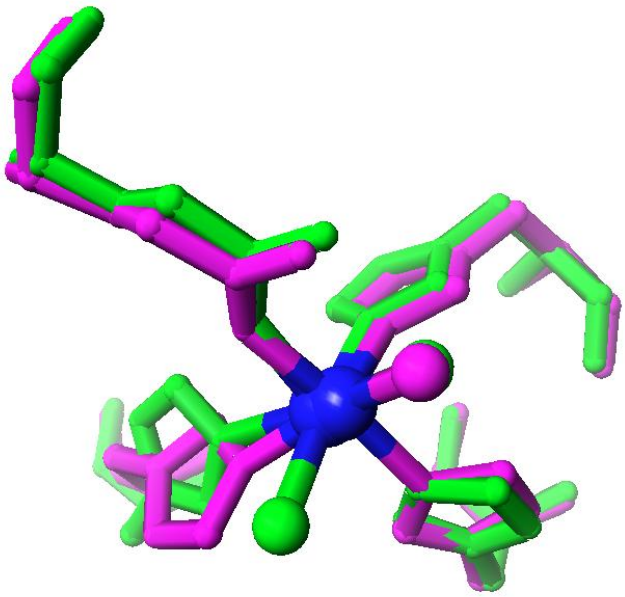

Figure 3-3 Overlay of the N-terminal (shown in magenta) and C-terminal (shown in green) manganese-coordinating ligands (PDB code: 1UW8) . The manganese ion is shown in blue. This image was prepared using the CAChe Worksystem Pro V6.5 software package (Fujitsu America Inc., Beaverton, OR).

A multifrequency EPR approach has been employed to address the question of whether it is possible to distinguish the two Mn ions in OxDC spectroscopically. Specifically this set of experiments was designed to (i) distinguish the two Mn(II) sites and to (ii) determine their respective magnetic parameters. The rationale of using this approach is based on the fact that Mn(II) linewidths generally become narrower at higher fields (and thus higher frequencies) allowing for better spectral resolution of small differences in g and A. Effects associated with differing fine structure parameters, however, are more prominent at low and intermediate fields (frequencies).

Results and Discussion

To avoid complications arising from the binding of ligands other than water to the two free ligand positions on each Mn, initial experiments used OxDC dissolved in 20 mM hexamethylenetetramine (HMTA) HCl buffer at pH6.0, 0.5 M NaCl (storage buffer). HMTA is not expected to bind to Mn(II) because it is positively charged and too bulky to fit into the Mn-binding pockets in the protein. OxDC has maximum activity at a pH value of around 4.0 and it is common practice in the literature to use various types of negatively charged buffer molecules to control pH for spectroscopic and kinetic analysis (*57, 72-74*). It was of interest, therefore, to investigate the effect of acetate buffer at pH 5.2 on the EPR spectra. At this pH value the enzyme possesses substantial activity but is also highly soluble.

X-band EPR

The X-band EPR spectrum of OxDC (Figure 3-4) at low temperature is distributed over a wide field range with a clearly discernable but weak group of lines at half-field indicating substantial fine-structure in the Mn(II) S=5/2 ions (71, 74) .

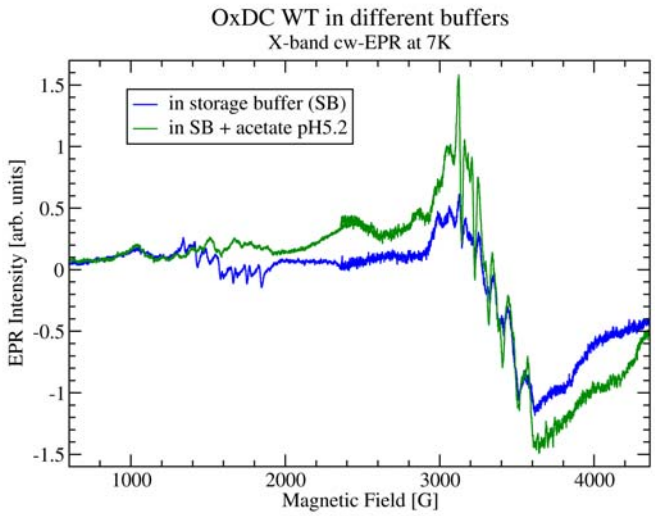

Figure 3-4 X-band cw-EPR spectra of wild type OxDC in storage buffer and in acetate buffer.

Figure 3-4 shows that there may be a mixture of Mn(II) species with similar g-(2.001) and A-(250 MHz) values but with different zero-field splitting constants D. When D is small compared to ν, the EPR signals are mostly around g ≈ 2. However, for large D, the signal is spread over a broad field range with only parts staying near g ≈ 2.

Field Dependence of the EPR Signal in Storage Buffer

Figure 3-5 shows the $g \approx 2$ region of the EPR spectra of OxDC in HMTA buffer pH 6.0 at frequencies ranging from X-band (corresponding to 0.34 T) to the sub-mm band (15 T). In Figure 3-5 the effect of increasing field on the central $+½ \rightarrow -½$ sextet of lines is clearly visible. They are substantially broadened at low frequencies due to higher order contributions of the zero-field splitting (zfs) (*117*), but broadening is reduced as the sample is moved toward its high-field limit. No broadening or field-dependent (*g*) or -independent (*A*) splitting of the central lines was observed up to 15 T where the linewidth is at its narrowest. This indicates that *g* and *A* are in fact very similar for the C- and N-terminal Mn(II) ions.

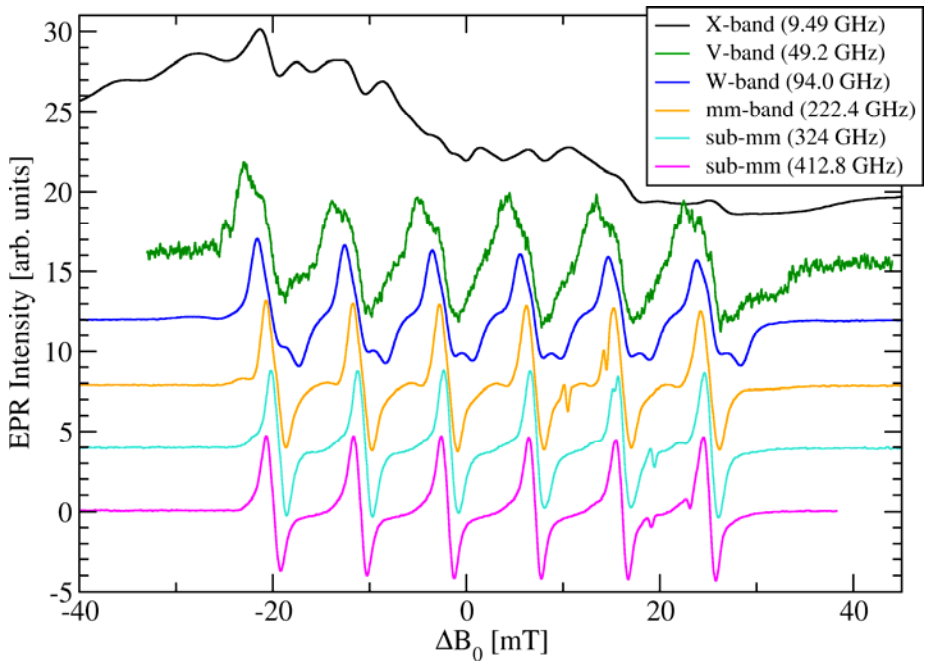

Figure 3-5 Field dependence of the EPR spectra of OxDC in storage buffer (20 mM Hexamethylenetetramine HCl, pH 6.0) with 0.5 M NaCl. To facilitate comparison of the +½ ↔–½ transitions spectra are shifted along the B0-axis. Field positions in T at the zero-points: 0.3340 (X-band, 9.4873 GHz), 1.7490 (V-band, 49.200 GHz), 3.3545 (W-band, 94.0214 GHz), 7.9427 (222.40 GHz), 11.567 (324.00 GHz), and 14.730 (412.80 GHz). All spectra were taken at temperatures between 5 and 20 K. Reprinted from (120) with permission.

Spectral Simulations and Magnetic Parameters

Spectral simulations were performed with the "easyspin" toolbox for Matlab (*121*) by Ines Garcia-Rubio and are shown along with the experimental settings in Appendix B. The main sextet lines could be simulated considering a Mn(II) center with zfs parameters D = 1200 MHz and E = 283 MHz (site I in table 3-1). However, this did not account for the weaker shoulders on the high- and low-field sides of the sextet lines and a second Mn(II) species was considered (site II in Table 3-1). Figure 3-6A shows the simulation together with the experimental W-band spectrum of OxDC in HMTA buffer. Note that both sites are present in the same proportion and site II has a considerably higher D-value (2700 MHz). This explains why its signal intensity is spread out over a broad field range and is seen only in the form of relatively weak shoulders on the narrow and intense lines of the site I signals, even at high frequencies. For this reason the

multi-frequency approach was crucial to detect, identify, and characterize the signals from the Mn(II) ion in site II.

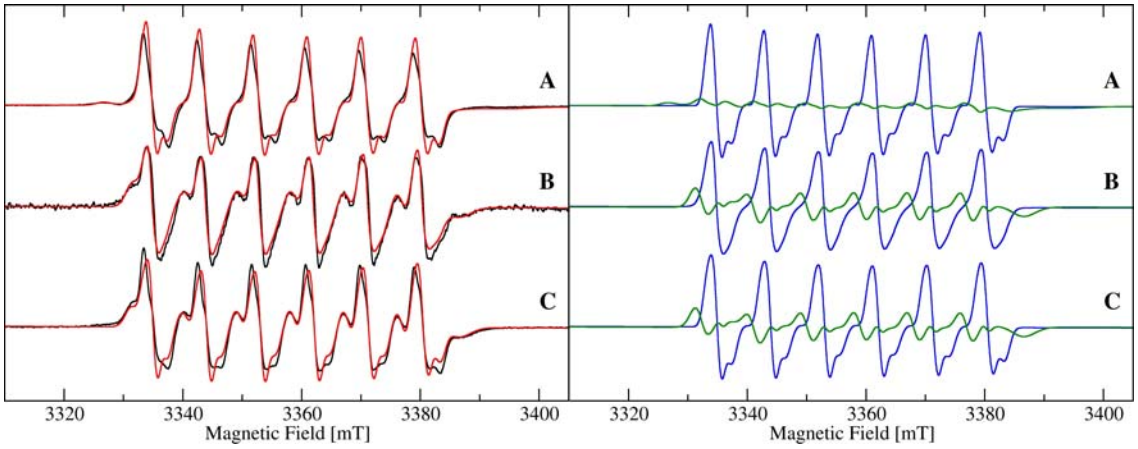

Figure 3-6 W-Band (94 GHz) EPR spectra of OxDC. A) HMTA buffer pH6.0. B) Acetate buffer pH5.2. C) HMTA buffer pH6.0 and 50 mM formate. The right panel shows the simulation of site I (blue) and site II (green) with the magnetic parameters given in Table 3-1. The left panel shows the experimental spectra (black) and the sum of the simulations of the two sites in the same proportion. Reprinted from (*120*) with permission.

Table 3-1 Magnetic parameters of OxDC species I and II. Modified from (*120*) with permission.

	g	A *[MHz]*	D *[MHz]*	E/D	*D- and E-Strain*
SB, site I	2.00087	253±2	1200 ± 50	0.23 ± 0.02	24% 24%
SB, site II	2.00094	250±3	2700 ± 50	0.25 ± 0.02	20% 20%
AB, site I	2.00086	252±2	1200 ± 50	0.23 ± 0.02	40% 40%
AB, site II	2.00086	250±3	2150 ± 50	0.05 ± 0.02	33% 60%
SB + formate, I	2.00087	253±2	1200 ± 50	0.23 ± 0.02	24% 24%
SB + formate, II	2.00086	250±3	2150 ± 50	0.05 ± 0.02	33% 60%

The best simulations required substantial D- and E-strain (20-24%) which is not uncommon for transition metal ions in proteins and in particular for Mn(II) (*117*). The E/D ratio was found to be approximately 25%, indicating considerable rhombicity of the distorted octahedral coordination environment of both Mn(II) ions.

Field Dependence of the EPR Signal in Acetate Buffer, pH 5.2

The spectra recorded at various frequencies from X-band to 420 GHz are shown in Figure 3-7. At high fields the wings that are characteristic for the fine structure are strongly suppressed compared to the main 6-line transitions. Therefore, the change in D upon acetate binding is less visible. The differences between this and the previous set of spectra are small and are most obvious in the intermediate to high frequency ranges (W-band and up). They mainly involve the shoulders associated with site II.

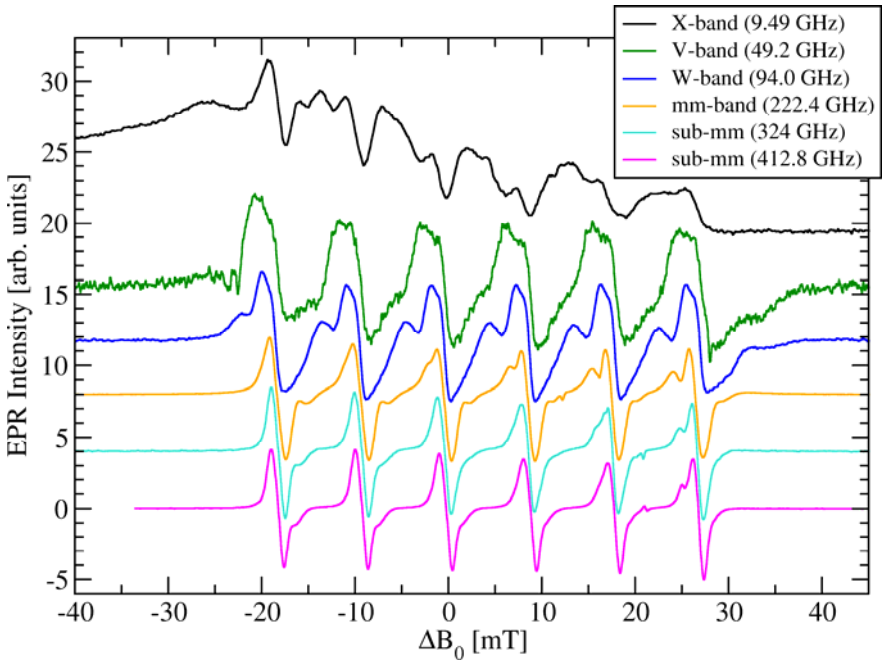

Figure 3-7 Field dependence of the EPR spectra of OxDC in acetate buffer (50 mM, pH 5.2) with 0.5 M NaCl. The spectra were shifted along the B_0-axis. Field positions in T at the zero-points: 0.3339 (X-band, 9.4853 GHz), 1.7470 (V-band, 49.200 GHz), 3.353 (W-band, 94.0206 GHz), 7.9415 (222.40 GHz), 11.563 (324.00 GHz), and 14.7253 (412.80 GHz). Temperatures were set between 5 K and 20 K. Reprinted from (*120*) with permission.

Figure 3-6B shows the experimental W-band signal of OxDC in acetate buffer pH5.2 with its simulation. The changes in the features of site II are mainly due to a decrease of *D* and *E* from 2700 to 2150 MHz, and 675 to 108 MHz, respectively as well as a small decrease in *g* (see

Table 3-1). The magnetic parameters of site I were unchanged except for an increase in zfs parameter strain which was also seen for site II. Note that the rather dramatic change in *E* indicates a more axial ligand field environment for site II in the presence of acetate.

The zfs parameters of Mn(II) have been demonstrated to be sensitive to electrostatic charges in their vicinity (*122*). The replacement of one or two water molecules in the coordination sphere of Mn by acetate is certainly expected to change the electrostatic potential around the Mn-center and could lead to the observed changes in *D* and *E*. The observation that only site II changes upon exposure to acetate buffer suggests that only site II is solvent-accessible. When formate is added to OxDC in HMTA buffer the spectral changes observed for site II are very similar to those found for acetate (see Figure 3-2C). This is not surprising given that formate and acetate are alike in the polar parts of their structure and are expected to show the same coordination geometries with the metal ion.

The simplest interpretation of these results points to a correlation between the two magnetic parameter sets and the two Mn-binding sites in the protein. The differences in the fine structure are due to subtle differences in the charge distribution in the N- and C-terminal binding sites while the almost identical *g* and *A* is due to similar octahedral coordination in both sites. The fact that both species are present in approximately the same concentration in all preparations investigated so far supports this interpretation.

The observation of changes in the fine structure parameters of only site II upon addition of acetate buffer or formate is intriguing and suggests that small molecule binding mainly takes place at site II and not site I under our experimental conditions. Just et al. (*73*) observed a channel leading from the N-terminal Mn binding site to the solvent which may be accessible by the hinge-motion of a flexible loop region while they report no obvious solvent channel available

for the C-terminal site. Moreover, formate was found coordinated to the N-terminal Mn(II) in the X-ray structure by Anand et al. (*72*). Therefore, it seems reasonable to identify site II with the N-terminal Mn-binding site, and site I with the C-terminal site.

The open and closed conformations (*72, 73*) of OxDC show the C-terminal Mn-binding site in hexa- and penta-coordinated forms, respectively. It is worth noting that *D*-values for penta-coordinated Mn(II) centers in MnSOD have been reported as one order of magnitude higher than what we found for site I (*123*). Therefore, our site I magnetic parameters are compatible with the hexa-coordinated Mn(II) ion in the C-terminal Mn site that is observed in the X-ray structure of OxDC published by Anand et al. (*72*).

A multi-frequency EPR approach has allowed us to spectroscopically distinguish two Mn(II) species that are present in equal proportions in the resting state of the enzyme oxalate decarboxylase in HMTA storage buffer. The main difference between these two species is the value of the fine structure parameters with $D_{\mathrm{I}} = 1200$ MHz, $D_{\mathrm{II}} = 2700$ MHz, and $E/D = 0.25$. When the enzyme is placed in acetate buffer pH5.2 or when formate is added, D_{II} is reduced to 2150 MHz and $E_{\mathrm{II}}/D_{\mathrm{II}} = 0.05$ while D_{I} and E_{I} remain the same indicating that only one Mn(II) is solvent accessible. Based on published crystal structure data, we conclude site I is the C-terminal Mn site while site II is the solvent-exposed N-terminal site and, therefore, the site of small molecule (acetate and formate) binding.

Experimental Section

Oxalate Decarboxylase Sample Preparation

Several different batches of OxDC enzyme preparations were used. They were prepared according to the procedures listed in Chapter 2. Final concentrations ranged from 7.7 to 12.3 mg/mL. Samples in HMTA pH6.0 were used without further modifications. Samples in 50mM acetate buffer (AB) pH5.2 were prepared from stock by addition of a concentrated acetate buffer

solution (500 mM, pH5.2). Typically, 90 μL of sample were mixed with 10 μL of concentrated AB buffer. The volumes were scaled in the same ratio for experiments requiring smaller (W-band) or larger quantities (sub-mm bands). The same procedure was used for the addition of formate to the HMTA buffered samples. 10 μL of 500 mM formate solution was added to 90 μL of HMTA pH6.0 buffered sample to arrive at a final concentration of 50 mM formate.

Electron Paramagnetic Resonance Spectroscopy

X-band spectra (9.5 GHz) were recorded on an Elexsys E580 spectrometer (Bruker Biospin Corp.) and the OxDC samples were placed in 3 x 4 mm2 (IDxOD) homemade clear fused quartz tubes and frozen in liquid nitrogen before insertion into the Oxford ESR900 cryostat which had been pre-cooled to ~10 K.

W-band (94 GHz) spectra were recorded on an Elexsys E680 spectrometer (Bruker Biospin Corp.) and the samples were placed into 0.7 x 0.79 mm^2 (IDxOD) clear fused quartz capillaries. The samples were then frozen in liquid nitrogen prior to insertion into the precooled Bruker ER4118CF-W cryostat.

V-band and sub-mm bands (50, 200-420 GHz) spectra were recorded with a home built instrument using a 15/17 T superconducting magnet as described by Hassan et al. (*124*). Samples were placed into 7.2 x 8.2 mm2 (IDxOD) home-made Teflon cups. The cups have a depth of 9.5 mm and were supplied with a Teflon stopper. Typically, 200 μL of sample was inserted into the cup which was then closed with the stopper to protect the sample from contamination. The sample was pre-frozen in liquid nitrogen, the field standard (P-doped Si sample) was then placed on top of the stopper before it was inserted into the sample holder. The sample holder was also pre-cooled to liquid nitrogen temperatures before it was inserted into the pre-cooled Oxford Spectrostat CF DY LT cryostat.

Experimental settings and simulations are givens in Appendix

CHAPTER 4
SPECTROSCOPIC CHANGES OF THE MANGANESE CENTERS IN THE PRESENCE OF SUBSTRATE

Introduction

Previous EPR spectroscopic characterization of the Mn centers in oxalate decarboxylase by workers in this laboratory identified a tyrosyl radical formed during oxalate turnover (*71*). Formation of this species requires OxDC, oxalate, and oxygen. The time course of radical formation and decay compared to the overall rate of enzyme turnover suggested that radical formation may be related to catalysis but is not on the catalytic pathway. Furthermore, no spectroscopic signature for Mn(III) or Mn(IV) was observed in samples frozen during catalytic turnover (*71*). X-band EPR spectral perturbations of the Mn centers have been observed upon oxalate addition indicating that EPR spectroscopic characterization of the manganese centers in the presence of substrate may yield insights into the mechanistic role that they play during catalysis (*74*). Since, as noted in Chapter 3, the effects of differing fine structure parameters are more prominent at low and intermediate fields and the fact that linewidths generally become narrower at higher fields allowing for better spectral resolution of small differences in g and A, multifrequency EPR characterization is a rational approach for characterizing the manganese centers in the presence of substrate. The scientific aim of the experiments described in this chapter is to follow the decarboxylation reaction of OxDC by monitoring both the Mn as well as the formation of any intermediate radicals as the reaction progresses. It is anticipated that experiments of this type will be essential to establishing the redox state of the active Mn site before, during, and after catalysis.

Results and Discussion

X-band (9.5 GHz)

Figure 4-1 shows spectral changes at X-band of the g ≈ 2 signal upon addition of acetate and oxalate to OxDC. The spectrum in storage buffer (HMTA, pH 6.0, 0.5 M NaCl) is shown in black. The sample is made 50 mM sodium acetate, pH 5.2 in order to decrease the pH to a level where OxDC is active yet still soluble enough to maintain the high protein concentration required (~10 mg/mL) to obtain high quality spectra.

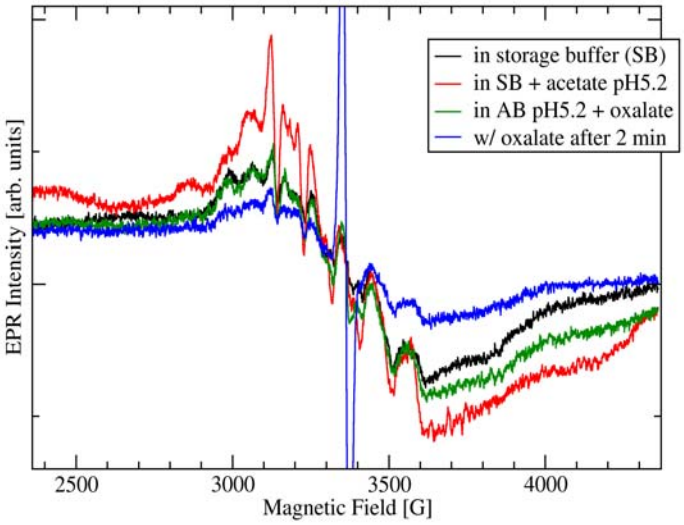

Figure 4-1 Spectral changes of the g ≈ 2 signal at X-band upon addition of acetate and oxalate to OxDC.

The intensity of the signal increases upon acetate addition (shown in red). The spectral intensity decreases to its original value when oxalate is added to 50 mM in acetate buffer pH 5.2 (shown in green) and flash frozen in liquid nitrogen. To detect the spectrum of the tyrosyl radical, the sample is thawed and allowed to react for 2 min, then freeze-quenched and re-inserted into the EPR cryostat (shown in blue). Formation of the tyrosyl radical is accompanied by a further decrease in spectral intensity.

To further explore the changes in spectral intensity during radical formation buffers other than acetate were used to lower the pH of the storage buffer. Buffers used were sodium citrate, pH 5.2, PIPES [piperazine-1,4-bis(2-ethanesulfonic acid)], pH 5.2, as well as the storage buffer adjusted to pH 5.2 (Figure 4-2). All tested buffers gave essentially the same spectra indicating that the effect of the change of the intensity during and after radical formation was not buffer dependent.

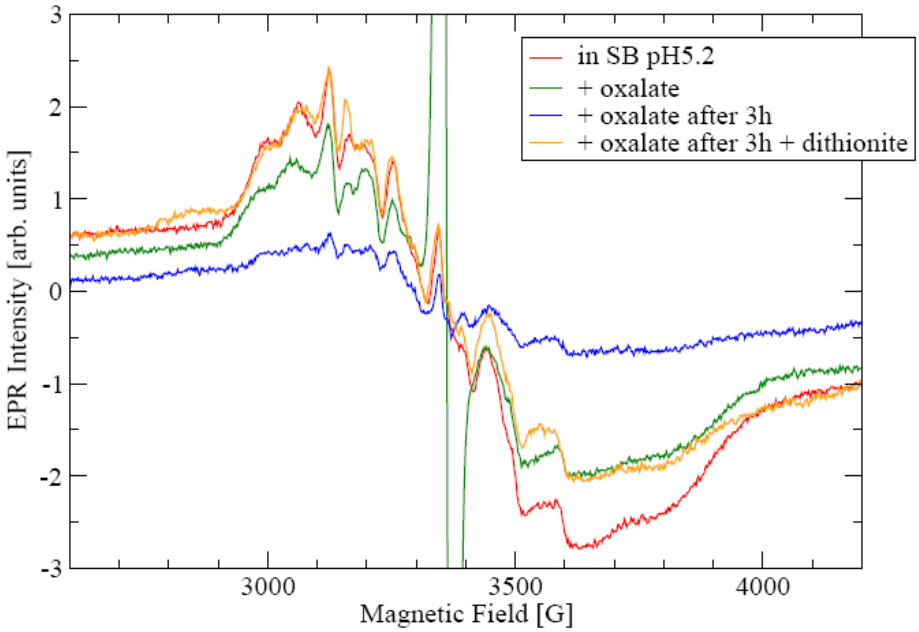

Figure 4-2 Spectral changes of the g ≈ 2 signal at X-band upon addition of oxalate to OxDC in storage buffer at pH 5.2.

Figure 4-2 shows the spectral changes of the g ≈ 2 signal at X-band upon addition oxalate to OxDC in storage buffer at pH 5.2. Upon making the sample 50 mM oxalate and flash freezing 2 minutes after mixing, the tyrosyl radical is observed (shown in green) as well as minor spectral changes and a reduction in the spectral intensity. After spectral acquisition the sample was thawed and stored on ice for 3 hours before being measured again (shown in blue). At this point the Mn(II) signal as well as the radical signal was almost gone. Upon making the sample 5 mM

dithionite almost all of the signal intensity was restored although spectral changes were observed, primarily in the wings of the sextet.

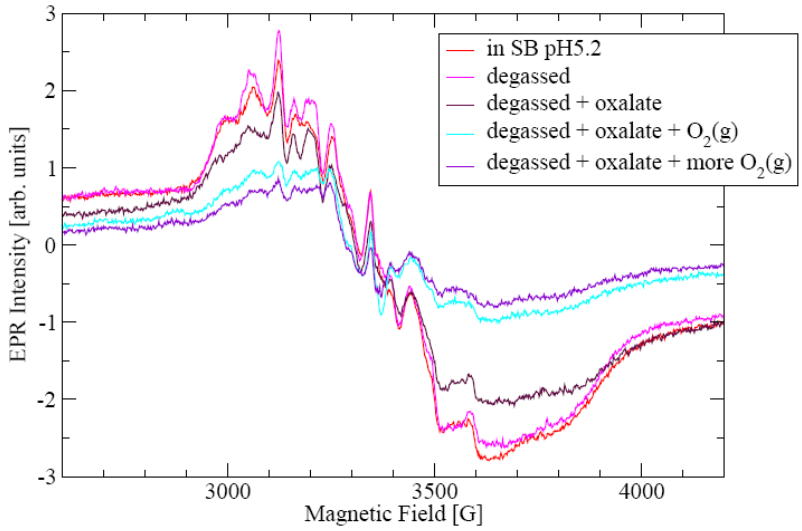

Figure 4-3 Spectral changes of the g ≈ 2 signal at X-band upon addition of oxalate to OxDC in storage buffer at pH 5.2 under anaerobic conditions followed by the reintroduction of air.

With respect to the half-field X-band signal (see Figure 3-1), oxalate almost completely destroys its multiplet pattern (data not shown) and leaves only a broad signal at 1560 G. Addition of dithionite does not rescue the low-field multiplet spectrum. The disappearance of the Mn(II) intensity and its almost complete restoration with dithionite is strong but indirect evidence for the formation of Mn(III) or Mn(IV). When, however, X-band spectra were taken of these identical series of experiments using a parallel mode cavity (data not shown), no spectroscopic signature of Mn(III) was observed. The parallel polarization experiments, however, do not preclude the possibility of the formation of long-lived, high-valent manganese species. It is conceivable that any high-valent manganese species might possess such large zero-

field splitting parameters that the anticipated signal in parallel mode would be unobservable at X-band or simply broadened beyond detection.

Figure 4-3 shows spectral changes of the $g \approx 2$ signal at X-band upon addition of oxalate to OxDC in storage buffer at pH 5.2 under anaerobic conditions followed by the reintroduction of air. Very little spectral changes are observed when OxDC in storage buffer at pH 5.2 (shown in red) is made anaerobic by gently bubbling the EPR tube containing the sample with $N_2(g)$ for 4 minutes inside a glove box (shown in pink). Addition of degassed oxalate decreases the Mn(II) signal dramatically (shown in brown) as in the case when oxygen is present (Figure 4-2), but no radical signal is observed. When the sample was thawed and air was allowed to enter the EPR tube, the Mn(II) signal intensity decreased further and surprisingly no radical was formed (Figure 4-2, shown in turquoise). Finally, when air was bubbled through the sample the Mn(II) signal only decreased slightly (shown in purple) and there was still no radical formation. This sample was then assayed for decarboxylase activity and remarkably showed an increase in specific activity from 51 U/mg to 88 U/mg. It was later confirmed that samples which have been made anaerobic then had oxygen reintroduced possessed an increase in specific activity of at least 50%.

Chemical Oxidation of OxDC Observed at X-band

The addition of potassium ferricyanide to 50 mM (or hydrogen peroxide to 3%) to OxDC did not have any appreciable effect on the Mn(II) signal (data not shown). The intensity of the Mn(II) signals could be decreased, however, by the addition of the strong oxidizing agents potassium hexachloroiridate (data not shown) and sodium (meta) periodate (Figure 4-4). In these experiments, a series of additions were made to the enzyme in storage buffer. At each concentration of oxidant an X-band spectrum was taken at 7 K. The decrease in signal intensity was small up to 2 mM of either of the oxidants used. Both of the oxidants showed a marked

decrease in signal intensity at about 4 mM with a concomitant appearance of a carbon-based radical. The linewidth of the radical signal is consistent with the previously described tyrosyl radical (*71*). The Mn(II) could be brought back with the addition of 5 mM dithionite (Figure 4-4). While it is difficult to interpret these intriguing observations with respect to the redox forms of the enzyme before, during, and after catalysis, these results indicate that molecules are able to enter into the Mn-binding sites facilitating future efforts to measure the reduction potentials of the two sites.

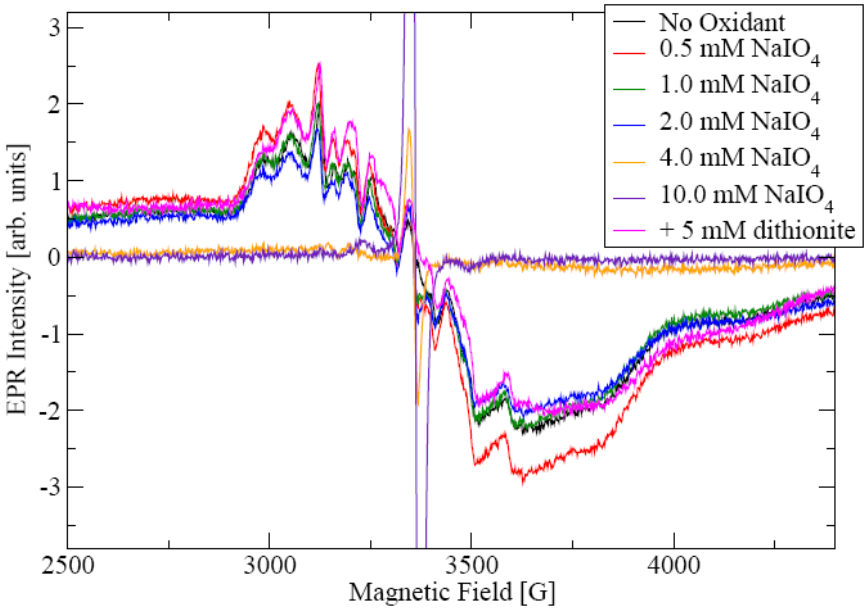

Figure 4-4 Mn(II) signal intensity and carbon-based radical formation as a function of the concentration of sodium (meta) periodate.

X-band Spin-Trapping of an Oxygen Species Formed During Oxalate Decarboxylase Turnover

In the spin-trapping technique, a diamagnetic spin-trap (EPR silent) compound reacts with reactive short-lived free radicals to form a more persistent spin adduct. From the EPR spectrum of the spin adduct, the structure of the reactive free radical can be deduced indirectly. The spin trapping experiments described here showed that this technique can be used to detect radical

species formed during OxDC turnover. These experiments employed the most commonly used nitrone spin trap 5,5-Dimethyl-1-pyrroline N-oxide (DMPO). The spectral shape of the EPR signal of the trapped radical shown in the time course (Figure 4-5) suggests that it may be a hydroxyl radical (*125, 126*), but this should be confirmed by analyzing the trapped product by mass spectroscopy.

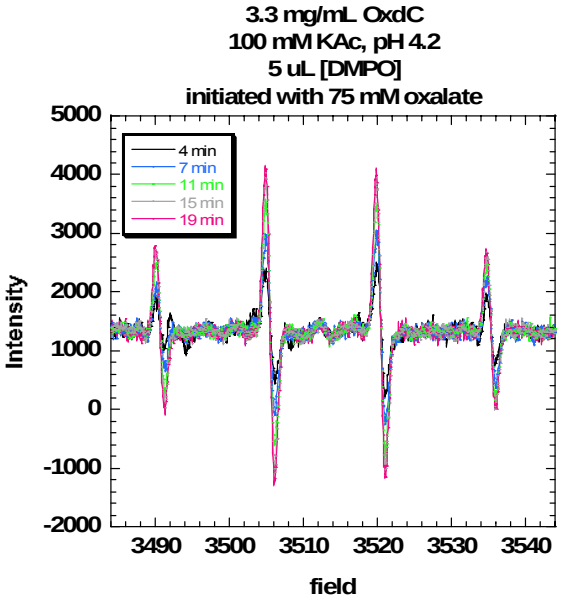

Figure 4-5 EPR spectra of the spin-trapped radical formed during OxDC turnover. The following blanks showed no significant signal: buffer + DMPO, buffer + DMPO + oxalate, and OxDC + buffer + DMPO.

One problem with the use of DMPO as a spin-trapping agent is that a DMPO-superoxide adduct has a half-life on the order of 1-2 minutes (*125, 126*) before decaying to the DMPO-hydroxide adduct. Since the hypothetical mechanism shown in Chapter 1 (Figure 1-5) proposes the formation of a manganese-bound superoxide radical, it was of interest to look at an earlier time point than those shown in Figure 4-5. A 2.5 minute time point is shown in Figure 4-6 and shows the appearance of a different signal that then decays to that shown in Figure 4-5 raising the possibility that it represents a DMPO-superoxide adduct. This should be explored further

using a spin trap with a longer-lived superoxide adduct species such as 2-ethoxycarbonyl-2-methyl-3,4-dihydro-2H-pyrrole-1-oxide (EMPO) or 5-diethoxyphosphoryl-5-methyl-1-pyrroline N-oxide (DEPMPO) (*127*).

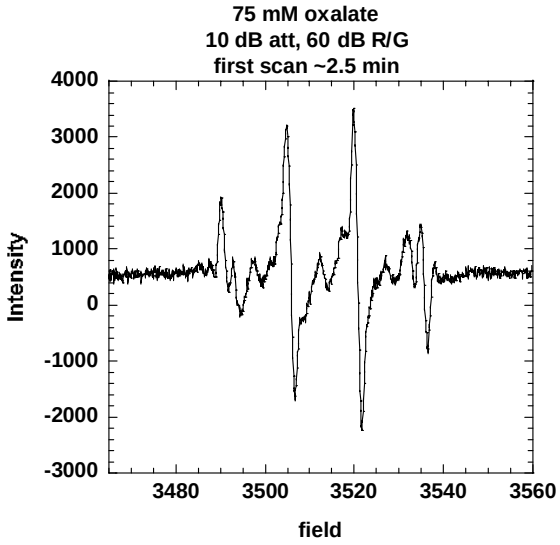

Figure 4-6 EPR spectrum of a short-lived DMPO-oxygen species.

Q-band (3Hz)

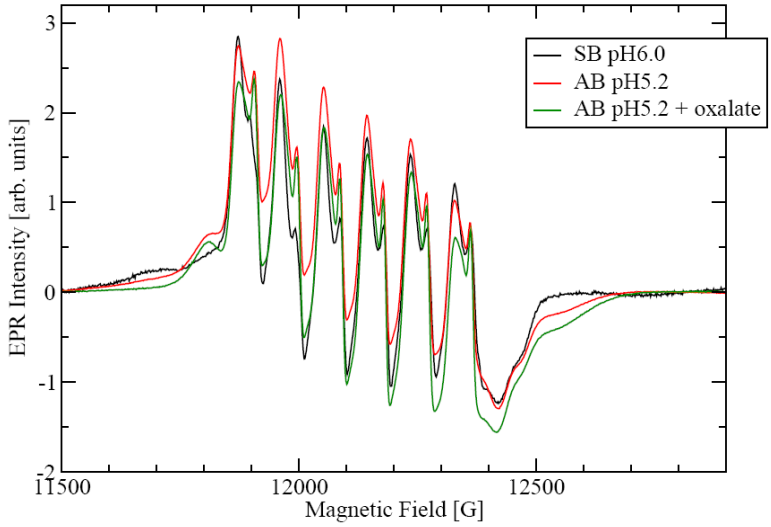

Figure 4-7 Spectral changes of the Mn(II) signal at Q-band upon addition of acetate and oxalate to OxDC.

Q-band EPR (Figure 4-7) was able to reveal the low- and high field- wings that belong to the higher spin manifolds (transitions outside the central +½ → –½ sextet of lines) at least for one of the Mn(II) species. The sample in storage buffer showed a true half field signal (data not shown) which becomes weaker when the sample is made pH 5.2 with the addition of acetate buffer.

W-band (94 GHz)

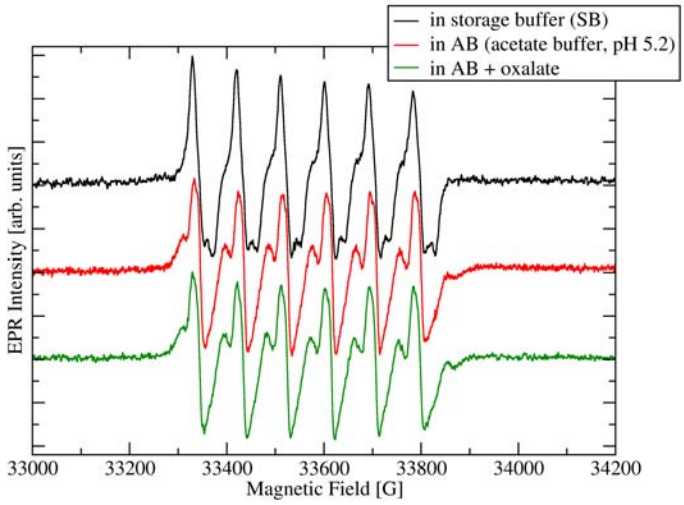

Figure 4-8 Spectral changes of the Mn(II) signal at W-band upon addition of acetate and oxalate to OxDC.

Just as in X-band, the wild-type enzyme shows an effect of acetate binding on its six line Mn(II) signal in W-band g ≈ 2 region (Figure 4-8). At this higher frequency, where there are no contributions from zero field splitting, there is no half field signal and all the signal is found at the g ≈ 2 region. The spectra taken in storage buffer (shown in black) display a clear spliiting in their negative troughs which is absent in those taken in acetate buffer, pH 5.2. There is very little difference in the spectra taken in acetate buffer with (shown in green) and without oxalate, which is in strong contrast with what is observed at X-band. No radical is observed at W-band.

324 GHz

Figure 4-9 shows the very clean 324 GHz spectrum of OxDC in storage buffer (black). In this spectrum only a single species is visible (note the two lines of the phosphorus doped silicon field standard in the 5th line and between the 5th and 6th lines). Addition of acetate (red) leads to a broadening of the sextet lines especially in the higher field portions with a clear splitting of the weaker component. The lines narrow again with the addition of substrate (green).

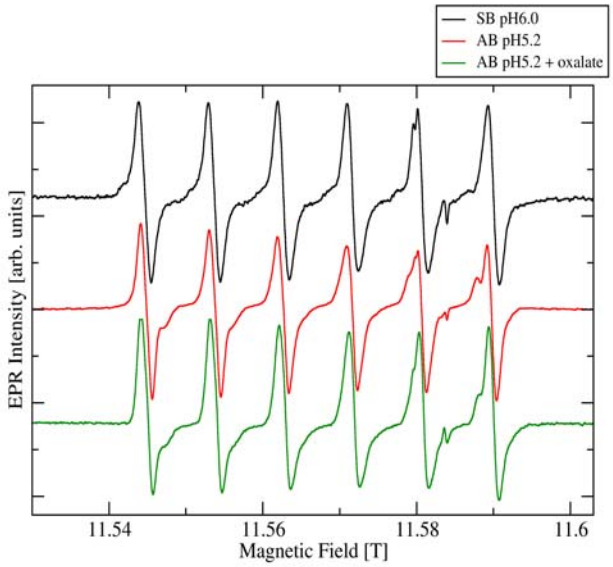

Figure 4-9 Spectral changes of the Mn(II) signal at 324 GHz upon addition of acetate and oxalate to OxDC.

690 GHz

The spectra shown in Figure 4-10 were acquired at the highest field available, 690 GHz. The larger linewidth of all the spectra displayed may be due to the fact that the Keck magnet (Bitter type magnet) is less homogeneous or this may be the first indication of an effect of *g*-anisotropy. The two Mn(II) species are indistinguishable from each other in the spectrum taken in storage buffer (shown in black). Addition of acetate buffer broadens the six lines and begins to split the lower field lines (shown in red). The spectrum taken after the addition of substrate

(shown in green) splits approximately 50 % of its signal intensity off into additional sextet signals. The observed spectrum is consistent with the hypothesis that only one Mn-binding site is available for substrate binding. This experiment clearly demonstrates that substrate binding to Mn(II) can be followed spectroscopically by very high field EPR.

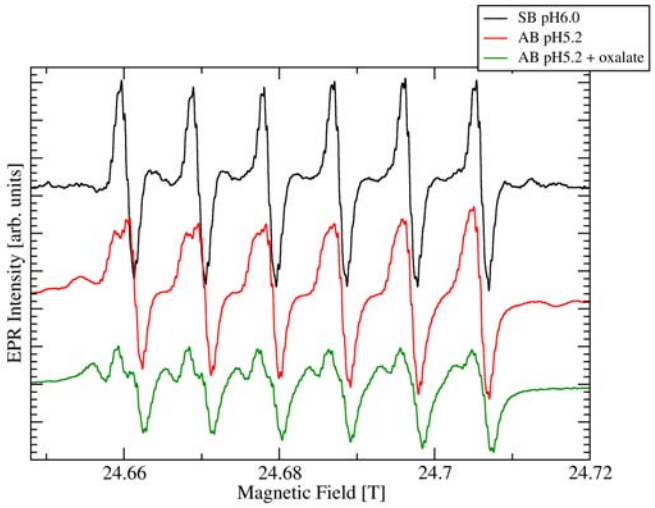

Figure 4-10 Spectral changes of the Mn(II) signal at 690 GHz upon addition of acetate and oxalate to OxDC.

Experimental Section

OxDC was purified as described in Chapter 2.

Sample preparation and EPR spectroscopy was as described in Chapter 3.

X-band spectra: microwave frequency 9.48731 GHz, microwave power 0.64 mW, modulation frequency 100 kHz, modulation amplitude 10 G, receiver gain 60 dB, time constant 41 ms, conversion time 41 ms, 1 sweep, 1.465 G/data point.

Q-band spectra: microwave frequency 34.05197 GHz, microwave power 17 μW, modulation frequency 100 kHz, modulation amplitude 10 G, receiver gain 60 dB, time constant 10 ms, conversion time 41 ms, 1 sweep, 1.953 G/data point.

W-band spectra: Microwave frequency 94.02141 GHz, microwave power 0.6 μW, modulation frequency 100 kHz, modulation amplitude 2 G, receiver gain 40 dB, time constant 82 ms, conversion time 82 ms, 1 sweep, 1.172 G/data point.

324 GHz spectra: Microwave frequency 324.00 GHz, modulation frequency 41.8 kHz, modulation amplitude 0.5 G, lock-in sensitivity 50 μV, time constant 100 ms, sweep speed 5.01 G/s, 1 sweep, 0.367 G/data point.

CHAPTER 5
SITE-DIRECTED MUTAGENESIS STUDIES TO PROBE WHICH MANGANESE-BINDING SITE(S) IS INVOLVED IN CATALYSIS

Introduction

The fact that the OxDC contains Mn in both the N- and C-terminal cupin domains raises the question of whether catalysis takes place in only one or both of the two Mn-binding sites. Multifrequency EPR studies (Chapter 3) suggest that only one Mn-binding site binds acetate and formate. Two structural observations can be cited as support for the hypothesis that the active site of the enzyme is located in the N-terminal domain. First, this domain appears to contain a channel along which oxalate can diffuse from solution, which can exist in an "open" or "closed" form as a result of the conformational rearrangement of residues 161-165 (*73*). Second, formate has been observed to coordinate the N-terminal Mn ion in one of the OxDC crystal structures (*72*). Site-directed mutagenesis studies of conserved arginine (Arg-92 and Arg-270) and glutamate (Glu-162 and Glu-333) residues in the two Mn-binding sites (Figure 1-4) have, however, provided conflicting evidence for which of the two domains might mediate catalysis (*72*, *73*). Interpretation of these studies is complicated by the presence of polyhistidine purification tags in the recombinant OxDC mutant enzymes, and/or a lack of quantitative information on their Mn content (*37*, *73*). Resolving the location of the active site(s) in OxDC is an important problem because if only a single site mediates the OxDC-catalyzed reaction, legitimate issues are raised concerning the function (if any) of the second Mn-binding domain, and the extent to which local protein structure in each domain results in the differential reactivity of the two metal centers.

Results and Discussion

Design and Steady-State Characterization of OxDC Mutants with Domain-Specific Modified Mn Affinity

Given the possibility that both Mn sites catalyze the decarboxylation reaction, a series of OxDC mutants were constructed designed to disrupt the Mn-binding capability of a given cupin domain by modifying the side chains of either Glu-101 and Glu-280, which coordinate the metal in the N- and C-terminal domains, respectively (Figure 1-4). Prior studies of *Flammulina* OxDC had shown that mutation of Mn-binding histidine residues in either cupin domain yielded only inactive enzyme (*128*). A series of site-specific OxDC mutants was, therefore, constructed in which Mn-binding glutamate residues in each of the two domains (Figure 1-4) were replaced by alanine, aspartate and glutamine residues (Table 5-1). It was anticipated that the affinity of the binding site containing the mutated residue would be severely reduced so as to yield enzyme in which Mn was incorporated preferentially into the other domain. If catalysis was mediated independently by both Mn-binding sites, we anticipated these OxDC metal-binding mutants would exhibit activities reduced by approximately 50% from that of wild type enzyme (assuming metal incorporation proceeded to give 1 Mn/monomer).

Table 5-1 Mn incorporation and steady-state kinetic parameters for metal-binding OxDC mutants

Enzyme	Spe. Act.	Mn content	K_m (mM)	k_{cat} (s^{-1})	k_{cat}/K_m ($M^{-1}s^{-1}$)
WT OxDC	61.2 U/mg	1.87	8.4 ± 0.7	53 ± 1.5	6309
E101A	0.05 U/mg	0.18	2.9 ± 0.3	0.046 ± 0.002	16
E101D	0.79 U/mg	0.09	3.4 ± 0.1	0.49 ± 0.01	144
E101Q	0.63 U/mg	0.11	4.0 ± 0.2	0.62 ± 0.01	155
E280A	0.03 U/mg	0.67	3.0 ± 0.2	0.019 ± 0.001	6
E280D	0.69 U/mg	0.64	5.4 ± 0.4	0.14 ± 0.01	26
E280Q	0.15 U/mg	0.73	10.1 ± 0.6	0.62 ± 0.01	61
E101Q/E280Q	0.01 U/mg	0.07	2.9 ± 0.3	0.012 ± 0.0003	4

Contrary to this expectation, the steady-state kinetic parameters for the series of OxDC mutants showed that catalytic turnover was significantly lower than expected on the basis of Mn incorporation even though the oxalate K_m values were not greatly perturbed (Table 5-1). In the case of the E280Q OxDC mutant, the Mn content was 39% of that present in fully active, wild type OxDC yet the specific activity of the same mutant was only about 1% of the wild type activity. In other words, all Mn-binding mutants fell significantly below the line constructed in Figure 2-1 (the dependence of OxDC specific activity on the extent of Mn incorporation). In addition, none of the mutant enzymes were found to exhibit oxalate oxidase activity, at least as assayed with a dye oxidation method to monitor oxalate-dependent hydrogen peroxide formation (*129*).

Table 5-2 Metal content of Mn-binding OxDC mutants[a].

Enzyme Preparation	Mn	Co	Zn	Fe	Cu	Mg	Specific Activity[b]
WT OxDC	1.87	n.d.[c]	0.51	0.07	0.01	0.01	100%
E101A	0.18	< 0.01	0.17	< 0.01	< 0.01	n.d.[c]	< 0.1%
E101D	0.11	< 0.01	0.08	< 0.01	< 0.01	n.d.[c]	1.0%
E101Q	0.09	< 0.01	0.05	0.30	< 0.01	n.d.[c]	1.3%
E280A	0.67	< 0.01	0.12	< 0.01	< 0.01	n.d.[c]	< 0.1%
E280D	0.64	< 0.01	0.07	0.04	< 0.01	n.d.[c]	0.3%
E280Q	0.73	n.d.[c]	0.11	< 0.01	< 0.01	< 0.01	1.1%
E101Q/E280Q	0.07	< 0.01	0.12	0.04	< 0.01	n.d.[c]	< 0.1%

[a] Number of metal ions/OxDC monomer. [b] Value is relative to that of wild type OxDC. [c] Value was not determined.

In designing these experiments, it was assumed that the absence of Mn in the domain lacking a key glutamate side chain would not dramatically affect the three-dimensional fold of the β-barrel domain structure. This assumption seems reasonable given the existence of stable, metal-free cupin domains that lack metal-binding residues (*130, 131*). Unexpectedly, these experiments showed that Mn incorporation at the C-terminal binding site appears to require the presence of Mn in the N-terminal domain. Thus, replacement of Glu-101 by alanine, aspartate or

glutamine gave OxDC mutants containing approximately 0.1-0.2 Mn/monomer (Table 5-1). That this was not merely an effect associated with expressing the OxDC mutant in *Escherichia coli* was demonstrated by the failure of efforts to introduce Mn into the E101Q OxDC mutant using our well-defined *in vitro* conditions for metal substitution and re-folding. OxDC molecules containing Mn bound only in the C-terminal domain may be absent in solution, and hence the activity of samples of recombinant OxDC containing less than 2 Mn/monomer is associated with enzyme species containing Mn in both domains and/or one Mn in the N-terminal binding site.

Size-Exclusion Chromatography (SEC)

Because modification of the metal-binding glutamates gave OxDC mutants with catalytic activities far below those anticipated from their Mn content (assuming two independent catalytic sites) it was of interest to investigate whether changes to the metal binding glutamate residues might have caused large perturbations in enzyme structure. X-ray crystal structures show that *Bacillus subtilis* OxDC adopts a quaternary structure consisting of a hexamer in which two trimers are packed face to face so that the complex possesses 32 (D_3) point symmetry (*72*) (Figure 1-3). Because this crystallographic observation is consistent with PAGE studies of native OxDC (*34*), we employed size-exclusion chromatography to investigate the quaternary structures adopted by the series of OxDC mutants (Table 5-3).

Although recombinant, wild type OxDC seemed to elute as a hexamer under our conditions, approximately 85% of the purified protein sample was present as oligomers of higher apparent mass, corresponding to complexes formed from approximately 12-18 monomers. Perhaps more importantly, however, replacement of either of the Mn-binding glutamate residues did not yield oligomeric forms of the OxDC mutants that were significantly different to those

adopted by the wild type enzyme, although small populations of dimers (based on their elution properties) were observed for several of the mutants.

Table 5-3 Estimates of size for the oligomeric forms of recombinant wild type OxDC and OxDC Mn-binding mutants obtained using size exclusion chromatography. [a]Values shown are those given for the molecular weight standards. [b]Estimates obtained from size exclusion chromatography. Asterix indicates the predominant species observed under elution conditions. [c]Double mutant in which Glu-101 and Glu-280 are both replaced by glutamine residues.

	Actual MW (kDa)[a]	Estimated MW (kDa)[b]	Number of OxDC monomers
Carbonic Anhydrase	29	27	-
Albumin	66	93	-
Alcohol Dehydrogenase	150	103	-
Amylase	200	259	-
Apoferritin	443	433	-
Thyroglobulin	669	579	-
Wt OxDC	-	596*, 310	14,7
E101A	-	589*, 208, 80	13, 5, 2
E101D	-	666	15
E101Q	-	500* 196	12, 5
E280A	-	603*, 272, 222, 105	14, 6, 5, 3
E280D	-	602	14
E280Q	-	617*, 216	14, 5
E101Q/E280Q[c]	-	572*, 189	13, 4

Circular Dichroism Measurements

Circular dichroism (CD) measurements were employed to evaluate the extent of secondary structural changes resulting from site-specific replacement of the metal-binding glutamate residues (Figure 5-1). The utility of circular dichroism in the analysis of proteins is derived from the fact that the polypeptide backbone is optically active in the far ultraviolet (170-250 nm) and that different secondary structures produce characteristic spectra (*132*). Since CD measurements give estimates of the fraction of residues in α- helical, β- sheet, β-turn, and unordered conformations, the effects of mutations, denaturants, and temperature can be studied and the

kinetics of protein folding and unfolding can be investigated much more efficiently than by high resolution methods such as X-ray crystallography. Technical considerations of CD data collection include sample preparation in a buffer which does not absorb in the region of interest and balancing the factors of sample concentration, background signal, and cuvette pathlength.

As expected on the basis of the X-ray crystal structures, the CD spectrum of wild type OxDC showed features consistent with the largely β-strand character of the cupin domains together with minima at 222 and 205 nm that are presumably associated with the α-helices that mediate monomer/monomer contacts (Figure 5-1). The three OxDC mutants containing perturbations in the C-terminal Mn-binding site (E280A, E280D and E280Q) exhibited very similar CD spectra, but which differed considerably from that of wild type OxDC.

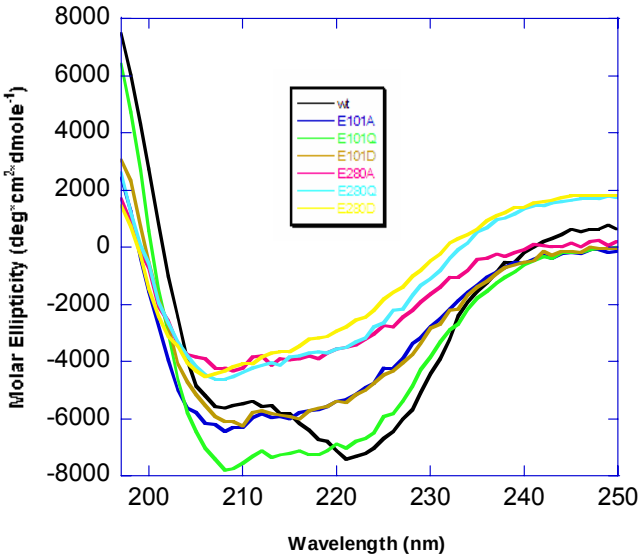

Figure 5-1 CD spectra of recombinant wild type OxDC and the Mn-binding OxDC mutants.

Because these three proteins still bind relatively large amounts of Mn/monomer, the simplest interpretation of the CD spectra is that they reflect the β-strand character of the N-terminal (and possibly the C-terminal) cupin domain(s). Thus, the observed changes likely reflect changes in the amount of α-helix, especially in light of the decreased molar ellipticities observed

at wavelengths between 190 nm and 200 nm. For OxDC mutants in which Glu-101 was replaced by other residues (E101A, E101D and E101Q) the picture was complicated by the finding that only E101A and E101D exhibited similar CD spectra. Although there are differences in the absolute molar ellipticities observed in the CD spectra for E101A, E101D and the three C-terminal OxDC mutants, the overall shape of the curves for the five enzymes were similar, suggesting a resemblance of their overall secondary structures. In the case of the E101Q OxDC mutant, however, the observed spectrum resembled that of the apo-form of *Thermococcus litoralis* phosphoglucose isomerase, a cupin for which activity is thought to be Fe-dependent (*133*). In many respects, the CD spectrum of the E101Q OxDC mutant is consistent with a higher proportion of α-helix, and similar levels of β-strand, secondary structure, relative to wild type OxDC.

Electron Paramagnetic Resonance Properties

To gain additional insight into the structure of the Mn-binding pocket in the OxDC mutants, we compared the EPR properties (see Chapter 3 for an introduction to the technique) of the Mn(II) center in the E280Q OxDC mutant with those of the wild type enzyme (Figure 5-2). In spectra taken for aerobic solutions of the enzyme at 10 K, the six-line Mn signals for the two proteins showed a strong resemblance, suggesting that the Mn(II) ions in both proteins were coordinated in similar environments, and the isotropic g-factor (g_{iso} = 2.00087) was identical for the two preparations within experimental limits (±0.00001). Differences were observed, however, in the signal linewidths (Figure 5-2). The linewidth for the E280Q mutant was 0.85 mT and that for the wild type enzyme was 1.1 mT (see simulations in Appendix C).

The spectra also revealed very little g- and A-strain, because the peak-to-peak amplitude was approximately the same within each six-line pattern, and did not show any trace of transitions between the higher electron spin manifolds. The latter is due to relatively large fine

structure values of the order of about 1000 MHz (Table 3-1). Similarly large fine structure parameters have been observed for the Mn(II) centers in the superoxide dismutases from *Rhodobacter capsulatus* and *Escherichia coli (134)*. Taken together, these spectral features suggest that the Mn ions in both samples are located in a very homogeneous ligand environment, supporting the proposal that the cupin structure of the N-terminal domain of wild type OxDC is retained in the Mn-binding mutant enzyme (E280Q).

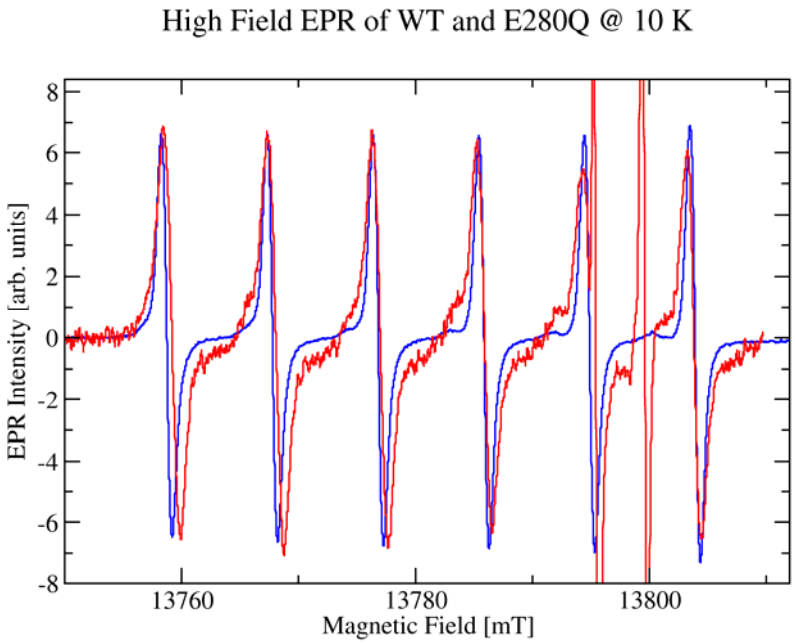

Figure 5-2 EPR spectra of the Mn(II) signals in wild type OxDC (red) and the E280Q OxDC mutant (blue) at 10 K**.** For the wild type enzyme, these experiments were performed at 386.116 GHz, with a modulation amplitude and modulation frequency of 2 G and 40 kHz, respectively. The main coil was slowly swept over a range of 13.75-13.81 T at 0.1 mT/s. In the case of the E280Q OxDC mutant, EPR experiments were performed at 382.826 GHz, with a modulation amplitude and modulation frequency of 2 G and 43 kHz, respectively. The main coil was slowly swept over a range of 13.628-13.698 T at 0.1 mT/s. For ease of comparison, the spectrum for the E280Q OxDC mutant (blue) is offset by 108.8 mT along the magnetic field axis. The additional sharp lines visible at 13796 and 13800 mT arise from the P-doped silicon field standard employed to calibrate the magnetic field sweep during acquisition of the spectrum for wild type OxDC (red).

Relaxation Enhancement Measurements

The significant difference in the spectral linewidth observed for the Mn signal in the two samples, however, suggested that a line broadening mechanism was operative in wild type OxDC that was absent in the E280Q OxDC mutant, perhaps because only one Mn-binding site was occupied in this protein. To answer this question, we measured the inversion recovery kinetics of the Mn signals for wild type OxDC and the E280QOxDC mutant of OxDC (Figure 5-3). Relaxation refers to the recovery from a non-equilibrium state to an equilibrium state. The characteristic time is called the relaxation time and is strongly dependent on the electronic structure of the paramagnetic center and on its interactions with its environment. The spin-lattice relaxation time, T_1, is the time constant for equilibration of the populations of the two electron spin Zeeman energy levels. The transverse relaxation time (or spin-spin relaxation time), T_2, is due to the variation in resonant fields that result from other spins in the vicinity. T_1 is usually much longer than T_2 (*135*).

These relaxation studies were performed using echo-detected EPR spectra for the samples, which were acquired at 3700 G and 3675 G for the wild type and mutant enzyme, respectively. For both samples, the observed T_1 decay was bi-exponential, with values of 9.25 and 55.4 μsec being obtained for the Mn signal in wild type OxDC. In the case of the E280Q OxDC mutant, however, the corresponding T_1 values were 16.3 and 92.5 μsec, meaning that relaxation was enhanced in the sample of wild type OxDC by a factor of approximately 1.7.A similar enhancement was observed for T_m (T_2) in the two samples (Figure 5-4).

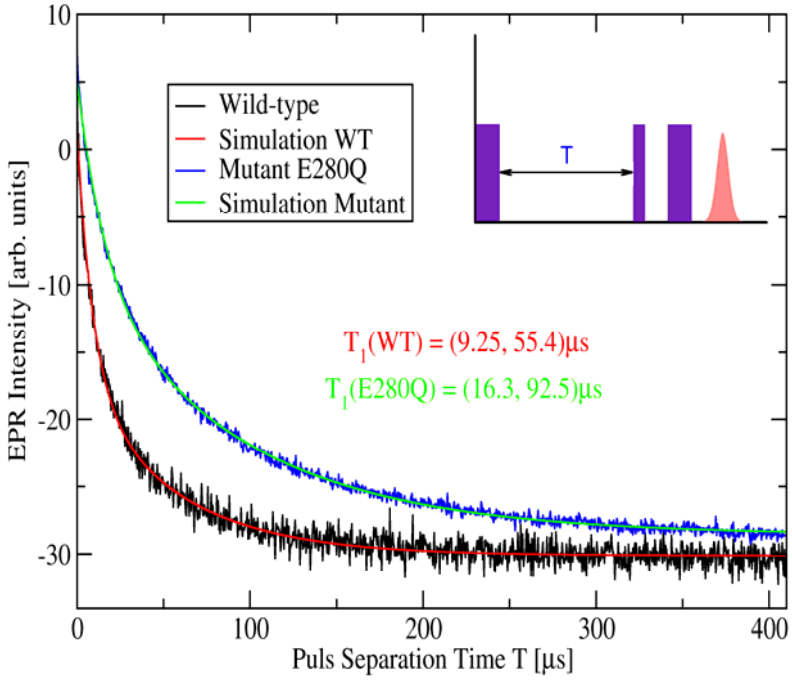

Figure 5-3. Inversion-recovery experiments on wild type OxDC (12.3 mg/mL) and the E280Q OxDC mutant (16.8 mg/mL). Samples were dissolved in 20 mM hexamethylenetetramine-HCl, pH 6.0, containing 0.5 M NaCl (100 µL total volume), and both spectra were taken at 5 K with a microwave frequency of 9.70703 GHz. The fields for the wild type OxDC and the E280Q OxDC mutant samples were 370 mT and 367.5 mT, respectively. The pulse sequence (see inset) employed π/2 and π pulses of 16 ns and 32 ns, respectively, and a 2-phase CYCLOPS sequence was used to separate the echo from unwanted spurious echoes. The data in the figure is the sum of 5 individual pulse trains per CYCLOPS phase, separated by a repetition time of 5.1 ms. Microwave attenuation was set to 11 dB. The echo amplitude from the Hahn readout sequence was integrated and plotted as a function of the pulse separation time T, with a pulse separation τ for the Hahn readout sequence of 140 ns. Both traces were simulated with bi-exponential recovery kinetics.

The observed changes in both T_1 and T_2 for the Mn signals in the two spectra demonstrated that the relaxation kinetics for metal centers in the wild-type enzyme were enhanced when compared to those of the single Mn in the E280Q OxDC mutant (Figures 5-3 and 5-4). The inter-monomer Mn-Mn distance of approximately 21 Å observed in the wild type OxDC hexamer is close enough for a dipolar interaction between the two metal ions to be observable in the EPR spectrum.

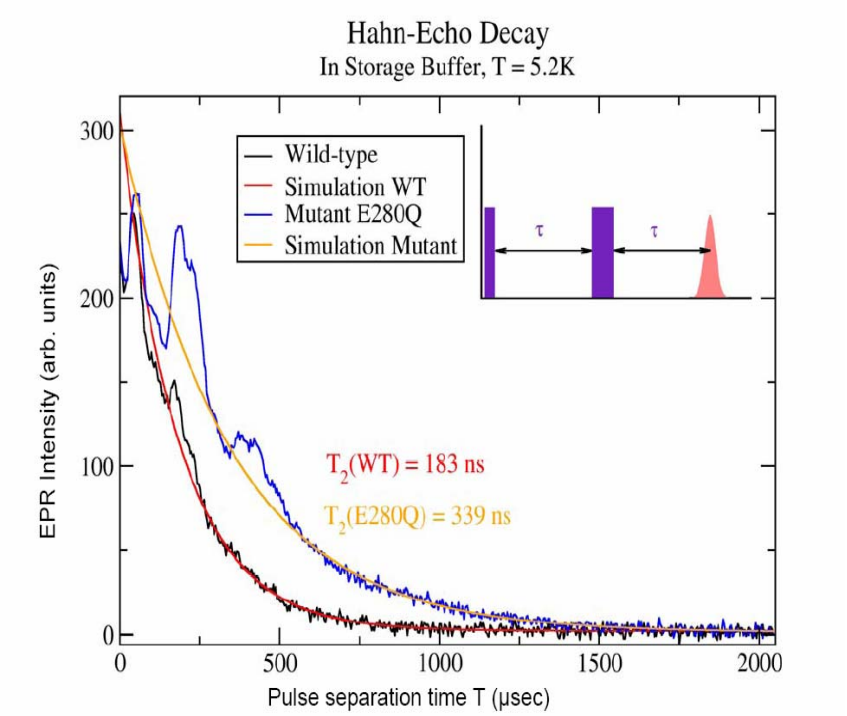

Figure 5-4 Data for the Hahn-echo decay experiment on wild-type OxDC and the E280Q mutant. Samples and fields were as for Figure 3-3. The experiment (inset) employed the usual $\pi/2$-τ-π Hahn echo pulse sequence with 16 and 32 ns pulses, respectively. A 2-phase CYCLOPS sequence was used to separate the echo from artifacts, and echo modulations were observed on the decay traces. Simulations were performed using a mono-exponential model taking points after the decay modulations.

Similar relaxation enhancements over distances of 15-30 Å have been seen in other proteins, including the bacterial photosynthetic reaction center (52) and metmyoglobin (53). Assuming that E280Q assembles in the same quaternary structure, its closest Mn-Mn distance would be almost twice as great (39-40 Å) as in the wild type hexamer, reducing the effect of the magnetic moment of one Mn ion on the relaxation dynamics of its nearest neighbor. Hence, it seems likely that the difference in the high-field EPR linewidths in the two spectra is due to paramagnetic relaxation broadening.

Implications for the Location of the Catalytic Site(s) in OxDC

As discussed in Chapter 2, the observation of a linear relationship between Mn occupancy and activity is consistent with three kinetic models, the simplest of which postulates that both Mn-binding sites are catalytically active. If the sites are also independent, then we anticipated the absence of Mn in one domain would yield a mutant enzyme exhibiting 50% of wild type activity (assuming insignificant structural changes and full metal incorporation). This proved not to be the case, however, with OxDC mutants (even those containing up to 0.73 Mn/monomer) exhibiting much lower activity than expected based on their Mn content (Figure 2-1). In fact, the level of activity observed for the E280Q OxDC mutant was significantly reduced in light of its Mn occupancy even though EPR experiments showed that Mn coordination by residues in the N-terminal domain was unaffected. Size-exclusion chromatography also supports the assumption that the E280Q OxDC mutant is correctly folded, and hence this result implies that (i) either the C-terminal Mn site mediates catalysis, or (ii) the N-terminal site catalyzes decarboxylation if, and only if, metal is bound in the C-terminal site. Unfortunately for the first of these two hypotheses, the E101D and E101Q OxDC mutants (in which Mn binding to the N-terminal domain is disrupted) exhibit catalytic activity that is lower than that observed for wild type OxDC containing an equivalent amount of bound Mn. This observation is therefore consistent with decarboxylation being mediated by the N-terminal Mn site, unless activity in the C-terminal site is dependent on the presence of metal in the N-terminal domain. Kinetic simulations in which the activity of one active site is dependent on metal occupancy of the other non-catalytic site, however, do not predict a linear relationship between bound Mn and catalytic activity, with one exception (case 6) in which Mn binding in one site causes a significant increase in Mn affinity of the second site while assuming that both sites have equal affinities prior to metal binding (Figure 2-2). Although these data rule out the hypothesis that both Mn binding sites can

independently degrade oxalate, this mutagenesis strategy does not permit us to define the location of the Mn(II) site that mediates catalysis.

Motivation for the Preparation of Single Domain OxDC Mutants

As noted in Chapter 1, it has been suggested that the two domains of oxalate decarboxylase arose from a gene duplication event (*28, 37, 43-46*). Two disparate sets of enzymological studies influenced the preparation of single domain mutants of OxDC. Gerlt and Babbitt (*136*) raised the possibility that $(\beta/\alpha)_8$-barrel fold proteins (unrelated to OxDC) may be derived from mixing and matching of $(\beta/\alpha)_4$-half barrels as well as other $(\beta/\alpha)_8$-barrels by divergent evolution. Crystallographic studies (*137*) indicated that imidazole glycerol phosphate synthase (HisF) from *Thermatoga maritima* is a $(\beta/\alpha)_8$-barrel composed of two superimposable domains (HisF-N and HisF-C). To examine the possibility that HisF evolved from duplication and fusion from and ancestral half barrel, the N- and C-terminal $(\beta/\alpha)_4$-half barrels of HisF (His-N and HisF-C) were produced in *Escherichia coli* purified and characterized (*138*). Separately, HisF-N and HisF-C are folded proteins, but are catalytically inactive. However, coexpression *in vivo* or joint refolding *in vitro*, resulted in these two domains assembling into a stoichiometric and catalytically active HisF-NC complex (*138*).

Another example of the expression of single domains in the literature was that of *E. coli* catalase-peroxidase (KatG) (*139, 140*), which is composed of two peroxidase-like domains. The N-terminal domain ($KatG^N$) contains the heme-dependent bifunctional site and the C-terminal domain ($KatG^C$) which does not bind heme, has no catalytic activity, and is separated from the activie site by 30 Å. $KatG^N$ expressed separately possesses neither catalase nor peroxidase activity (*139, 140*). However, separately expressed $KatG^C$ is able to restructure separately expressed $KatG^N$ to its bifunctional conformation (*141*).

N-Terminal OxDC Single Domain Mutant (OxDC-N1) Does Not Catalyze the Decarboxylation Reaction

This construct begins at the N-terminus and ends at glutamine-233. It includes a beta strand which contributes to the C-terminal domain (Figure 5-5).

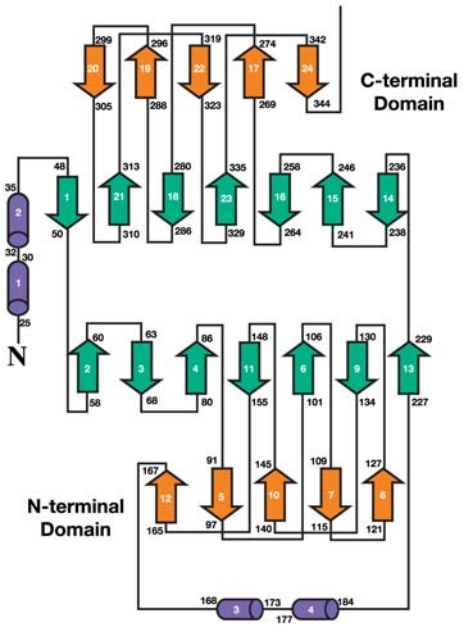

Figure 5-5 Topology diagram of OxDC. Figure adapted from (*72*).

This mutant did not contain Mn as determined by ICPMS, but did contain up to 1.01 mole Zn/mole of monomer (Table 5-4). It was possible, however, to incorporate up to 0.14 moles Mn/mole of monomer (0.45 moles Zn/ mole of monomer remaining) by the method described in Chapter 2 for the preparation of the "apoenzyme" and reconstitution of wild type recombinant OxDC (Table 5-4). This mutant was not found to possess OxDC activity by the OxDC-FDH linked enzyme assay. A small but detectable amount of oxalate oxidase activity, however, was detected in the manganese reconstituted sample by the dye oxidation assay described in the Experimental Section.

Table 5-4 Metal content of single domain mutant preparations

Sample	Spe. Act.	Mn	Fe	Cu	Zn	Co
OxDC-N1	0 U/mg	<0.01	<0.01	<0.01	1.01	<0.01
Recon OxDC-N1	0 U/mg	0.14	<0.01	<0.01	0.45	<0.01
OxDC-N1#2	0 U/mg	0.01	<0.04	<0.01	0.74	<0.01
Recon OxDC-N1#2	0 U/mg	0.06	0.02	<0.01	0.65	<0.01
OxDC-C	0 U/mg	0.08	0.02	<0.01	0.33	<0.01

EPR Characterization of Reconstituted N-terminal OxDC Single Domain Mutant (OxDC-N1)

Figure 5-6 shows the spectra of OxDC-N1 in 20 mM hexamethylenetetramine (HMTA) HCl buffer, pH6.0, 0.5 M NaCl (storage buffer) (shown in black). The six line spectra is typical of the Mn(II) centers in both the wild-type OxDC and in the E280Q mutant.

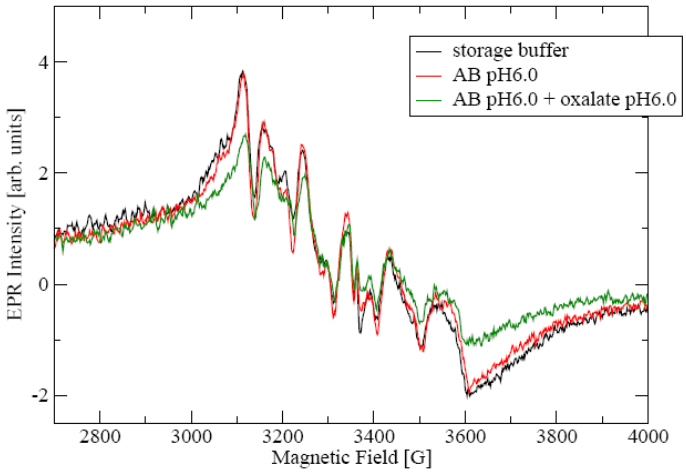

Figure 5-6 Effect of buffer and oxalate on the g ≈ 2 X-band Mn(II) signal of reconstituted N-terminal OxDC mutant (OxDC-N1)

A series of spectra were taken in order to make comparisons with the wild-type enzyme (see Chapters 3 and 4). In an effort to reduce the pH into the range of OxDC activity for the wild-type, the sample was made 50 mM sodium acetate, pH 5.2. Upon this treatment, some of the protein precipitated and what appeared as the sharp lines of hexaaquo manganese(II) appeared (spectrum not shown). Unlike the wild-type enzyme (but similar to the E2809Q mutant – data not shown), the spectrum changes very little if at all by the addition of sodium acetate and/or oxalate at pH 6.0.

C-Terminal OxDC Single Domain Mutant (OxDC-C) Does Not Catalyze the Decarboxylation Reaction

This construct begins with an engineered methione followed by leucine-231 and ends at the end of the wild type protein. Although this construct did contain a small amount of Mn as determined by ICPMS and by EPR at 324 GHz it was subjected to the reconstitution procedure described in Chapter 2 for the wild type full length enzyme. These spectra suggest that more Mn is in the purified than the reconstituted sample (no ICPMS data for reconstituted sample). This mutant was not found to possess neither OxDC activity by the OxDC-FDH linked enzyme assay nor oxalate oxidase activity by the dye oxidation assay. Furthermore, the OxDC-C did not show any signs of acetate or oxalate binding (data not shown).

Combining the N- and C-Terminal Single Domain Mutants Did Not Result in Decarboxylase Activity

Neither combining reconstituted OxDC-N-1 and OxDC-C in storage buffer nor putting the two single domain mutants through the reconstitution procedure together resulted in any detectable decarboxylation activity.

Experimental Section

Expression and Purification of Site-Specific OxDC Mutants.

All site-specific OxDC mutants were constructed using the overlap extension method (*142*) and the OxdC:pET-9a plasmid containing the gene coding for *Bacillus subtilis* OxDC (*57*). Thus, primers (Table 5-4) for mutagenesis were designed such that the desired mutation was located at the 5'-end. Primers overlapped 10 to 12 bases and included restriction sites to facilitate cloning into pET9a. The 3'- and 5'- fragments were amplified independently and a third PCR combined these two fragments to yield the full length gene. The resulting products were digested with BamHI and NdeI and cloned into pET9a. Constructs were transformed into JM109 competent cells, and transformants screened by restriction enzyme digestions using BamHI and NdeI. Plasmids containing the desired clones were sequenced to confirm PCR fidelity and transformed into BL21(DE3) competent cells.

Table 5-5 Primers used in the construction of Mn-binding mutants

Enzyme	Type	Primer Sequence
WT OxDC [a]	Forward	5'-GGAGGAAAC**ATCATATG**AAAAAACAAAATG-3'
WT OxDC [b]	Reverse	5'-GCGGCA**GGATCC**TTATTTACTGCATTTC-3'
E101A	Forward	5'-GCTGCATGGGCTTATATGATTTACGG-3'
E101A	Reverse	5'-GCCCATGCAGCTTCTTTATGCCAGTG-3'
E101D	Forward	5'-GCTGACTGGGCTTATATGATTTACGG-3'
E101D	Reverse	5'-GCCCAGTCAGCTTCTTTATGCTGCCAGTG-3'
E101Q	Forward	5'-GCTCAATGGGCTTATATGATTTACGG-3'
E101Q	Reverse	5'-GCCCATTGAGCTTCTTTATGCCAGTG-3'
E280A	Forward	5'-CCCACGCATGGCAATACTACATCTCC-3'
E280A	Reverse	5'-GCCATGCGTGGGTATTCGGGTGCC-3'
E280D	Forward	5'-GCTCATTGGGCTTATATGATTTACGG-3'
E280D	Reverse	5'-GCCCAATGAGCTTCTTTATGCCAGTG-3'
E280Q	Forward	5'-CCCACCAATGGCAATACTACATCTCC-3'
E280Q	Reverse	5'-GCCATTGGTGGGTATTCGGGTGCC-3'

[a] NdeI restriction site engineered (residues shown in bold). [b] BamHI restriction site engineered (residues shown in bold)

Expression of the OxDC mutants was carried out as for the wild type enzyme (Chapter 2). After an initial purification using DEAE-Sepharose Fast Flow column chromatography, (Chapter 2), OxDC mutants were precipitated from 50 mM imidazole-Cl, pH 7.0, containing 1.7 M $(NH_4)_2SO_4$. The precipitate was then centrifuged (10,000 rpm, 20 min, 4 ^oC), and re-suspended in 20 mM hexamethylenetetramine-HCl, pH 6.0 containing 0.5 M NaCl to yield solutions of the site-specific OxDC mutants at concentrations ranging from 3.5 to 19.6 mg/mL. This abbreviated purification procedure gave mutant enzymes of > 90% purity, as evaluated by SDS-PAGE.

Oxalate Oxidase Assays

The level of oxalate oxidase activity for wild type OxDC and the series of OxDC mutants at ambient temperatures (21-23 ^oC), using a continuous assay in which H_2O_2 production was coupled to the horseradish peroxidase (HRP) catalyzed oxidation of 2,2'-azinobis-(3-ethylbenzthiazoline-6-sulphonic acid) (ABTS) (*129*). Reaction mixtures contained 25 U HRP, 5 mM ABTS, 50 mM potassium oxalate, wild type OxDC or the metal-binding OxDC mutants (at concentrations up to 0.035 mg/mL) dissolved in 50 mM sodium acetate, pH 4.0 (total volume 1 mL). An extinction coefficient of 10,000 M^{-1} cm^{-1} for the ABTS radical product was assumed in these experiments. Control samples omitted HRP so as to differentiate between H_2O_2 production and any oxalate-dependent dye oxidation activity by wild type OxDC or the OxDC mutant.

Size-Exclusion Chromatography Measurements

The oligomeric state of the wild type enzyme was compared with that of the metal-binding mutants by size exclusion chromatography using a BIOSEP-S2000 column (300 x 7.8 mm with 75 x 7.8 mm guard column) (Phenomenex, Torrance, CA) was equilibrated with 20 mM hexamethylenetetramine hydrochloride, pH 6.0, containing 0.5 M NaCl (buffer C), and calibrated using carbonic anhydrase (29.0 kDa), bovine serum albumin (66.0 kDa), alcohol dehydrogenase (150 kDa), β-amylase (200 kDa), apoferritin (443 kDa), and thyroglobulin (669

kDa). The void volume was measured by injecting blue dextran. Samples of recombinant, wild type OxDC or the site-specific OxDC mutants were then injected onto the column and eluted with buffer C, at a flow rate of 1 mL/min with UV detection at 280 nm, to assign the oligomeric form of the enzyme.

Circular Dichroism Studies

Recombinant, wild type OxDC was dialyzed into 25 mM potassium phosphate, pH 7.0 containing 100 mM NaCl, and the protein concentration adjusted to a final value of 185 μg/mL. A similar procedure was performed for all 9 site-specific OxDC mutants. In cases where the protein precipitated (8/10 samples), the precipitate was removed by microcentrifugation, The CD spectrum of the protein was then obtained using an Aviv 215 spectrometer (Aviv Associates, Lakewood, NJ) at wavelengths over the range of 190-250 nm (1 mm path length). All spectra were corrected by subtracting the CD spectrum of the buffer over this range of wavelengths.

Electron Paramagnetic Resonance Spectroscopy

EPR spectra were determined using samples of wild type OxDC (12.3 mg/mL) or the E280Q OxDC mutant (16.8 mg/mL) dissolved in 20 mM hexamethylenetetramine-HCl, pH 6.0, containing 0.5 M NaCl (100 μL total volume). The metal contents of the wild type and mutant enzymes were 1.63 and 0.73 Mn/monomer, respectively. All high-field EPR experiments were performed using a custom-built spectrometer operating in transmission mode (*124*). Far IR radiation was generated by a Gunn source at W-band (94-97 GHz or 105-110 GHz), which was frequency tripled and/or quadrupled to achieve frequencies of 320 or 380 GHz with a radiation power of 2-10 mW, and transmitted through an oversized waveguide so as to pass through the sample once before being detected by an InSb hot-electron bolometer (QMC Instruments Ltd, Cardiff, UK). The analog signal from the bolometer was fed into a Stanford Instrument SR830 lock-in detector, which was referenced to the field modulation at the sample. The magnetic field

sweep was carried out by either sweeping the main coil or a custom-built auxiliary 1000 G sweep coil. Field calibration was performed using a piece of P-doped silicon, which has a *g*-value of 1.99854 and a hyperfine coupling constant of 117.507 MHz (*143*). Spectral simulations were done with the EasySpin toolbox (*121*) in the MATLAB computing environment (The MathWorks, Natick, MA), and with in-house programs written Andrew Ozarowski. The time-dependent EPR spectra required for the relaxation rate studies were taken with a Bruker Elexsys E580 pulse/cw spectrometer equipped with a 5 mm Bruker Flexline dielectric resonator. The Flexline resonator and the samples were cooled using cold helium gas in an Oxford CF935 cryostat, and the temperature during acquisition was controlled with an ITC4 temperature controller and a VC40 gas flow controller (Oxford Instruments, Eynsham, UK). Standard pulse sequences were employed in these experiments (*144*).

Expression of OxDC Single Domain Mutants

Three single domain mutants were independently amplified from pET9a plasmid containing the gene coding for *Bacillus subtilis* OxDC (*57*). 1) OxDC-N1 (YD1) was amplified using primers OxdC fwd and Domain-1 rev (Table 4-3). This construct begins at the N-terminus and ends at glutamine-233. It includes a beta strand which contributes to the C-terminal domain. 2) OxDC-N2 (DD1) was amplified using primers Domain-1 fwd and Domain-1 reverse (Table 3-6). This construct does not contain the N-terminal beta strand that contributes to the C-terminal domain. It begins with an engineered methionine followed by serine-53 and ends at glutamine-233. 3) OxDC-C was amplified using primers Domain-2 fwd and OxdC rev. This construct begins with an engineered methione followed by leucine-231 and ends at the end of the wild type protein. The resulting products were digested with BamHI and NdeI and cloned into the pET9a plasmid. Constructs were transformed into JM109 competent cells, and transformants were screened by restriction enzyme digestions using BamHI and NdeI. Plasmids containing the

desired clones were sequenced to confirm PCR fidelity and were transformed into BL21(DE3) competent cells. Expression of the OxDC mutants carried out as for the wild type enzyme.

Table 5-6 Primers used in the preparation of OxDC single domain mutants

Primer Name	Primer sequence
OxdC * fwd	5'-GGAGGAAACATCATATGAAAAAACAAAATG-3'
OxdC ** rev	5'-GCGGCAGGATCCTTATTTACTGCATTTC-3'
Domain-1 fwd	5'-GGAGGAAACATATGTCTGATACTCATAACC-3'
Domain-1 rev	5'-GCGGCAGGATCCCTATTGTTCAAGAAGGCG-3'
Domain-2 fwd	5'-TTTACTTACCATATGCTTGAACAAGAGCCG-3'
* NdeI restriction site engineered (underlined)	
** BamHI restriction site engineered (underlined)	

Purification of Single Domain OxDC Mutant OxDC-N1

Expression of OxDC-N1 was confirmed by comparing cell lysates before and after induction by 12% SDS PAGE. The appearance of a band in the induced cells at the calculated molecular weight of 26.4 kd (http://www.scripps.edu/cgi-bin/cdputnam/protcalc3) confirmed expression. Cells were lysed, extracted, and purified by DEAE column chromatography as described for recombinant wild-type OxDC. Fractions containing OxDC-N1 as determined by electrophoretic mobility were pooled and dialyzed for 4 h against 50 mM imidazole-HCl buffer, pH 7.0 (2 L). The resulting sample was then applied to a Q-Sepharose Hi-Performance column (2.5 x 18 cm) column equilibrated with 50 mM imidazole-HCl buffer, pH 7.0, and eluted using a 500 mL linear gradient from the column buffer to the same containing 1 M NaCl. Fractions containing OxDC were pooled and exhaustively dialyzed against 20 mM hexamethylenetetramine hydrochloride, pH 6.0, containing 0.5 M NaCl. Purified OxDC-N1 (> 90 % as determined by SDS PAGE) was concentrated to 5.3 mg/mL and stored as at -80 ^{o}C.

Purification of Single Domain OxDC Mutant OxDC-C

Expression of CTD was confirmed by comparing cell lysates before and after induction by 12% SDS PAGE. The appearance of a band in the induced cells at the calculated molecular weight of 17.7 kd (http://www.scripps.edu/cgi-bin/cdputnam/protcalc3) confirmed expression. OxDC-C was purified (>90% purity as determined by SDS PAGE) by the method described above for OxDC-N1.

CHAPTER 6
CONCLUSIONS AND FUTURE WORK

We have demonstrated a linear dependence of oxalate decarboxylase specific activity on the Mn incorporation. This observation is consistent with only three of the seven kinetic models studied. The simplest model is that both Mn-binding sites are catalytically active. If the sites are also independent, the absence of Mn in one domain would yield a mutant enzyme with 50% of wild type activity (assuming insignificant structural changes and full metal incorporation). OxDC Mn-binding mutants, however, exhibited much lower activity than expected based on their Mn content (Figure 2-1). For example, the level of activity observed for the E280Q OxDC mutant was significantly reduced in light of its Mn occupancy (0.73 Mn/monomer) even though EPR experiments showed that Mn coordination by residues in the N-terminal domain was unaffected. Size-exclusion chromatography is consistent with the assumption that the E280Q OxDC mutant is correctly folded. This result implies that (i) either the C-terminal Mn site mediates catalysis, or (ii) the N-terminal site catalyzes decarboxylation if, and only if, metal is bound in the C-terminal site. That the E101D and E101Q OxDC mutants (in which Mn binding to the N-terminal domain is disrupted) exhibit catalytic activity that is lower than that observed for wild type OxDC containing an equivalent amount of bound Mn argues against the first of these two hypotheses. This observation is therefore consistent with decarboxylation being mediated by the N-terminal Mn site, unless activity in the C-terminal site is dependent on the presence of metal in the N-terminal domain.

Kinetic simulations in which the activity of one active site is dependent on metal occupancy of the other non-catalytic site, however, do not predict a linear relationship between bound Mn and catalytic activity, with one exception (case 6) in which Mn binding in one site causes a significant increase in Mn affinity of the second site while assuming that both sites have

equal affinities prior to metal binding (Figure 2-3). Although these data rule out the hypothesis that both Mn binding sites can independently degrade oxalate, this mutagenesis strategy does not permit us to define the location of the Mn(II) site that mediates catalysis.

A multi-frequency EPR approach has allowed us to spectroscopically distinguish two Mn(II) species that are present in equal proportions in the resting state of oxalate decarboxylase in storage buffer. The main difference between these two species is the value of the fine structure parameters with D_{I} = 1200 MHz and D_{II} = 2700 MHz. When the enzyme is placed in acetate buffer pH5.2 or when formate is added, D_{II} is reduced to 2150 MHz while D_{I} remains the same indicating that only one Mn(II) is solvent accessible. Based on published crystal structure data, we suggest site I is the C-terminal Mn site while site II is the solvent-exposed N-terminal site and, therefore, the site of small molecule (acetate and formate) binding.

It would be of interest in terms of the catalytic mechanism to determine the redox properties of OxDC. The observation that the Mn(II) EPR signal can be decreased with the addition of sodium (meta) periodate and potassium hexachloroiridate with a concomitant appearance of a carbon-based radical should be explored further and is significant in that it demonstrates that oxidants can reach the manganese ions and that potentiometric titrations can be carried out on OxDC. It would also be of interest to use an oxygen electrode to characterize the oxygen dependence of the bacterial form of OxDC. Questions about the binding of substrate to the Mn-binding site(s) could be addressed by crystallographic structure solution of the Co substituted enzyme in the presence of oxalate.

APPENDIX A
KINETIC PARAMETERS USED IN GEPASI SIMULATIONS

Case 1 (site 2 unimportant or inactive)

1(a)	**1(b)**	**1(c)**
R1 (Mass action (reversible))	R1 (Mass action (reversible))	R1 (Mass action (reversible))
k1 = 1.0000e+009	k1 = 1.0000e+009	k1 = 1.0000e+009
k2 = 5.0000e+000	k2 = 5.0000e+003	k2 = 5.0000e+000
R2 (Mass action (reversible))	R2 (Mass action (reversible))	R2 (Mass action (reversible))
k1 = 1.0000e+009	k1 = 1.0000e+009	k1 = 1.0000e+009
k2 = 5.0000e+000	k2 = 5.0000e+000	k2 = 5.0000e+003
R3 (Mass action (reversible))	R3 (Mass action (reversible))	R3 (Mass action (reversible))
k1 = 1.0000e+009	k1 = 1.0000e+009	k1 = 1.0000e+009
k2 = 5.0000e+000	k2 = 5.0000e+003	k2 = 5.0000e+000
R4 (Mass action (reversible))	R4 (Mass action (reversible))	R4 (Mass action (reversible))
k1 = 1.0000e+009	k1 = 1.0000e+009	k1 = 1.0000e+009
k2 = 5.0000e+000	k2 = 5.0000e+000	k2 = 5.0000e+003
R5 (Mass action (reversible))	R5 (Mass action (reversible))	R5 (Mass action (reversible))
k1 = 1.0000e+008	k1 = 1.0000e+008	k1 = 1.0000e+008
k2 = 8.4000e+005	k2 = 8.4000e+005	k2 = 8.4000e+005
R6 (Mass action (irreversible))	R6 (Mass action (irreversible))	R6 (Mass action (irreversible))
k = 5.3000e+001	k = 5.3000e+001	k = 5.3000e+001
R7 (Mass action (reversible))	R7 (Mass action (reversible))	R7 (Mass action (reversible))
k1 = 1.0000e+008	k1 = 1.0000e+008	k1 = 1.0000e+008
k2 = 8.4000e+005	k2 = 8.4000e+005	k2 = 8.4000e+005
R8 (Mass action (reversible))	R8 (Mass action (reversible))	R8 (Mass action (reversible))
k1 = 1.0000e+008	k1 = 1.0000e+008	k1 = 1.0000e+008
k2 = 8.4000e+005	k2 = 8.4000e+005	k2 = 8.4000e+005
R9 (Mass action (irreversible))	R9 (Mass action (irreversible))	R9 (Mass action (irreversible))
k = 5.3000e+001	k = 5.3000e+001	k = 5.3000e+001
R10 (Mass action (irreversible))	R10 (Mass action (irreversible))	R10 (Mass action (irreversible))
k = 5.0000e-006	k = 5.0000e-006	k = 5.0000e-006

Case 1’ (site 2 unimportant or inactive)

1(a)'	1(b)'	1(c)'
R1 (Mass action (reversible))	R1 (Mass action (reversible))	R1 (Mass action (reversible))
k1 = 1.0000e+009	k1 = 1.0000e+009	k1 = 1.0000e+009
k2 = 5.0000e+000	k2 = 5.0000e+003	k2 = 5.0000e+000
R2 (Mass action (reversible))	R2 (Mass action (reversible))	R2 (Mass action (reversible))
k1 = 1.0000e+009	k1 = 1.0000e+009	k1 = 1.0000e+009
k2 = 5.0000e+000	k2 = 5.0000e+000	k2 = 5.0000e+003
R3 (Mass action (reversible))	R3 (Mass action (reversible))	R3 (Mass action (reversible))
k1 = 1.0000e+009	k1 = 1.0000e+009	k1 = 1.0000e+009
k2 = 5.0000e+000	k2 = 5.0000e+003	k2 = 5.0000e+000
R4 (Mass action (reversible))	R4 (Mass action (reversible))	R4 (Mass action (reversible))
k1 = 1.0000e+009	k1 = 1.0000e+009	k1 = 1.0000e+009
k2 = 5.0000e+000	k2 = 5.0000e+000	k2 = 5.0000e+003
R5 (Mass action (reversible))	R5 (Mass action (reversible))	R5 (Mass action (reversible))
k1 = 1.0000e+008	k1 = 1.0000e+008	k1 = 1.0000e+008
k2 = 8.4000e+005	k2 = 8.4000e+005	k2 = 8.4000e+005
R6 (Mass action (irreversible))	R6 (Mass action (irreversible))	R6 (Mass action (irreversible))
k = 5.3000e+001	k = 5.3000e+001	k = 5.3000e+001
R7 (Mass action (reversible))	R7 (Mass action (reversible))	R7 (Mass action (reversible))
k1 = 1.0000e+008	k1 = 1.0000e+008	k1 = 1.0000e+008
k2 = 8.4000e+005	k2 = 8.4000e+005	k2 = 8.4000e+005
R8 (Mass action (reversible))	R8 (Mass action (reversible))	R8 (Mass action (reversible))
k1 = 1.0000e+008	k1 = 1.0000e+008	k1 = 1.0000e+008
k2 = 8.4000e+005	k2 = 8.4000e+005	k2 = 8.4000e+005
R9 (Mass action (irreversible))	R9 (Mass action (irreversible))	R9 (Mass action (irreversible))
k = 2.6500e+001	k = 2.6500e+001	k = 2.6500e+001
R10 (Mass action (irreversible))	R10 (Mass action (irreversible))	R10 (Mass action (irreversible))
k = 5.0000e-006	k = 5.0000e-006	k = 5.0000e-006

Case 2 (site 1 most active)

2(a)	2(b)	2(c)
R1 (Mass action (reversible))	R1 (Mass action (reversible))	R1 (Mass action (reversible))
k1 = 1.0000e+009	k1 = 1.0000e+009	k1 = 1.0000e+009
k2 = 5.0000e+000	k2 = 5.0000e+003	k2 = 5.0000e+000
R2 (Mass action (reversible))	R2 (Mass action (reversible))	R2 (Mass action (reversible))
k1 = 1.0000e+009	k1 = 1.0000e+009	k1 = 1.0000e+009
k2 = 5.0000e+000	k2 = 5.0000e+000	k2 = 5.0000e+003
R3 (Mass action (reversible))	R3 (Mass action (reversible))	R3 (Mass action (reversible))
k1 = 1.0000e+009	k1 = 1.0000e+009	k1 = 1.0000e+009
k2 = 5.0000e+000	k2 = 5.0000e+003	k2 = 5.0000e+000
R4 (Mass action (reversible))	R4 (Mass action (reversible))	R4 (Mass action (reversible))
k1 = 1.0000e+009	k1 = 1.0000e+009	k1 = 1.0000e+009
k2 = 5.0000e+000	k2 = 5.0000e+000	k2 = 5.0000e+003
R5 (Mass action (reversible))	R5 (Mass action (reversible))	R5 (Mass action (reversible))
k1 = 1.0000e+008	k1 = 1.0000e+008	k1 = 1.0000e+008
k2 = 8.4000e+005	k2 = 8.4000e+005	k2 = 8.4000e+005
R6 (Mass action (irreversible))	R6 (Mass action (irreversible))	R6 (Mass action (irreversible))
k = 5.3000e+001	k = 5.3000e+001	k = 5.3000e+001
R7 (Mass action (reversible))	R7 (Mass action (reversible))	R7 (Mass action (reversible))
k1 = 1.0000e+008	k1 = 1.0000e+008	k1 = 1.0000e+008
k2 = 8.4000e+005	k2 = 8.4000e+005	k2 = 8.4000e+005
R8 (Mass action (reversible))	R8 (Mass action (reversible))	R8 (Mass action (reversible))
k1 = 1.0000e+008	k1 = 1.0000e+008	k1 = 1.0000e+008
k2 = 8.4000e+005	k2 = 8.4000e+005	k2 = 8.4000e+005
R9 (Mass action (irreversible))	R9 (Mass action (irreversible))	R9 (Mass action (irreversible))
k = 3.5000e+001	k = 3.5000e+001	k = 3.5000e+001
R10 (Mass action (irreversible))	R10 (Mass action (irreversible))	R10 (Mass action (irreversible))
k = 8.0000e+000	k = 8.0000e+000	k = 8.0000e+000

Case 3 (site 2 required, site 1 is active)

3(a)	3(b)	3(c)
R1 (Mass action (reversible))	R1 (Mass action (reversible))	R1 (Mass action (reversible))
k1 = 1.0000e+009	k1 = 1.0000e+009	k1 = 1.0000e+009
k2 = 5.0000e+000	k2 = 5.0000e+003	k2 = 5.0000e+000
R2 (Mass action (reversible))	R2 (Mass action (reversible))	R2 (Mass action (reversible))
k1 = 1.0000e+009	k1 = 1.0000e+009	k1 = 1.0000e+009
k2 = 5.0000e+000	k2 = 5.0000e+000	k2 = 5.0000e+003
R3 (Mass action (reversible))	R3 (Mass action (reversible))	R3 (Mass action (reversible))
k1 = 1.0000e+009	k1 = 1.0000e+009	k1 = 1.0000e+009
k2 = 5.0000e+000	k2 = 5.0000e+003	k2 = 5.0000e+000
R4 (Mass action (reversible))	R4 (Mass action (reversible))	R4 (Mass action (reversible))
k1 = 1.0000e+009	k1 = 1.0000e+009	k1 = 1.0000e+009
k2 = 5.0000e+000	k2 = 5.0000e+000	k2 = 5.0000e+003
R5 (Mass action (reversible))	R5 (Mass action (reversible))	R5 (Mass action (reversible))
k1 = 1.0000e+008	k1 = 1.0000e+008	k1 = 1.0000e+008
k2 = 8.4000e+005	k2 = 8.4000e+005	k2 = 8.4000e+005
R6 (Mass action (irreversible))	R6 (Mass action (irreversible))	R6 (Mass action (irreversible))
k = 5.3000e+001	k = 5.3000e+001	k = 5.3000e+001
R7 (Mass action (reversible))	R7 (Mass action (reversible))	R7 (Mass action (reversible))
k1 = 1.0000e+008	k1 = 1.0000e+008	k1 = 1.0000e+008
k2 = 8.4000e+005	k2 = 8.4000e+005	k2 = 8.4000e+005
R8 (Mass action (reversible))	R8 (Mass action (reversible))	R8 (Mass action (reversible))
k1 = 1.0000e+008	k1 = 1.0000e+008	k1 = 1.0000e+008
k2 = 8.4000e+005	k2 = 8.4000e+005	k2 = 8.4000e+005
R9 (Mass action (irreversible))	R9 (Mass action (irreversible))	R9 (Mass action (irreversible))
k = 5.0000e-006	k = 5.0000e-006	k = 5.0000e-006
R10 (Mass action (irreversible))	R10 (Mass action (irreversible))	R10 (Mass action (irreversible))
k = 5.0000e-006	k = 5.0000e-006	k = 5.0000e-006

Case 4 (sites 1 and 2 have equal activity)

4(a)	**4(b)**	**4(c)**
R1 (Mass action (reversible))	R1 (Mass action (reversible))	R1 (Mass action (reversible))
k1 = 1.0000e+009	k1 = 1.0000e+009	k1 = 1.0000e+009
k2 = 5.0000e+000	k2 = 5.0000e+003	k2 = 5.0000e+000
R2 (Mass action (reversible))	R2 (Mass action (reversible))	R2 (Mass action (reversible))
k1 = 1.0000e+009	k1 = 1.0000e+009	k1 = 1.0000e+009
k2 = 5.0000e+000	k2 = 5.0000e+000	k2 = 5.0000e+003
R3 (Mass action (reversible))	R3 (Mass action (reversible))	R3 (Mass action (reversible))
k1 = 1.0000e+009	k1 = 1.0000e+009	k1 = 1.0000e+009
k2 = 5.0000e+000	k2 = 5.0000e+003	k2 = 5.0000e+000
R4 (Mass action (reversible))	R4 (Mass action (reversible))	R4 (Mass action (reversible))
k1 = 1.0000e+009	k1 = 1.0000e+009	k1 = 1.0000e+009
k2 = 5.0000e+000	k2 = 5.0000e+000	k2 = 5.0000e+003
R5 (Mass action (reversible))	R5 (Mass action (reversible))	R5 (Mass action (reversible))
k1 = 1.0000e+008	k1 = 1.0000e+008	k1 = 1.0000e+008
k2 = 8.4000e+005	k2 = 8.4000e+005	k2 = 8.4000e+005
R6 (Mass action (irreversible))	R6 (Mass action (irreversible))	R6 (Mass action (irreversible))
k = 5.3000e+001	k = 5.3000e+001	k = 5.3000e+001
R7 (Mass action (reversible))	R7 (Mass action (reversible))	R7 (Mass action (reversible))
k1 = 1.0000e+008	k1 = 1.0000e+008	k1 = 1.0000e+008
k2 = 8.4000e+005	k2 = 8.4000e+005	k2 = 8.4000e+005
R8 (Mass action (reversible))	R8 (Mass action (reversible))	R8 (Mass action (reversible))
k1 = 1.0000e+008	k1 = 1.0000e+008	k1 = 1.0000e+008
k2 = 8.4000e+005	k2 = 8.4000e+005	k2 = 8.4000e+005
R9 (Mass action (irreversible))	R9 (Mass action (irreversible))	R9 (Mass action (irreversible))
k = 2.6500e+001	k = 2.6500e+001	k = 2.6500e+001
R10 (Mass action (irreversible))	R10 (Mass action (irreversible))	R10 (Mass action (irreversible))
k = 2.6500e+001	k = 2.6500e+001	k = 2.6500e+001

Case 5 (site 2 required, fully occupied enzyme twice as active)

5(a)	5(b)	5(c)
R1 (Mass action (reversible))	R1 (Mass action (reversible))	R1 (Mass action (reversible))
k1 = 1.0000e+009	k1 = 1.0000e+009	k1 = 1.0000e+009
k2 = 5.0000e+000	k2 = 5.0000e+003	k2 = 5.0000e+000
R2 (Mass action (reversible))	R2 (Mass action (reversible))	R2 (Mass action (reversible))
k1 = 1.0000e+009	k1 = 1.0000e+009	k1 = 1.0000e+009
k2 = 5.0000e+000	k2 = 5.0000e+000	k2 = 5.0000e+003
R3 (Mass action (reversible))	R3 (Mass action (reversible))	R3 (Mass action (reversible))
k1 = 1.0000e+009	k1 = 1.0000e+009	k1 = 1.0000e+009
k2 = 5.0000e+000	k2 = 5.0000e+003	k2 = 5.0000e+000
R4 (Mass action (reversible))	R4 (Mass action (reversible))	R4 (Mass action (reversible))
k1 = 1.0000e+009	k1 = 1.0000e+009	k1 = 1.0000e+009
k2 = 5.0000e+000	k2 = 5.0000e+000	k2 = 5.0000e+003
R5 (Mass action (reversible))	R5 (Mass action (reversible))	R5 (Mass action (reversible))
k1 = 1.0000e+008	k1 = 1.0000e+008	k1 = 1.0000e+008
k2 = 8.4000e+005	k2 = 8.4000e+005	k2 = 8.4000e+005
R6 (Mass action (irreversible))	R6 (Mass action (irreversible))	R6 (Mass action (irreversible))
k = 5.3000e+001	k = 5.3000e+001	k = 5.3000e+001
R7 (Mass action (reversible))	R7 (Mass action (reversible))	R7 (Mass action (reversible))
k1 = 1.0000e+008	k1 = 1.0000e+008	k1 = 1.0000e+008
k2 = 8.4000e+005	k2 = 8.4000e+005	k2 = 8.4000e+005
R8 (Mass action (reversible))	R8 (Mass action (reversible))	R8 (Mass action (reversible))
k1 = 1.0000e+008	k1 = 1.0000e+008	k1 = 1.0000e+008
k2 = 8.4000e+005	k2 = 8.4000e+005	k2 = 8.4000e+005
R9 (Mass action (irreversible))	R9 (Mass action (irreversible))	R9 (Mass action (irreversible))
k = 2.6000e+001	k = 2.6000e+001	k = 2.6000e+001
R10 (Mass action (irreversible))	R10 (Mass action (irreversible))	R10 (Mass action (irreversible))
k = 5.0000e-006	k = 5.0000e-006	k = 5.0000e-006

Case 6 (site 1 active, cooperative binding)

6(a)	6(b)	6(c)
R1 (Mass action (reversible))	R1 (Mass action (reversible))	R1 (Mass action (reversible))
k1 = 1.0000e+009	k1 = 1.0000e+009	k1 = 1.0000e+009
k2 = 5.0000e+002	k2 = 5.0000e+002	k2 = 5.0000e+000
R2 (Mass action (reversible))	R2 (Mass action (reversible))	R2 (Mass action (reversible))
k1 = 1.0000e+009	k1 = 1.0000e+009	k1 = 1.0000e+009
k2 = 5.0000e+002	k2 = 5.0000e+000	k2 = 5.0000e+002
R3 (Mass action (reversible))	R3 (Mass action (reversible))	R3 (Mass action (reversible))
k1 = 1.0000e+009	k1 = 1.0000e+009	k1 = 1.0000e+009
k2 = 5.0000e+000	k2 = 5.0000e+000	k2 = 5.0000e-002
R4 (Mass action (reversible))	R4 (Mass action (reversible))	R4 (Mass action (reversible))
k1 = 1.0000e+009	k1 = 1.0000e+009	k1 = 1.0000e+009
k2 = 5.0000e+000	k2 = 5.0000e-002	k2 = 5.0000e+000
R5 (Mass action (reversible))	R5 (Mass action (reversible))	R5 (Mass action (reversible))
k1 = 1.0000e+008	k1 = 1.0000e+008	k1 = 1.0000e+008
k2 = 8.4000e+005	k2 = 8.4000e+005	k2 = 8.4000e+005
R6 (Mass action (irreversible))	R6 (Mass action (irreversible))	R6 (Mass action (irreversible))
k = 5.3000e+001	k = 5.3000e+001	k = 5.3000e+001
R7 (Mass action (reversible))	R7 (Mass action (reversible))	R7 (Mass action (reversible))
k1 = 1.0000e+008	k1 = 1.0000e+008	k1 = 1.0000e+008
k2 = 8.4000e+005	k2 = 8.4000e+005	k2 = 8.4000e+005
R8 (Mass action (reversible))	R8 (Mass action (reversible))	R8 (Mass action (reversible))
k1 = 1.0000e+008	k1 = 1.0000e+008	k1 = 1.0000e+008
k2 = 8.4000e+005	k2 = 8.4000e+005	k2 = 8.4000e+005
R9 (Mass action (irreversible))	R9 (Mass action (irreversible))	R9 (Mass action (irreversible))
k = 5.3000e+001	k = 5.3000e+001	k = 5.3000e+001
R10 (Mass action (irreversible))	R10 (Mass action (irreversible))	R10 (Mass action (irreversible))
k = 5.0000e-006	k = 5.0000e-006	k = 5.0000e-006

Case 7 (only full enzyme active, cooperative binding)

7(a)	**7(b)**	**7(c)**
R1 (Mass action (reversible))	R1 (Mass action (reversible))	R1 (Mass action (reversible))
k1 = 1.0000e+009	k1 = 1.0000e+009	k1 = 1.0000e+009
k2 = 5.0000e+002	k2 = 5.0000e+002	k2 = 5.0000e+000
R2 (Mass action (reversible))	R2 (Mass action (reversible))	R2 (Mass action (reversible))
k1 = 1.0000e+009	k1 = 1.0000e+009	k1 = 1.0000e+009
k2 = 5.0000e+002	k2 = 5.0000e+000	k2 = 5.0000e+002
R3 (Mass action (reversible))	R3 (Mass action (reversible))	R3 (Mass action (reversible))
k1 = 1.0000e+009	k1 = 1.0000e+009	k1 = 1.0000e+009
k2 = 5.0000e+000	k2 = 5.0000e+000	k2 = 5.0000e-002
R4 (Mass action (reversible))	R4 (Mass action (reversible))	R4 (Mass action (reversible))
k1 = 1.0000e+009	k1 = 1.0000e+009	k1 = 1.0000e+009
k2 = 5.0000e+000	k2 = 5.0000e-002	k2 = 5.0000e+000
R5 (Mass action (reversible))	R5 (Mass action (reversible))	R5 (Mass action (reversible))
k1 = 1.0000e+008	k1 = 1.0000e+008	k1 = 1.0000e+008
k2 = 8.4000e+005	k2 = 8.4000e+005	k2 = 8.4000e+005
R6 (Mass action (irreversible))	R6 (Mass action (irreversible))	R6 (Mass action (irreversible))
k = 5.3000e+001	k = 5.3000e+001	k = 5.3000e+001
R7 (Mass action (reversible))	R7 (Mass action (reversible))	R7 (Mass action (reversible))
k1 = 1.0000e+008	k1 = 1.0000e+008	k1 = 1.0000e+008
k2 = 8.4000e+005	k2 = 8.4000e+005	k2 = 8.4000e+005
R8 (Mass action (reversible))	R8 (Mass action (reversible))	R8 (Mass action (reversible))
k1 = 1.0000e+008	k1 = 1.0000e+008	k1 = 1.0000e+008
k2 = 8.4000e+005	k2 = 8.4000e+005	k2 = 8.4000e+005
R9 (Mass action (irreversible))	R9 (Mass action (irreversible))	R9 (Mass action (irreversible))
k = 5.0000e-006	k = 5.0000e-006	k = 5.0000e-006
R10 (Mass action (irreversible))	R10 (Mass action (irreversible))	R10 (Mass action (irreversible))
k = 5.0000e-006	k = 5.0000e-006	k = 5.0000e-006

APPENDIX B
SIMULATIONS OF EPR SPECTRA AT DIFFERENT FIELD/FREQUENCY COMBINATIONS OF OXALATE DECARBOXYLASE IN STORAGE BUFFER

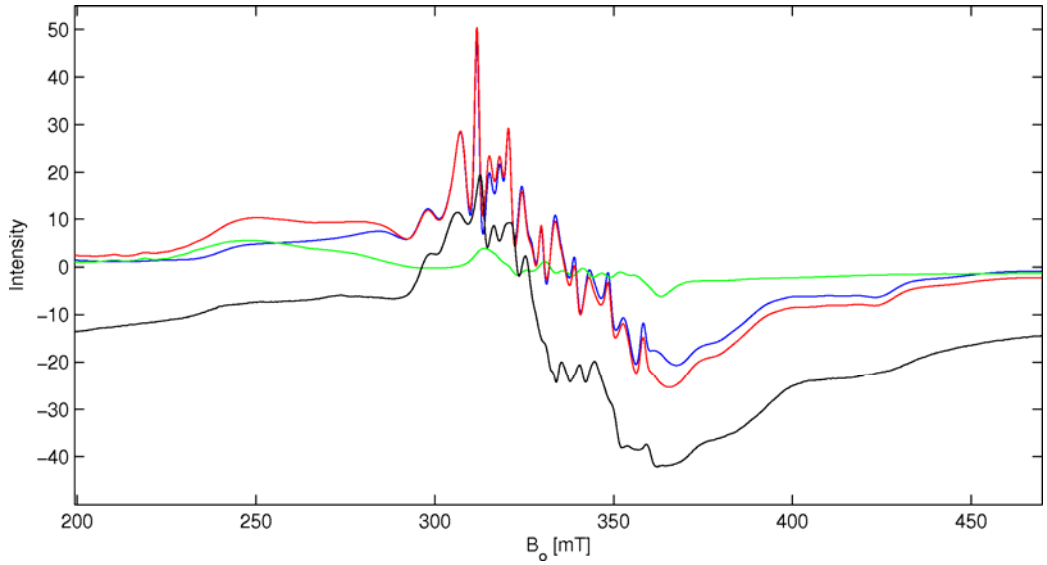

Figure B-1 X-band spectrum of OxDC in SB pH6.0 at T = 10 K. Experimental spectrum is shown in black. Simulations for sites I and II are shown in blue and green, respectively. The sum of the simulation of the two sites is shown in red.Experimental parameters: Microwave frequency 9.48731 GHz, microwave power 0.64 mW, modulation frequency 100 kHz, modulation amplitude 10 G, receiver gain 60 dB, time constant 41 ms, conversion time 41 ms, 1 sweep, 1.465 G/data point.Simulation parameters for site I: g_{iso} = 2.000865, A_{iso} = 254 MHz, D = 1200 MHz, E = 252 MHz, D-Strain = 0.24×D, E-Strain = 0.24×E, linewidthiso = 33 MHz.Simulation parameters for site II: g_{iso} = 2.00094, A_{iso} = 248 MHz, D = 2750 MHz, E = 660 MHz, D-Strain = 0.20×D, E-Strain = 0.20×E, $linewidth_{iso}$ = 33 MHz.

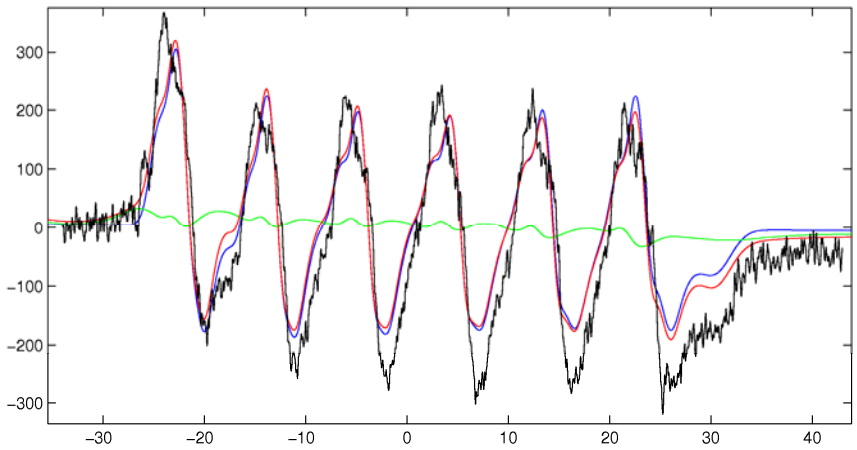

Figure B-2 V-band spectrum of OxDC in SB pH6.0 at T = 20 K. Experimental spectrum is shown in black. Simulations for sites I and II are shown in blue and green, respectively. The sum of the simulation of the two sites is shown in red.Experimental parameters: Microwave frequency 49.200 GHz, microwave power corresponding to a dector signal of 500 mV, modulation frequency 41.68 kHz, modulation amplitude 4 G, lock-in sensitivity 200 μV, time constant 300 ms, sweep speed 1 G/s, 1 sweep, 0.250 G/data point, center field 1.753 T.Simulation parameters for site I: g_{iso} = 2.000865, A_{iso} = 254 MHz, D = 1200 MHz, E = 276 MHz, D-Strain = 0.24×D, E-Strain = 0.30×E, $linewidth_{iso}$ = 33 MHz. Simulation parameters for site II: g_{iso} = 2.00094, A_{iso} = 248 MHz, D = 2700 MHz, E = 675 MHz, D-Strain = 0.25×D, E-Strain = 0.20×E, $linewidth_{iso}$ = 33 MHz.

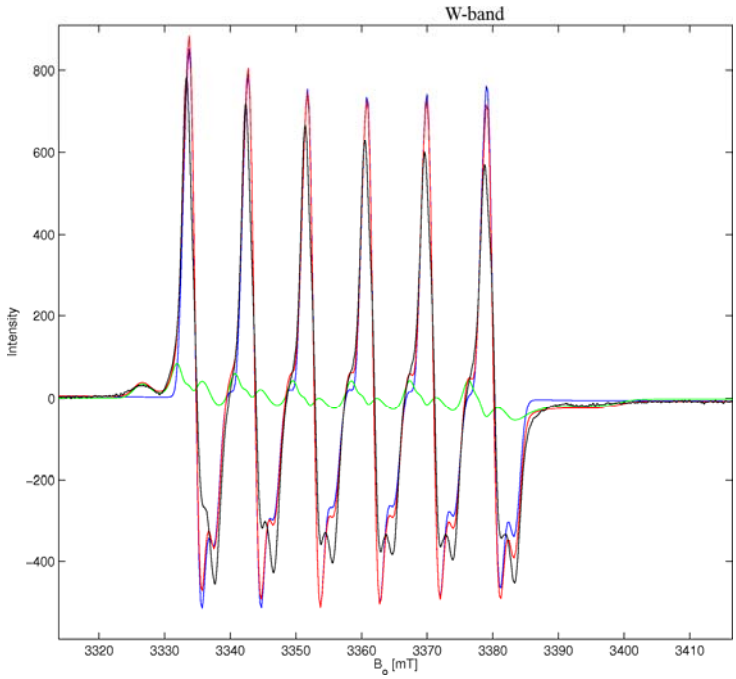

Figure B-3 W-band EPR spectrum of OxDC in SB pH6.0 at T = 50 K. Experimental spectrum is shown in black. Simulations for sites I and II are shown in blue and green, respectively. The sum of the simulation traces of the two sites is given in red. Experimental parameters: Microwave frequency 94.02141 GHz, microwave power 0.6 μW modulation frequency 100 kHz, modulation amplitude 2 G, receiver gain 40 dB, time constant 164 ms, conversion time 164 ms, 1 sweep, 1.172 G/data point. Simulation parameters for site I: g_{iso} = 2.000865, A_{iso} = 254 MHz, D = 1200 MHz, E = 252 MHz, D-Strain = 0.24×D, E-Strain = 0.24×E, linewidth$_{iso}$ = 33 MHz. Simulation parameters for site II: g_{iso} = 2.00094, A_{iso} = 248 MHz, D = 2700 MHz, E = 648 MHz, D-Strain = 0.20×D, E-Strain = 0.20×E, linewidth$_{iso}$ = 33 MHz.

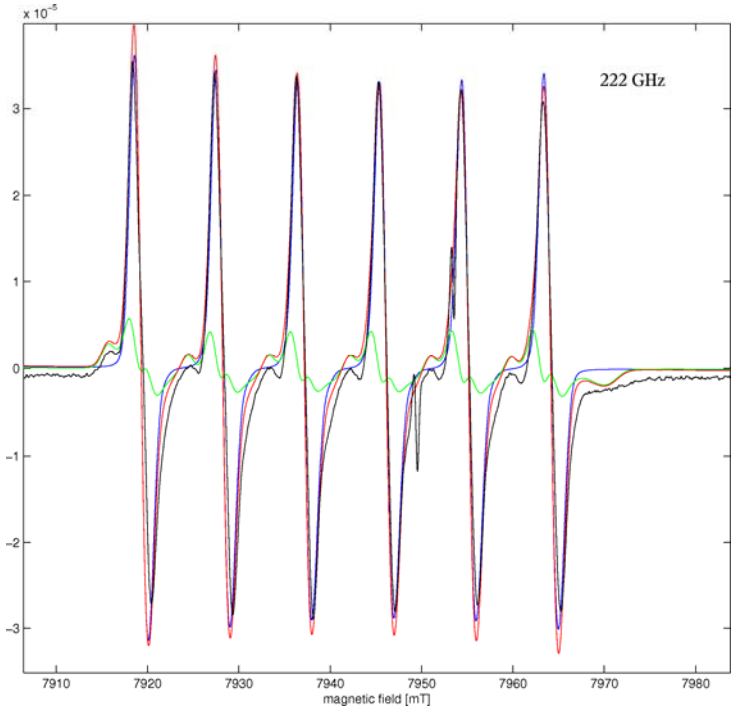

Figure B-4 Sub-mm EPR spectrum of OxDC in SB pH6.0 at T = 20 K and 222 GHz. Experimental spectrum is shown in black. Simulations for sites I and II are shown in blue and green, respectively. The sum of the simulation of the two sites is shown in red. Experimental parameters: Microwave frequency 222.400 GHz, modulation frequency 41.8 kHz, modulation amplitude 0.5 G, lock-in sensitivity 500 μV, time constant 100 ms, sweep speed 5.01 G/s, 1 sweep, 0.368 G/data point. Simulation parameters for site I: g_{iso} = 2.000865, A_{iso} = 251 MHz, D = 1200 MHz, E = 252 MHz, D-Strain = 0.24×D, E-Strain = 0.24×E, linewidth$_{iso}$ = 33 MHz. Simulation parameters for site II: g_{iso} = 2.00094, A_{iso} = 247 MHz, D = 2700 MHz, E = 675 MHz, D-Strain = 0.20×D, E-Strain = 0.20×E, linewidth$_{iso}$ = 33 MHz.

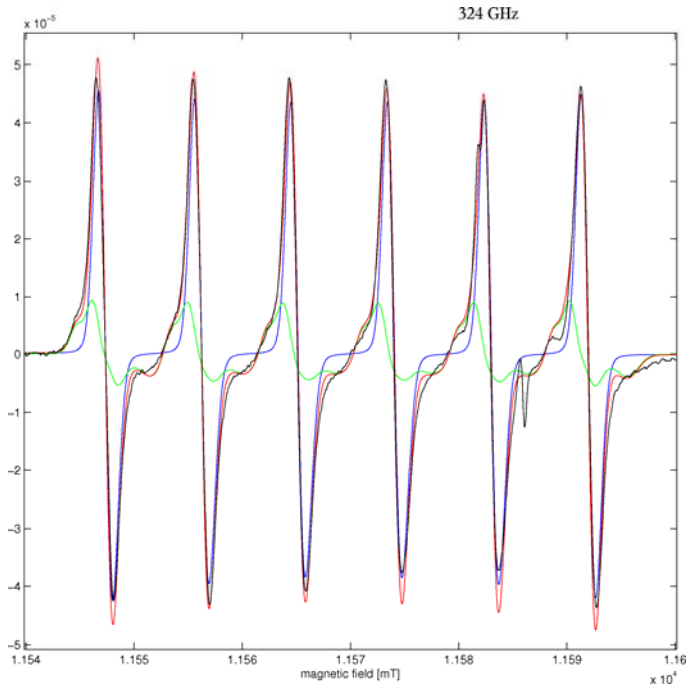

Figure B-5 Sub-mm EPR spectrum of OxDC in SB pH6.0 at T = 20 K and 324 GHz. Experimental spectrum is shown in black. Simulations for sites I and II are shown in blue and green, respectively. The sum of the simulation traces of the two sites is given in red. Experimental parameters: Microwave frequency 324.00 GHz, modulation frequency 41.8 kHz, modulation amplitude 0.5 G, lock-in sensitivity 50 μV, time constant 100 ms, sweep speed 5.01 G/s, 1 sweep, 0.367 G/data point.Simulation parameters for site I: g_{iso} = 2.000865, A_{iso} = 250 MHz, D = 1200 MHz, E = 252 MHz, D-Strain = 0.24×D, E-Strain = 0.24×E, linewidth$_{iso}$ = 33 MHz.Simulation parameters for site II: g_{iso} = 2.00094, A_{iso} = 247 MHz, D = 2700 MHz, E = 675 MHz, D-Strain = 0.20×D, E-Strain = 0.20×E, linewidth$_{iso}$ = 33 MHz.

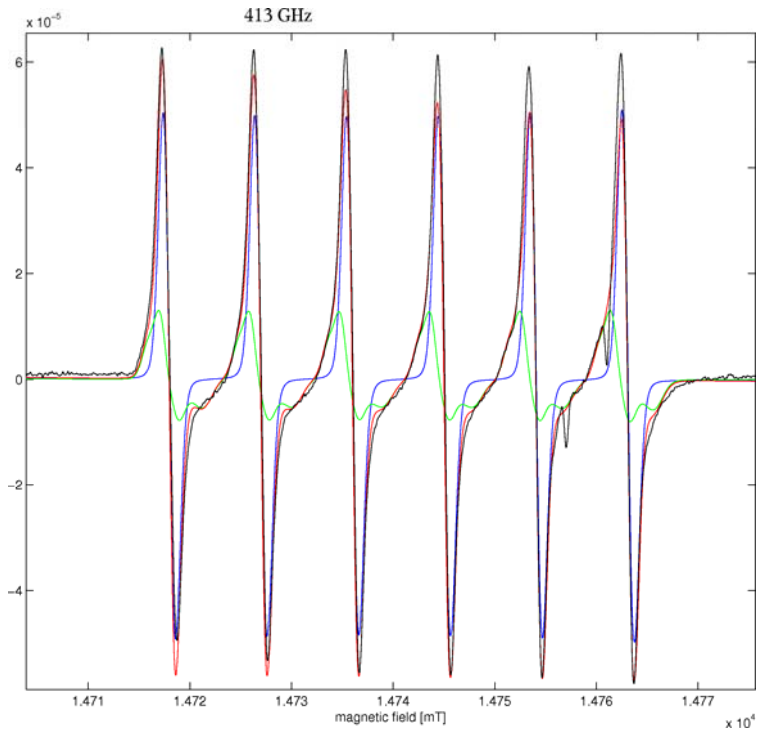

Figure B-6 Sub-mm EPR spectrum of OxDC in SB pH6.0 at T = 20 K and 412.8 GHz. Experimental spectrum is shown in black. Simulations for sites I and II are shown in blue and green, respectively. The sum of the simulation traces of the two sites is given in red. Experimental parameters: Microwave frequency 412.800 GHz, modulation frequency 41.8 kHz, modulation amplitude 4 G, lock-in sensitivity 500 μV, time constant 100 ms, sweep speed 5.01 G/s, 1 sweep, 0.369 G/data point. Simulation parameters for site I: g_{iso} = 2.000865, A_{iso} = 253 MHz, D = 1200 MHz, E = 252 MHz, D-Strain = 0.24×D, E-Strain = 0.24×E, linewidth$_{iso}$ = 33 MHz.Simulation parameters for site II: g_{iso} = 2.00093, A_{iso} = 249 MHz, D = 2700 MHz, E = 675 MHz, D-Strain = 0.25×D, E-Strain = 0.25×E, linewidth$_{iso}$ = 33 MHz.

APPENDIX C
HIGH FIELD SPECTRA AND SIMULATIONS OF WT OXDC AND THE E280Q MUTANT

Figures C-1, C-2, and C-3 show the results of the best fits obtained for simulations of the EPR spectra obtained for wild type OxDC and the E280Q mutant. All simulations were performed with the Easy Spin toolbox (*121*) in the MATLAB computing environment (The MathWorks, Natick, MA) by Dr. Ines Garcia-Rubio at ETH-Zurich. We assumed isotropic g- and A-tensors while using an anisotropic fine structure tensor, and the fits improved considerably by choosing a mixture of Lorentzian and Gaussian lineshapes. Nine independent fit parameters were used for the main Mn(II) species in each spectrum. Given that only the region around g~2 was measured in these experiments, fine structure values and associated strain parameters have a large uncertainty (conservatively estimated to be ±50% of the fit values). On the other hand, the hyperfine coupling constant could be extracted from the first with more confidence. Changing A by ± 1 MHz considerably worsened agreement between the simulated and the experimental spectrum, and, similarly, the margin of error for the isotropic g-value is small being estimated as approximately ± 0.00001. Apparent linewidths are somewhat dependent on the choice of D and E, although reducing both fine structure constants to almost zero only reduces the linewidth by a few Gauss (0.85 mT and 1.1 mT for E280Q and wild-type enzyme respectively), and these simulations suffer from lack of accuracy in the wings of the six lines.

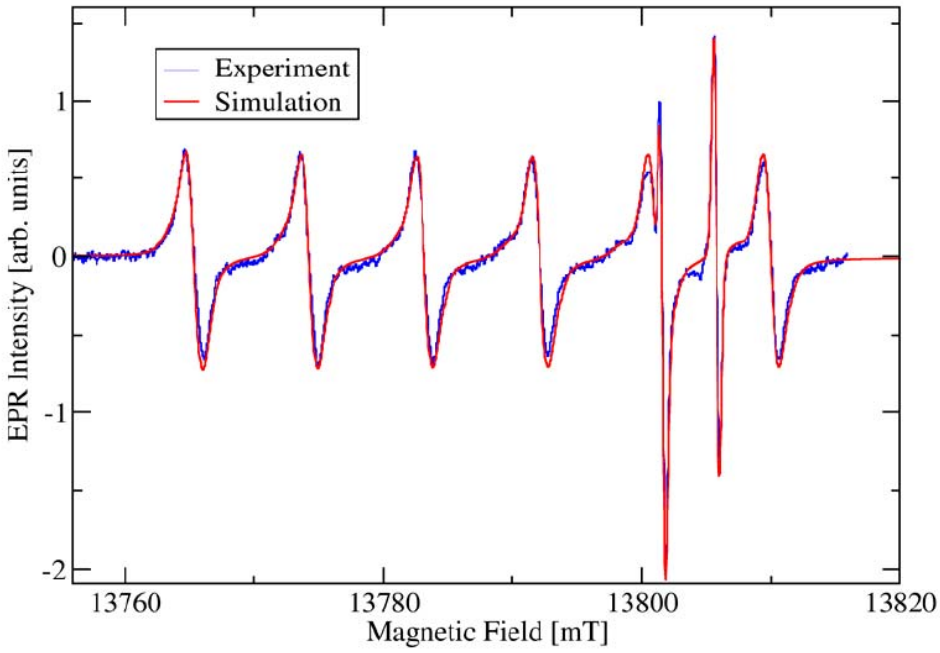

Figure C-1 High field EPR of wild-type OxDC enzyme at 386.116 GHz and 10 K. The experimental and simulated spectra are displayed in blue and red, respectively. Simulation parameters for the majority Mn(II) component are: g-factor = 2.00087, D = 1200 MHz, E = 240 MHz, D-Strain: 40% of D, E-Strain: 40% of E, hyperfine coupling, A: 250 MHz, A-Strain: 1% of A, linewidth: 1.5 mT, lineshape: 90% Lorentzian, 10% Gaussian. A minority component was assumed to be present to explain the low field shoulders on the main six-line spectrum, contributing approximately 4% of the spectral intensity, with simulation parameters: g-factor = 2.00107, D = E = 0 MHz, hyperfine coupling, A: 245 MHz, linewidth: 1.8 mT, lineshape: 100% Lorentian.

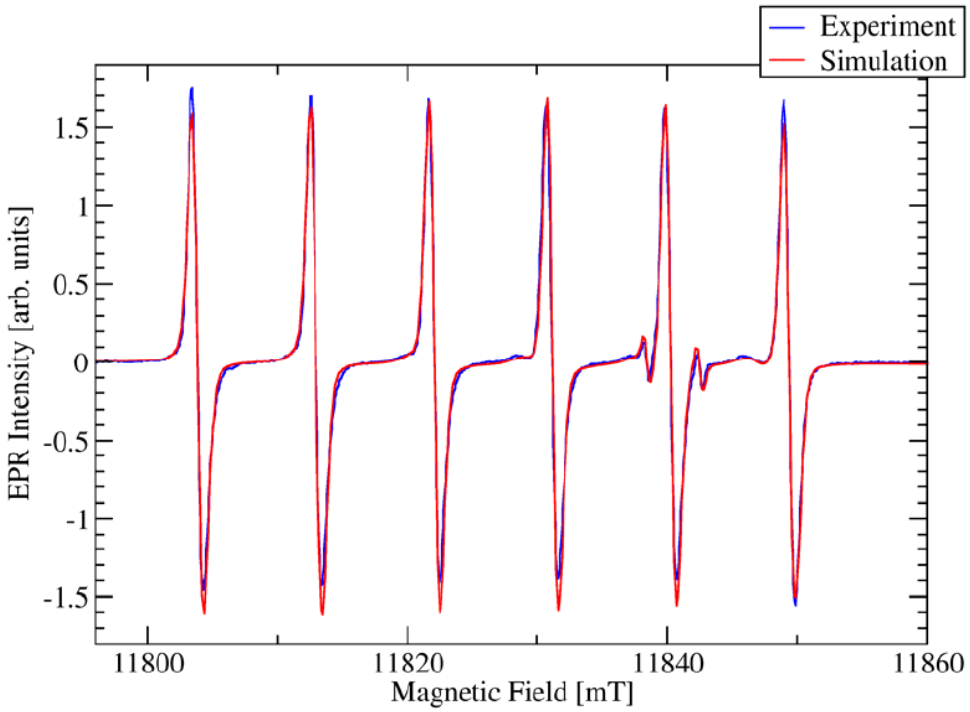

Figure C-2 High field EPR of E280Q OxDC mutant at 331.2 GHz and 20 K. The experimental and simulated spectra are displayed in blue and red, respectively. Simulation parameters for the majority Mn(II) component are: g-factor = 2.00087, D = 850 MHz, E = 85 MHz, D-Strain: 40% of D, E-Strain: 40% of E, hyperfine coupling, A: 255 MHz, A-Strain: 2% of A, linewidth: 0.9 mT, lineshape: 50% Lorentzian, 50% Gaussian. A minority component was assumed to be present to explain the low field shoulders on the main six-line spectrum, contributing approximately 7.5% of the spectral intensity, with simulation parameters: g-factor = 2.00109, D = E = 0 MHz, hyperfine coupling, A: 242 MHz, linewidth: 1.8 mT, lineshape: 100% Lorentian.

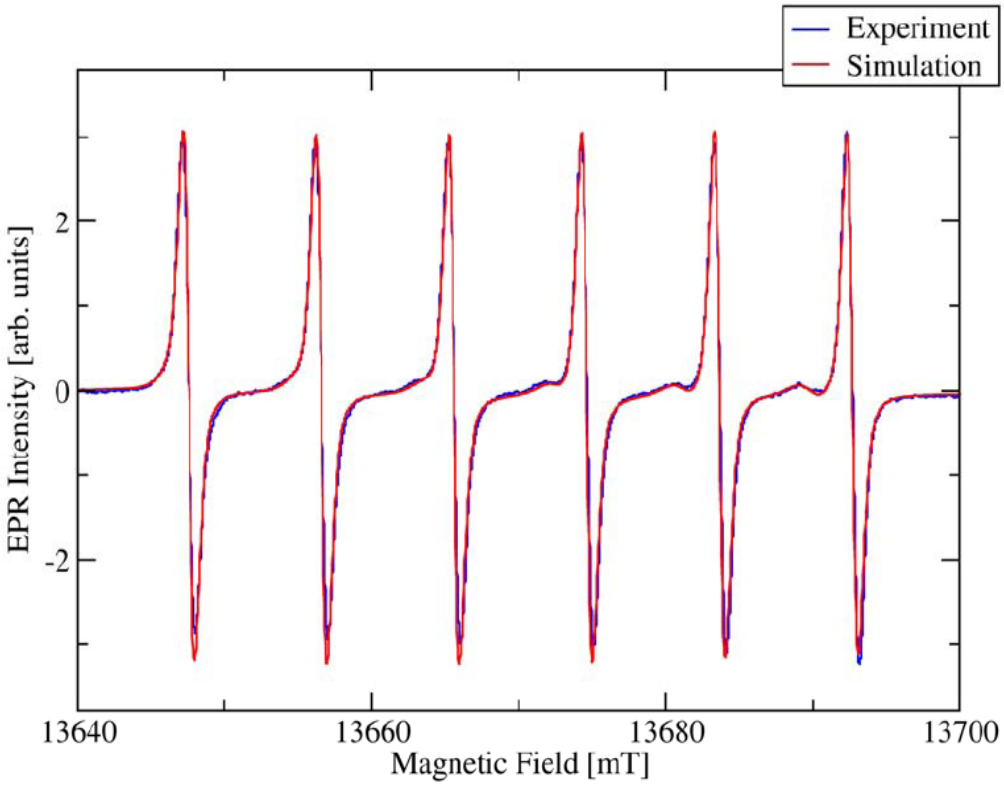

Figure C-3 High field EPR of E280Q OxDC mutant at 382.826 GHz and 10 K. The experimental and simulated spectra are displayed in blue and red, respectively. Simulation parameters for the majority Mn(II) component are: g-factor = 2.00087, D = 850 MHz, E = 85 MHz, D-Strain: 40% of D, E-Strain: 40% of E, hyperfine coupling, A: 253 MHz, A-Strain: 1% of A, linewidth: 1.0 mT, lineshape: 80% Lorentzian, 20% Gaussian. A minority component was assumed to be present to explain the low field shoulders on the main six-line spectrum, contributing approximately 7.5% of the spectral intensity, with simulation parameters: g-factor = 2.00111, D = E = 0 MHz, hyperfine coupling, A: 240 MHz, linewidth: 1.8 mT, lineshape: 100% Lorentian. This spectrum taken at 382 GHz did not have a field standard, and to simulate the 382 GHz spectrum, the field axis was adjusted to yield the same isotropic g-factor in the simulation in essence using the six-line spectrum as the field standard for that particular frequency made possible using the calibrated spectrum taken for the E280Q OxDC mutant at 331 GHz.

LIST OF REFERENCES

1. Holmes, R. P., and Kennedy, M. (2000) *Kidney Int 57*, 1662-7.

2. Libert, B., Franceschi, V. R. (1987) *J. Agric. Food Chem. 35*, 926-938.

3. Massey, L. K. (2003) *Front Biosci 8*, s584-94.

4. Franceschi, V. R., and Nakata, P. A. (2005) *Annu Rev Plant Biol 56*, 41-71.

5. Franceschi, V. R., Loewus, F.A. (1995) in *Calcium Oxalate in Biological Systems* (Khan, S. R., Ed.) pp 113-130, CRC, Boca Raton.

6. Richardson, K. E., and Tolbert, N. E. (1961) *J Biol Chem 236*, 1280-4.

7. Seal, S. N., Sen, S. P. (1970) *Plant Cell Physiol. 11*, 119-128.

8. Giachetti, E., Pinzauti, G., Bonaccorsi, R., and Vanni, P. (1988) *Eur J Biochem 172*, 85-91.

9. Pinzauti, G., Giachetti, E., Camici, G., Manao, G., Cappugi, G., and Vanni, P. (1986) *Arch Biochem Biophys 244*, 85-93.

10. Franceschi, V. (2001) *Trends Plant Sci 6*, 331.

11. Houck, D. R., and Inamine, E. (1987) *Arch Biochem Biophys 259*, 58-65.

12. Kubicek, C. P., Schreferl-Kunar, G., Wohrer, W., and Rohr, M. (1988) *Appl Environ Microbiol 54*, 633-7.

13. Stone, H. E., Amentrout, V. N. (1985) *Mycologia 77*, 526-532.

14. Kritzman, G., Chet, I., Henis, I. (1977) *Exper. Mycol. 1*, 280-289.

15. Akamatsu, Y., Ma, D. B., Higuchi, T., and Shimada, M. (1990) *FEBS Lett 269*, 261-3.

16. Espejo, E., and Agosin, E. (1991) *Appl Environ Microbiol 57*, 1980-1986.

17. Goodwin, D. C., Barr, D. P., Aust, S. D., and Grover, T. A. (1994) *Arch Biochem Biophys 315*, 267-72.

18. Dutton, M. V., Kathiara, M., Gallagher, I. M., and Evans, C. S. (1994) *Fems Microbiology Letters 116*, 321-325.

19. Allison, M. J., Daniel, S. L., Cornick, N. A. (1995) in *Calcium Oxalate in Biological Systems* (Khan, S. R., Ed.) pp 131-168, CRC, Boca Raton.

20. Hodgkinson, A. (1977) *Oxalic acid in biology and medicine*, Academic Press, London ; New York.

21. Elder, T. D., and Wyngaarden, J. B. (1960) *J Clin Invest 39*, 1337-44.

22. Sidhu, H., Schmidt, M. E., Cornelius, J. G., Thamilselvan, S., Khan, S. R., Hesse, A., and Peck, A. B. (1999) *J Am Soc Nephrol 10 Suppl 14*, S334-40.

23. Sidhu, H., Allison, M., and Peck, A. B. (1997) *J Clin Microbiol 35*, 350-3.
24. Williams, H. E., and Wandzilak, T. R. (1989) *J Urol 141*, 742-9.

25. Hoppe, B., von Unruh, G., Laube, N., Hesse, A., and Sidhu, H. (2005) *Urol Res 33*, 372-5.

26. Hesse, A., Bongartz, H. Heynck, H., Berg, W. (1996) *Clin. Biochem. 29*, 467-472.

27. Honow, R., Bongartz, D., Hesse, A. (1997) *Clin. Chim. Acta 261*.

28. Dunwell, J. M., Khuri, S., and Gane, P. J. (2000) *Microbiol Mol Biol Rev 64*, 153-79.

29. Thompson, C., Dunwell, J. M. Johnstone, C. E., Lay, V., Ray, J., Schmitt, H., Watson, H., Nisbet, G. (1995) *Euphytica 85*, 169-172.

30. Wei, Y., Zhang, Z., Andersen, C. H., Schmelzer, E., Gregersen, P. L., Collinge, D. B., Smedegaard-Petersen, V., and Thordal-Christensen, H. (1998) *Plant Mol Biol 36*, 101-12.

31. Strasser, H., Burgstaller, W., and Schinner, F. (1994) *FEMS Microbiol Lett 119*, 365-70.

32. Kotsira, V. P., and Clonis, Y. D. (1997) *Arch Biochem Biophys 340*, 239-49.

33. Shimazono, H. (1955) *J Biochem 42*, 321-340.

34. Tanner, A., and Bornemann, S. (2000) *J Bact 182*, 5271-5273.

35. Quayle, J. R. (1963) *Biochem J 87*, 368-73.

36. Whittaker, M. M., and Whittaker, J. W. (2002) *J Biol Inorg Chem 7*, 136-45.

37. Svedruzic, D., Jonsson, S., Toyota, C. G., Reinhardt, L. A., Ricagno, S., Lindqvist, Y., and Richards, N. G. J. (2005) *Arch Biochem Biophys 433*, 176-192.

38. Wojtaszek, P. (1997) *Biochem J 322 (Pt 3)*, 681-92.

39. Dumas, B., Freyssinet, G., and Pallett, K. E. (1995) *Plant Physiol 107*, 1091-1096.

40. Showalter, A. M. (1993) *Plant Cell 5*, 9-23.

41. Woo, E. J., Dunwell, J. M., Goodenough, P. W., and Pickersgill, R. W. (1998) *FEBS Letters 437*, 87-90.

42. Woo, E. J., Dunwell, J. M., Goodenough, P. W., Marvier, A. C., and Pickersgill, R. W. (2000) *Nat Struct Biol 7*, 1036-1040.

43. Dunwell, J. M., Purvis, A., and Khuri, S. (2004) *Phytochemistry 65*, 7-17.

44. Dunwell, J. M., and Gane, P. J. (1998) *J Mol Evol 46*, 147-54.

45. Dunwell, J. M., Culham, A., Carter, C. E., Sosa-Aguirre, C. R., and Goodenough, P. W. (2001) *Trends Biochem Sci 26*, 740-6.

46. Dunwell, J. M. (1998) *Biotechnol Genet Eng Rev 15*, 1-32.

47. Park, J. S., Wood, P. M., Davies, M. J., Gilbert, B. C., and Whitwood, A. C. (1997) *Free Radic Res 27*, 447-58.

48. Opaleye, O., Rose, R. S., Whittaker, M. M., Woo, E. J., Whittaker, J. W., and Pickersgill, R. W. (2006) *J Biol Chem 281*, 6428-33.

49. Sahin, N. (2003) *Res Microbiol 154*, 399-407.

50. Baetz, A. L., and Allison, M. J. (1989) *J Bacteriol 171*, 2605-8.

51. Baetz, A. L., and Allison, M. J. (1990) *J Bacteriol 172*, 3537-40.

52. Maloney, P. C., Anantharam, V., and Allison, M. J. (1992) *J Biol Chem 267*, 10531-6.

53. Ruan, Z. S., Anantharam, V., Crawford, I. T., Ambudkar, S. V., Rhee, S. Y., Allison, M. J., and Maloney, P. C. (1992) *J Biol Chem 267*, 10537-43.

54. Abe, K., Ruan, Z. S., and Maloney, P. C. (1996) *J Biol Chem 271*, 6789-93.

55. Anantharam, V., Allison, M. J., and Maloney, P. C. (1989) *J Biol Chem 264*, 7244-50.

56. Kuhner, C. H., Hartman, P. A., and Allison, M. J. (1996) *Appl Environ Microbiol 62*, 2494-500.

57. Reinhardt, L. A., Svedruzic, D., Chang, C. H., Cleland, W. W., and Richards, N. G. (2003) *J Am Chem Soc 125*, 1244-52.

58. Shimazono, H., and Hayaishi, O. (1957) *J Biol Chem 227*, 151-9.

59. Magro, P., Marciano, P., and Dilenna, P. (1988) *Fems Microbiology Letters 49*, 49-52.

60. Lillehoj, E. B., Smith, F. G. (1965) *Arch Biochem Biophys 105*, 216-220.

61. Emiliani, E., and Bekes, P. (1964) *Arch Biochem Biophys 105*, 488-93.

62. Emiliani, E., and Riera, B. (1968) *Biochim Biophys Acta 167*, 414-20.

63. Kathiara, M., Wood, D. A., and Evans, C. S. (2000) *Mycological Research 104*, 345-350.

64. Micales, J. A. (1997) *Int. J.Biodeter. Biodegr. 39*, 125-132.

65. Makela, M., Galkin, S., Hatakka, A., and Lundell, T. (2002) *Enzyme and Microbial Technology 30*, 542-549.

66. Mehta, A., and Datta, A. (1991) *Journal of Biological Chemistry 266*, 23548-23553.

67. Azam, M., Kesarwani, M., Chakraborty, S., Natarajan, K., and Datta, A. (2002) *Biochemical Journal 367*, 67-75.

68. Azam, M., Kesarwani, M., Natarajan, K., and Datta, A. (2001) *Biochem Biophys Res Commun 289*, 807-12.

69. Cotter, P. D., and Hill, C. (2003) *Microbiol Mol Biol Rev 67*, 429-53, table of contents.

70. Tanner, A., Bowater, L., Fairhurst, S. A., and Bornemann, S. (2001) *J Biol Chem 276*, 43627-43634.

71. Chang, C. H., Svedruzic, D., Ozarowski, A., Walker, L., Yeagle, G., Britt, R. D., Angerhofer, A., and Richards, N. G. J. (2004) *J Biol Chem 279*, 52840-52849.

72. Anand, R., Dorrestein, P. C., Kinsland, C., Begley, T. P., and Ealick, S. E. (2002) *Biochem 41*, 7659-7669.

73. Just, V. J., Stevenson, C. E., Bowater, L., Tanner, A., Lawson, D. M., and Bornemann, S. (2004) *J Biol Chem 279*, 19867-74.

74. Muthusamy, M., Burrell, M. R., Thorneley, R. N., and Bornemann, S. (2006) *Biochemistry 45*, 10667-73.

75. Kunst, F., Ogasawara, N., Moszer, I., Albertini, A. M., Alloni, G., Azevedo, V., Bertero, M. G., Bessieres, P., Bolotin, A., Borchert, S., Borriss, R., Boursier, L., Brans, A., Braun, M., Brignell, S. C., Bron, S., Brouillet, S., Bruschi, C. V., Caldwell, B., Capuano, V., Carter, N. M., Choi, S. K., Codani, J. J., Connerton, I. F., Danchin, A., and et al. (1997) *Nature 390*, 249-56.

76. Bowater, L., Fairhurst, S. A., Just, V. J., and Bornemann, S. (2004) *FEBS Lett 557*, 45-8.

77. Brahms, S., Brahms, J., Spach, G., and Brack, A. (1977) *Proc Natl Acad Sci U S A 74*, 3208-12.

78. Gopal, B., Madan, L. L., Betz, S. F., and Kossiakoff, A. A. (2005) *Biochem 44*, 193-201.

79. Thompson, J. D., Higgins, D. G., and Gibson, T. J. (1994) *Nucleic Acids Res 22*, 4673-80.

80. Jeanmougin, F., Thompson, J. D., Gouy, M., Higgins, D. G., and Gibson, T. J. (1998) *Trends Biochem Sci 23*, 403-5.

81. Anantharaman, V., Aravind, L., and Koonin, E. V. (2003) *Curr Opin Chem Biol 7*, 12-20.

82. Murzin, A. G., Brenner, S. E., Hubbard, T., and Chothia, C. (1995) *J Mol Biol 247*, 536-40.

83. Lo Conte, L., Brenner, S. E., Hubbard, T. J., Chothia, C., and Murzin, A. G. (2002) *Nucleic Acids Res 30*, 264-7.

84. Andreeva, A., Howorth, D., Brenner, S. E., Hubbard, T. J., Chothia, C., and Murzin, A. G. (2004) *Nucleic Acids Res 32*, D226-9.

85. Gerlt, J. A., and Babbitt, P. C. (1998) *Curr Opin Chem Biol 2*, 607-12.

86. Gerlt, J. A., and Babbitt, P. C. (2001) *Annu Rev Biochem 70*, 209-46.

87. Anantharaman, V., Koonin, E. V., and Aravind, L. (2001) *J Mol Biol 307*, 1271-92.

88. Woo, E. J., Bauly, J., Chen, J. G., Marshall, J., Macdonald, H., Lazarus, C., Goodenough, P., Venis, M., Napier, R., and Pickersgill, R. (2000) *Acta Crystallogr D Biol Crystallogr 56 (Pt 11)*, 1476-8.

89. Olivares, J. A. (1988) *Methods Enzymol 158*, 205-232.

90. Chang, C. H., Richards, N. G. J. (2005) *J. Chem. Theory Comput. 1*, 994-1007.

91. Escutia, M. R., Bowater, L., Edwards, A., Bottrill, A. R., Burrell, M. R., Polanco, R., Vicuna, R., and Bornemann, S. (2005) *Appl Environ Microbiol 71*, 3608-16.

92. Cleland, W. W. (2003) *J Biol Chem 278*, 51975-84.

93. Cleland, W. W. (1995) *Methods Enzymol 249*, 341-73.

94. Klinman, J. P. (2001) *J Biol Inorg Chem 6*, 1-13.

95. Su, Q., and Klinman, J. P. (1998) *Biochemistry 37*, 12513-25.

96. Armstrong, R. N. (2000) *Biochemistry 39*, 13625-13632.

97. Schaab, M. R., Barney, B. M., and Francisco, W. A. (2006) *Biochemistry 45*, 1009-16.

98. Schute, H., Flossdorf, J., Sahm, H., and Kula, M. R. (1976) *Eur J Biochem 62*, 151-60.

99. Kehres, D. G., and Maguire, M. E. (2003) *FEMS Microbiol Rev 27*, 263-290.

100. Que, Q., and Helmann, J. D. (2000) *Molec Microbiol 35*, 1454-1468.

101. Moore, C. M., and Helmann, J. D. (2005) *Curr Opin Microbiol 8*, 188-95.

102. Zaharik, M. L., and Finlay, B. B. (2004) *Front Biosci 9*, 1035-42.

103. Horsburgh, M. J., Wharton, S. J., Karavolos, M., and Foster, S. J. (2002) *Trends Microbiol 10*, 496-501.

104. Gonzalez, J. C., Peariso, K., Penner-Hahn, J. E., and Matthews, R. G. (1996) *Biochem 35*, 12228-34.

105. Whitfield, C. D., and Weissbach, H. (1970) *Journal of Biological Chemistry 245*, 402-409.

106. Mizuno, K., Whittaker, M. M., Bachinger, H. P., and Whittaker, J. W. (2004) *J Biol Chem 279*, 27339-44.

107. Yamakura, F., Kobayashi, K., Ue, H., and Konno, M. (1995) *European Journal of Biochemistry 227*, 700-706.

108. Quijano, C., Hernandez-Saavedra, D., Castro, L., McCord, J. M., Freeman, B. A., and Radi, R. (2001) *J Biol Chem 276*, 11631-8.

109. Li, T., Walker, A. L., Iwaki, H., Hasegawa, Y., and Liu, A. (2005) *J Am Chem Soc 127*, 12282-90.

110. Vance, C. K., and Miller, A. F. (1998) *Biochemistry 37*, 5518-5527.

111. Ose, D. E., and Fridovich, I. (1976) *J Biol Chem 251*, 1217-8.

112. Ose, D. E., and Fridovich, I. (1979) *Arch Biochem Biophys 194*, 360-4.

113. Mendes, P. (1993) *Comput Appl Biosci 9*, 563-71.

114. Mendes, P. (1997) *Trends Biochem Sci 22*, 361-3.

115. Cleland, W. W. (1979) *Methods Enzymol 62*, 151-160.

116. Weil, J. A., Bolton, J. R., and Wertz, J. E. (1994) *Electron Paramagnetic Resonance*, John Wiley & Sons, Inc., New York.

117. Reed, G. H., and Markham, G. D. (1984) in *Biological Magnetic Resonance* (Berliner, L. J., and Reuben, J., Ed.) pp 73-142, Plenum Press, New York.

118. Van Wieringgen, J. S. (1955) *Diss. Faraday Soc. 19*, 118-124.

119. Hurd, F. K., Sachs, M., and Hershberger, W. D. (1954) *Phys. Rev. 93*, 373-376.

120. Angerhofer, A., Moomaw, E. W., Garcia-Rubio, I., Ozarowski, A., Krzystek, J., Weber, R. T., and Richards, N. G. (2007) *J Phys Chem B 111*, 5043-5046.

121. Stoll, S., and Schweiger, A. (2006) *J Magn Reson 178*, 42-55.

122. Garcia-Rubio, I., Angerhofer, A., and Schweiger, A. (2007) *J Magn Reson 184*, 130-42.

123. Tabares, L. C., Cortez, N., Hiraoka, B. Y., Yamakura, F., and Un, S. (2006) *Biochemistry 45*, 1919-29.

124. Hassan, A. K., Pardi, L. A., Krzystek, J., Sienkiewicz, A., Goy, P., Rohrer, M., and Brunel, L. C. (2000) *J Magn Reson 142*, 300-12.

125. Zhang, H., Joseph, J., Vasquez-Vivar, J., Karoui, H., Nsanzumuhire, C., Martasek, P., Tordo, P., and Kalyanaraman, B. (2000) *FEBS Lett 473*, 58-62.

126. Olive, G., Mercier, A., Le Moigne, F., Rockenbauer, A., and Tordo, P. (2000) *Free Radic Biol Med 28*, 403-8.

127. Frejaville, C., Karoui, H., Tuccio, B., Le Moigne, F., Culcasi, M., Pietri, S., Lauricella, R., and Tordo, P. (1995) *J Med Chem 38*, 258-65.

128. Chakraborty, S., Chakraborty, N., Jain, D., Salunke, D. M., and Datta, A. (2002) *Prot Sci 11*, 2138-2147.

129. Requena, L., and Bornemann, S. (1999) *Biochem J 343 Pt 1*, 185-90.

130. Christendat, D., Saridakis, V., Dharamsi, A., Bochkarev, A., Pai, E. F., Arrowsmith, C. H., and Edwards, A. M. (2000) *J Biol Chem 275*, 24608-12.

131. Lawrence, M. C., Izard, T., Beuchat, M., Blagrove, R. J., and Colman, P. M. (1994) *J Mol Biol 238*, 748-76.

132. Woody, R. W. (1995) *Methods Enzymol 246*, 34-71.

133. Jeong, J. J., Fushinobu, S., Ito, S., Jeon, B. S., Shoun, H., and Wakagi, T. (2003) *FEBS Lett 535*, 200-4.

134. Un, S., Dorlet, P., Voyard, G., Tabares, L. C., and Cortez, N. (2001) *J Am Chem Soc 123*, 10123-4.

135. Eaton, S. S. a. E., G. R. (2000) in *Biological Magnetic Resonance in Biological Systems by EPR* (Berliner, L. J., and Reuben, J., Ed.) pp 29-153, Academic/Plenum Publishers, New York.

136. Gerlt, J. A., and Babbitt, P. C. (2001) *Nat Struct Biol 8*, 5-7.

137. Lang, D., Thoma, R., Henn-Sax, M., Sterner, R., and Wilmanns, M. (2000) *Science 289*, 1546-50.

138. Hocker, B., Beismann-Driemeyer, S., Hettwer, S., Lustig, A., and Sterner, R. (2001) *Nat Struct Biol 8*, 32-6.

139. Li, Y., and Goodwin, D. C. (2004) *Biochem Biophys Res Commun 318*, 970-6.

140. Baker, R. D., Cook, C. O., and Goodwin, D. C. (2004) *Biochem Biophys Res Commun 320*, 833-9.

141. Baker, R. D., Cook, C. O., and Goodwin, D. C. (2006) *Biochemistry 45*, 7113-21.

142. Ho, S. N., Hunt, H. D., Horton, R. M., Pullen, J. K., and Pease, L. R. (1989) *Gene 77*, 51-9.

143. Petrenko, A., Maniero, A. L., van Tol, J., MacMillan, F., Li, Y., Brunel, L. C., and Redding, K. (2004) *Biochemistry 43*, 1781-6.

144. Schweiger, A., and Jeschke, G. (2001) *Principles of Pulse Electron Paramagnetic Resonance*, Oxford University Press, Oxford.

BIOGRAPHICAL SKETCH

Ellen Moomaw was born in Jacksonville, FL in 1960. After earning a master's of science degree in biochemistry in the laboratory of Dr. Dale Edmondson (Emory University, 1984), she worked in various biotechnology companies in San Diego. In 1987 Ellen was the 30th employee hired at a young company called Agouron Pharmaceuticals, Inc. where she purified and characterized a number of proteins including thymidylate synthetase, HIV reverse transcriptase and RNase H, DNA polymerase b, and HCV protease. By the time she left Agouron in 1999 to teach high school chemistry, Agouron (now part of Pfizer) had over 1200 employees and had gotten the 4th HIV protease inhibitor on the market (Viracept™). Ellen started graduate studies in the chemistry department of the University of Florida in 2003, where she joined the research group of Dr. Nigel G. J. Richards.